

# 学位論文

Quantum dynamics of H<sub>2</sub> molecule described by  
an electron-nuclear wave function with floating Gaussians

(浮動ガウシアン電子-原子核波動関数を用いた  
水素分子の量子動力学)

平成27年12月博士（理学）申請

東京大学大学院理学系研究科

化学専攻

市川 雄一



## Abstract

### Chapter 1

The object of this thesis and the background of the theory and field are introduced. First physical phenomena treated in the theory are described introducing previous experimental research. Second theoretical methods for simulation are described and compared.

### Chapter 2

Theoretical formulation using floating Gaussians for quantum dynamics of molecule is derived. Quantum mechanical equations of motion are derived and necessary terms with floating Gaussians are analytically derived.

### Chapter 3

General derivation in Chapter 2 is applied for H<sub>2</sub> molecule. Analytical formulations of electron-nuclear total wave functions, integrals, and differentials by parameters in wave function of H<sub>2</sub> molecule are obtained.

### Chapter 4

Calculation results of simulation for a ground state of electron-nuclear wave function of H<sub>2</sub> molecule are shown. Energies, periods of vibrations of squared inter-particle distances of electrons and nuclei, comparison of electronic excitation energies with the conventional HF methods, and non-adiabatic effects depending of the mass of nucleus are discussed.

### Chapter 5

Time-dependent quantal dynamics of H<sub>2</sub> molecule in intense laser fields are simulated. Molecular dynamics depending on laser parameters are discussed.

### Chapter 6

This thesis is summarized and perspectives are described.

## Contents

1. Introduction.....	6
1.1. Object of study .....	6
1.2. Dynamics in intense laser field .....	6
1.3. Classical approach .....	11
1.4. Grid method .....	12
1.5. Coupled coherent state (CCS) method.....	14
2. Quantum dynamics with floating Gaussians and general formulations .....	20
2.1. General equations of motion (EOMs) .....	20
2.1.1. In the case of unnormalized wave function .....	21
2.2. Derivation of Integrals for Gaussians .....	22
2.2.1. Overlap integral.....	22
2.2.2. Kinetic integral.....	26
2.2.3. Coulomb integral.....	27
2.3. Optimization methods.....	28
2.3.1. Gradient descent method (GDM).....	28
2.3.2. Imaginary time propagation (ITP) method.....	29
3. Theory for application to H <sub>2</sub> molecule .....	31
3.1. Total wave function.....	31
3.1.1. Expression of wave function with 4 orbital functions.....	31
3.1.2. Expression of each orbital with Gaussians .....	32
3.1.3. Expression of total Hamiltonian .....	33
3.2. Expression of each integral.....	33
3.2.1. Overlap integral.....	34
3.2.2. Kinetic integral.....	34
3.2.3. Coulomb integral .....	35
3.2.4. Integral for laser field .....	36
3.3. Differential of integral of Hamiltonian with each parameter .....	36
3.3.1. Differential by Gaussian label $g_x^i$ .....	39

3.3.2.	Differential by orbital coefficients.....	42
3.4.	Derivation of $c_{ij}$ .....	43
3.4.1.	Differential of $G_{t_x}$ .....	46
3.4.2.	Differential of $U_t^i$ .....	49
3.4.3.	Differential of $G_{t_x}$ by conjugate variables .....	51
3.4.4.	Differential of $U_t^i$ by orbital coefficients .....	53
4.	Ground state of H <sub>2</sub> molecule .....	56
4.1.	Optimization to ground-state.....	56
4.1.1.	Gradient descent .....	56
4.1.2.	Imaginary time propagation.....	59
4.1.3.	Discussion for ground-state wave function.....	68
4.2.	Time-dependent dynamics .....	70
4.2.1.	Real time propagation with orbital coefficients fixed.....	70
4.2.2.	Real time propagation with orbital coefficients varied.....	75
4.2.3.	Electronic excitation represented by floating Gaussian.....	78
4.2.4.	Assignment of the high frequency components .....	81
4.2.5.	Mass dependence of non-adiabatic coupling .....	88
5.	Application of laser fields to H <sub>2</sub> molecule .....	91
5.1.	Demonstration with 1.5 cycle pulse laser .....	91
5.2.	Ionization dependence on CEP and cycle of pulses .....	92
5.2.1.	Laser condition .....	93
5.2.2.	$E_0 = 0.3$ a.u. ....	94
5.2.3.	$E_0 = 0.25$ a.u. ....	100
5.2.4.	$E_0 = 1$ a.u. and 0.1 a.u. ....	103
6.	Summary and perspectives .....	105
6.1.	Summary.....	105
6.2.	Perspectives.....	107
	Acknowledgements .....	109

## 1. Introduction

### 1.1. Object of study

Unique molecular dynamics are observed in intense laser fields<sup>1), 2)</sup> such as tunnel ionization, electron recollision, proton migration<sup>3), 4)</sup>, Coulomb explosion of multiply charged ions, and molecular dynamics depending on carrier-envelope phase (CEP) of laser pulse<sup>5)</sup>. In order to describe such dynamics theoretically, it becomes necessary to treat the electronic motion associated with ionization induced by the interaction with the strong electric field and longtime dynamics during and after the duration of excitation laser pulse. It requires a large calculation cost to simulate these phenomena quantum mechanically and a method to deal quantum mechanically with the motion of nuclei is needed to be developed. Especially iterative simulation and the large calculation cost are required to investigate the dynamics under different conditions of laser pulses such as CEPs. Due to heavy calculation cost in the simulation of molecular dynamics in intense laser field, classical approach modified with some terms of quantum effect is still effective in this field because of these difficulties<sup>6), 7)</sup>. In this chapter, I will describe molecular dynamics in intense laser field first. Furthermore, previous approaches for these dynamics will be introduced and problems on previous works and the approach in present research will be described.

### 1.2. Dynamics in intense laser field

In intense laser field, the ionization of molecule occurs even if the photon energy is smaller than the ionization energy. This can be described with the mechanisms of multiphoton ionization and tunnel ionization. Figure 1-1 shows the pictorial sketch of mechanism of multiphoton ionization. The electron absorbs several photons simultaneously and is excited. If the energy level is higher than the potential barrier of nuclear, the electron can be ejected even if the energy of one photon is lower than the barrier. But the excitation probability is exponentially in proportion to the number of photon to absorb, so the probability of ionization is not high if the laser intensity is not strong. In further stronger laser field where laser field intensity is in the

range of  $10^{13}\sim 10^{15}$  W/cm<sup>2</sup>, the laser field will behave as electric field and tunnel ionization mechanism can be observed. Figure 1-2 shows the sketch of mechanism of tunnel ionization. If the laser field is strong enough, the potential curve of nuclear will be distorted by the electric field of laser pulse. At that time, the potential barrier against the bound state of electron will come lower and the probability of tunnel phenomenon will increase. Once the electron tunnels the barrier, then the electron can escape from the nuclear along the distorted potential. For those contribution, the ion yield will increase in strong laser field.

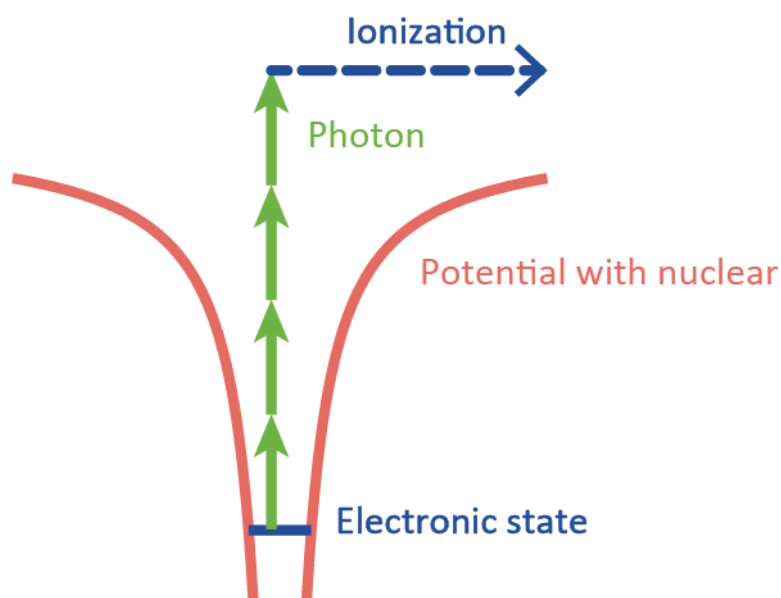


Figure 1-1 Sketch of multiphoton ionization

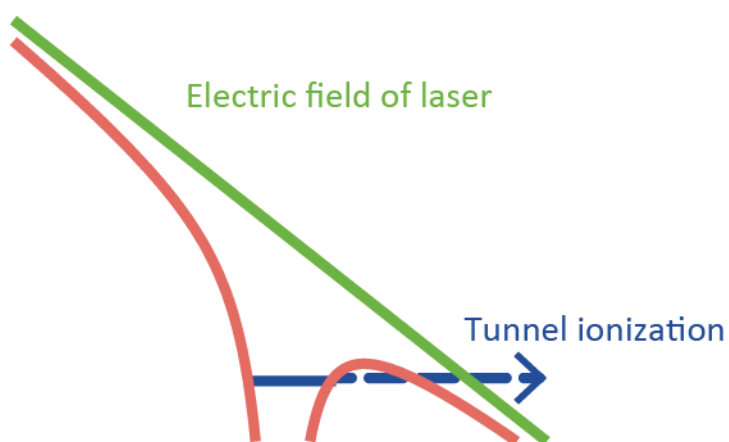
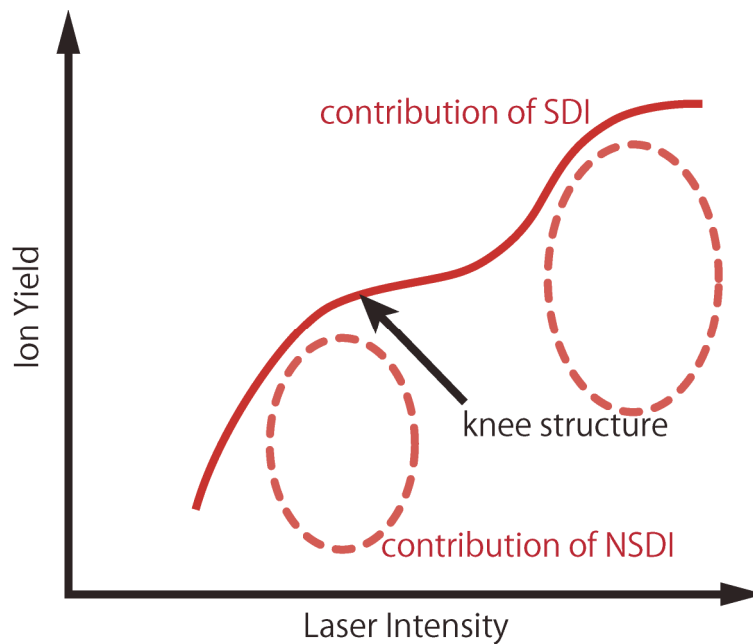


Figure 1-2 Sketch of tunnel ionization

However, if we measure the ion yield for double ionization for atoms or molecules which have several electrons such as He atom and H<sub>2</sub> molecule against the laser peak intensity, we will observe knee structure<sup>8)</sup> shown in Figure 1-3. This knee structure is described by two kinds of double-ionization mechanisms of sequential double ionization (SDI) and non-sequential ionization (NSDI).



**Figure 1-3 Sketch of relationship between laser intensity and ion field. Red solid line shows the ionization probability of doubly charged ion against the peak intensity variation.**

If the laser field is strong enough to detach two electrons from nuclear, electrons can be ionized independently without interaction between electrons. Then electrons are ejected sequentially from the atom or molecule and this ionization mechanism is called SDI. However, in a weaker laser field where the laser strength is not enough for SDI, there is another contribution of double ionization. This ionization mechanism is NSDI and it can be described by recollision of electron. Figure 1-4 shows the pictorial explanation about mechanism of recollision of electron. In the strong laser field, the laser field can be regarded as electric field and this electric field distorts the potential

of nuclear. At that time, one electron will tunnel the potential and the other electron will remain at the bound state in the core if the laser pulse is not strong for SDI. And first the electron which tunneled the potential will go away from the core. But in laser pulse, the electric field will alternate along the frequency of the pulse and the shape of potential will be reversed after some time pass. Then this electron is forced to be back to the core and it will collide with the core and the other electron. Then two electrons can be ejected together and this ionization mechanism with interaction between two electrons is called NSDI. NSDI will have the major contribution for the double ionization when the laser pulse is not strong enough for SDI.

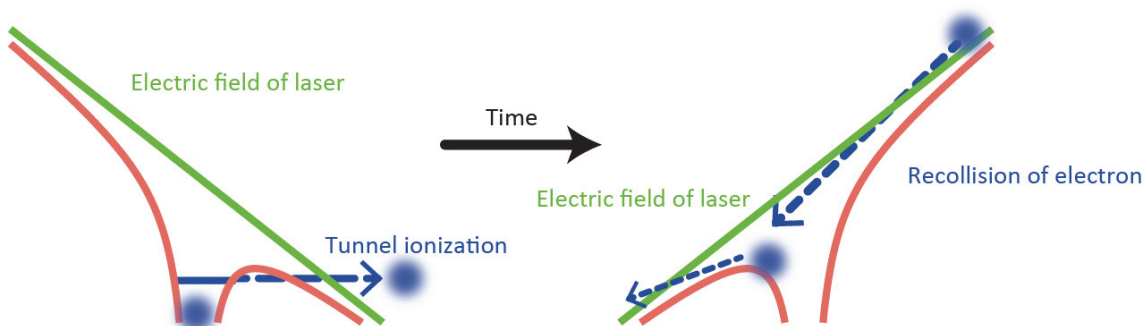


**Figure 1-4 Sketch of non-sequential ionization**

This NSDI mechanism suggests that we should treat the dynamics of electrons fully through the laser pulse duration and in the region of space which is distant from the atomic or molecular core to simulate quantum mechanically. It contributes to further heavier calculation cost than that of calculation for static state of ground-state.

Furthermore, those dynamics will depend on laser pulse condition. In strong laser field, carrier-envelope phase (CEP) at few-cycle pulse plays an important role for the ionization mechanism. Figure 1-5 shows the laser pulses which have different CEP against the same duration, cycle, intensity and frequency. In the previous experiment<sup>5)</sup>, the molecular dynamics of  $C_2D_2$  was reported. The location of ionization and direction of dissociation of  $D^+$  from molecular core will depend on the CEP difference and

eventually the direction of bond-breaking will change by CEP difference. This result suggests that the CEP will affect the chemical reaction and such a parameter in laser pulses has important role in dynamics. Not only the CEP, but also other parameters such as peak intensity, cycle, and wavelength contribute to dynamics in strong laser fields. From the aspect of quantum calculation, we need to calculate trajectories independently against the different laser conditions. In such a situation, the calculation cost is more and more important issue to investigate molecular dynamics in intense laser field.

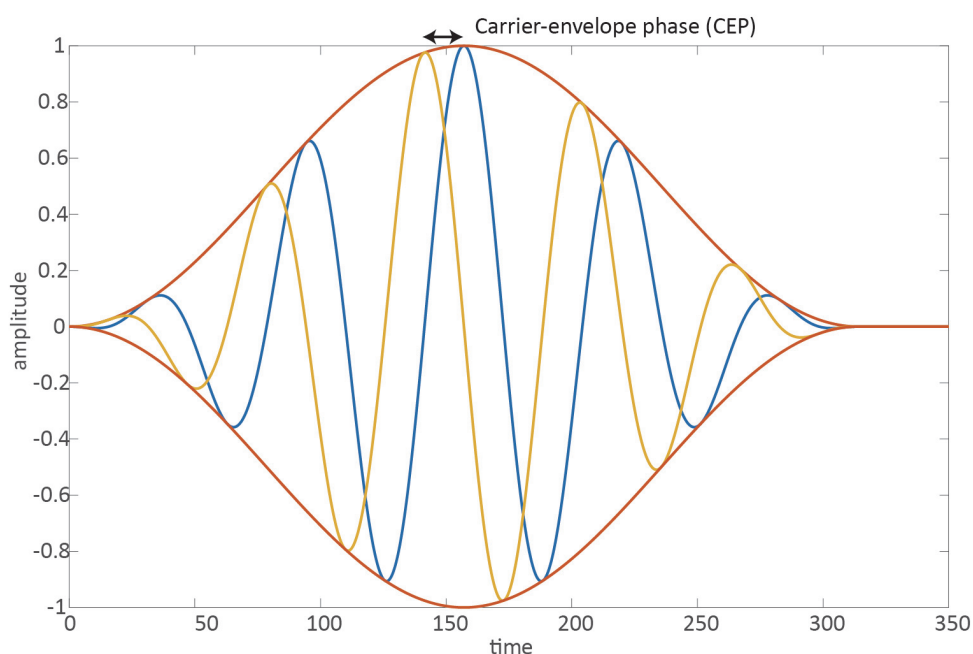


**Figure 1-5 Laser pulses which have different carrier envelope phase. Red lines represent envelope of laser pulses. Yellow and blue lines represent carrier of laser pulses.**

In intense laser field, the nuclei are not necessarily at standstill while laser pulse applied. In previous reports<sup>9), 10)</sup>, the ultrafast proton migration in methanol was observed as shown Figure 1-6. In the Born-Oppenheimer picture, it was considered that nuclei are much heavier than electrons and they can be treated as fixed Coulomb

points. But these experimental results show that protons are not fixed in the molecule in the reaction with laser pulses. This fact suggests that protons should not be treated as fixed Coulomb points in the theory to investigate molecular dynamics and construction of quantum mechanical theory for nuclei and electrons may give us new interesting results and point of view.

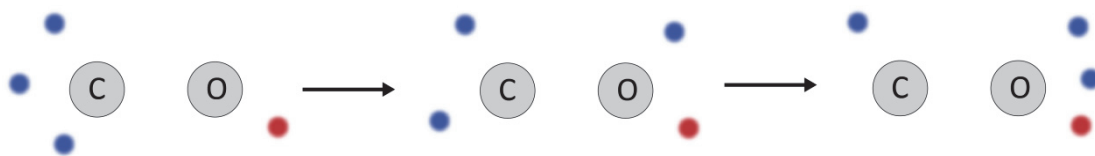


**Figure 1-6 Proton migration in  $\text{CH}_3\text{OH}^{2+}$ . Blue and red circles represent H atom.**

At above description about molecular dynamics in intense laser field, I described necessity to follow the electronic dynamics through the laser pulse and calculate trajectory on each laser condition. At that time, the calculation cost and time are the critical issue. Furthermore, we need to develop the theory to treat not only electrons but also protons quantum mechanically. From next section, I will explain about previous approaches for molecular dynamics calculation.

### 1.3. Classical approach

The one of approaches is a way to describe the ionization mechanism with classical dynamics. It is difficult to construct stable chemical bonds with pure classical dynamics. Then soft-core interaction potential<sup>11), 12)</sup> is used instead of Coulomb potential. Soft-core interaction potential is represented as

$$V(x) = \frac{1}{\sqrt{x^2 + a^2}} . \quad (1-1)$$

Here  $x$  is the coordinate and  $a$  the parameter. When charge points are far away enough this potential behaves as usual Coulomb potential and when they are close the potential is suppressed to finite. Hence the calculation of motion will be stabilized avoiding singularity. For example, in the simulation of ionization of  $\text{H}_2$  molecule in a

strong laser field with this method, the motions of 4 particles are chaotic and nonlinear, and the bond is unstable totally though there are periodic trajectories<sup>12)</sup>. Furthermore, there is a way to modify the classical approach with some additional terms of quantum effect to satisfy Heisenberg principle<sup>6), 7), 13-21)</sup>. In this method, the additional potential which satisfy the uncertainty principle

$$|p| \times |r| \geq \xi \hbar . \quad (1-2)$$

Here  $\xi$  is a parameter for the calculation. Through calculations with classical equations of motion, we can simulate many phenomena such as collisions of particles, ionizations and can obtain statics for the information of kinetic energy release (KER) and anisotropy of ionization and so on. On the other hand, we need parameters which are not *ab initio* and we should construct additional potential for each number of particles of the problem.

#### 1.4. Grid method

One conventional way of quantum mechanical calculation is grid approach. In ordinary grid approach, the grid space is used to represent the wave function. Figure 1-7 shows the pictorial example of grid representation. The strong point of grid method is flexibility to express the wave function. Any shape of function can be projected numerically into the grid space. But there are several weak points. In the grid method, the calculation cost is extremely heavy. Even if we assume the calculation for static state, we need huge memory to store the grid points. For example, in the case of H<sub>2</sub> molecule as 2 electron problem on cylindrical coordinate, the memory size required is

$$\psi(\rho_1, \rho_2, z_1, z_2, \phi): (50,50,200,200,20) \equiv 16 \text{ Gbytes} , \quad (1-3)$$

only for two electrons. If we want to treat electron-nuclear wave function for H<sub>2</sub> molecule, several billion times of this memory size will be required. In the present resource, it is actually difficult to use peta or exa bytes of memory. Not only the memory size, but also calculation time will be incredibly long.

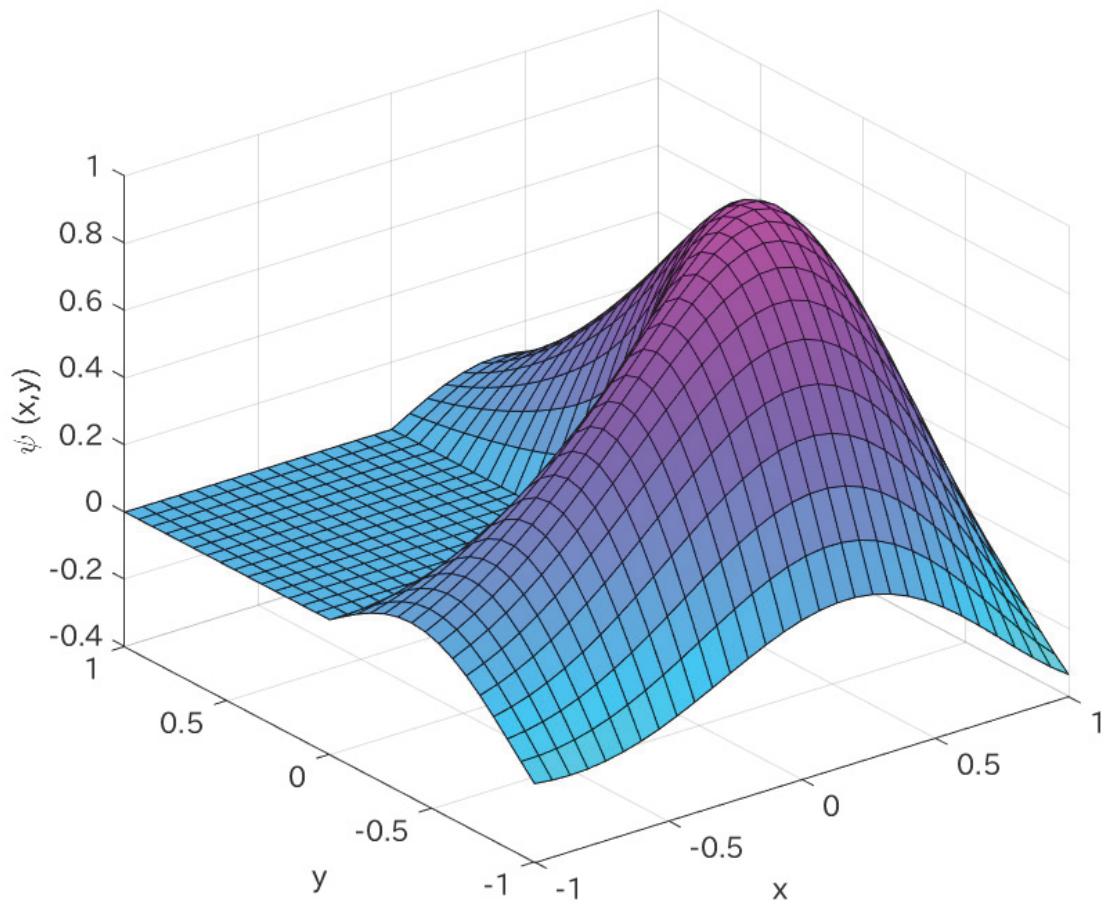


**Figure 1-7 Example of grid representation of wave function. Wave function  $\psi$  is defined discretely on  $x$  and  $y$ .**

Furthermore, it is necessary to prepare larger grid domain to simulate dynamics in strong laser fields compared to static state calculation because the recollision mechanism of electrons should be treated appropriately. As described in Figure 1-4, even once electron gets distant from the core, there is a possibility that the electron comes back and plays important role. Hence we should prepare larger grid domain to follow the motion of electron which is not near the core.

There are previous works for dynamics of  $H_2$  molecule in strong laser fields with grid methods. One is Belfast method<sup>22)</sup>. In this method, a mixed basis set was used for the wave function and finite-difference method was used for the time propagation. In this method, some dimensions are expressed with basis function and the application of

grid is restricted to some dimensions. In another previous report<sup>23)</sup>, the center-of-mass motion of the electrons was approximately reduced. Naturally, the motions of nuclei are fixed in the both simulations.

### 1.5. Coupled coherent state (CCS) method

Coupled coherent state (CCS) method is a way to deal with a time-variation wave function effectively with floating Gaussian bases<sup>24-34)</sup>. Coherent state is a state which returns complex number against operation of annihilation operator  $\hat{a}$  and creation operator  $\hat{a}^\dagger$  such as

$$\hat{a}|z\rangle = z|z\rangle, \quad (1-4)$$

$$\langle z|\hat{a}^\dagger = \langle z|z^*. \quad (1-5)$$

And for example, a Gaussian like

$$\langle x|z\rangle = \left(\frac{\gamma}{\pi}\right)^{\frac{1}{4}} \exp\left(-\frac{\gamma}{2}(x - q(t))^2 + \frac{i}{\hbar}p(t)(x - q(t)) + \frac{ip(t)q(t)}{2\hbar}\right) \quad (1-6)$$

is one of coherent states. Figure 1-8 shows the image of this function.

A wide spatial range of grid is required to follow the motion of electron at ionization, but in CCS method the motion of electrons can be expressed by variations of center positions and phases of floating Gaussian bases and it is not necessary to increase the number of basis against the spatial range of electronic motion at ionization. In CCS method, for calculation of wave function, the time complexity is  $O(M^4)$ , where  $M$  is total number of CCS bases. 4<sup>th</sup> order comes from the heaviest calculation part of 2 particle Coulomb integral. On the other hand, in grid method, the time complexity is  $O\left(\left(\frac{L}{\Delta l}\right)^{3N}\right)$  in 3-dimensional space, where  $L$  is range of grid per 1D,  $\Delta l$  is step width of each grid, and  $N$  is total number of particles. In grid method, necessity of large grid domain means increase of  $L$ . However, in CCS method, the floating Gaussian can follow the motion of electron which is distant from the core, then  $M$  is independent from the motion of electrons.

Furthermore, the calculation cost of grid method will exponentially increase against the number of particles. On the other hand, it is also necessary to increase the

number of bases in CCS method, but the order of dependence is polynomial. Hence it is practically impossible to use grid method but it is possible to apply CCS method for larger system for simulation.

In the previous study of CCS, electron dynamics in strong laser fields was investigated with CCS method in the system of He atom<sup>28)</sup> with the nucleus fixed. As seen in proton migration, nuclei move very fast in the intense laser field. As well as the deal with the electron dynamics, theoretical formulation of quantal dynamics of nuclei is a point of the present research. The dynamics of H<sub>2</sub> molecule in the strong laser field will be investigated in this paper as an example in the treatment of the electron-nuclear wave function.

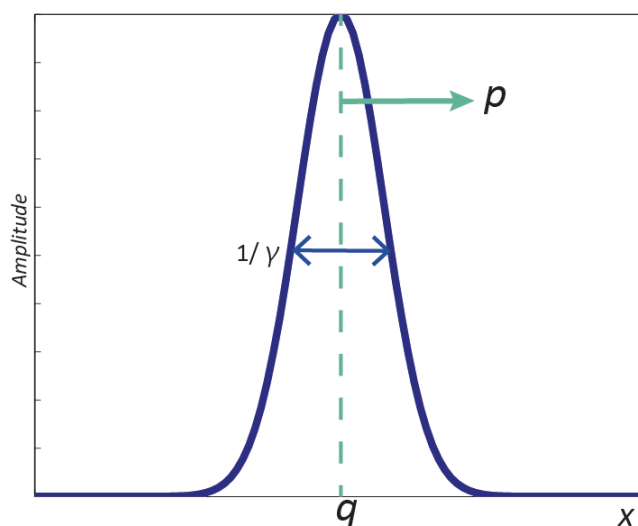


**Figure 1-8 One-dimensional coherent state with center position  $q$  and momentum  $p$ .**

There are previous works of the electron-nuclear wave function of H<sub>2</sub> molecule<sup>35-40)</sup> as nuclear orbital-molecular orbital (NOMO) method, but those are for time-independent static states. Previous works for CCS method to treat the dynamics of nuclei are also still limited in the framework of Ehrenfest approximation.

In this thesis, formulation of time-dependent quantum mechanics by the electron-nuclear wave function with CCS bases will be indicated. And the application for H<sub>2</sub> molecule and its results will be shown and discussed.

## References

1. K. Yamanouchi, "The Next Frontier" *Science* **295**, 1659-1660 (2002).
2. F. Krausz and M. Ivanov, "Attosecond physics" *Rev. Mod. Phys.* **81**, 163-234 (2009).
3. A. Hishikawa, H. Hasegawa and K. Yamanouchi, "Hydrogen migration in acetonitrile in intense laser fields in competition with two-body Coulomb explosion" *J. Electron Spectrosc.* **141**, 195-200 (2004).
4. H. Xu, T. Okino and K. Yamanouchi, "Tracing ultrafast hydrogen migration in allene in intense laser fields by triple-ion coincidence momentum imaging" *J. Chem. Phys.* **131**, 151102 (2009).
5. S. Miura, T. Ando, K. Ootaka, A. Iwasaki, H. Xu, T. Okino, K. Yamanouchi, D. Hoff, T. Rathje, G. G. Paulus, M. Kitzler, A. Baltuška, G. Sansone and M. Nisoli, "Carrier-envelope-phase dependence of asymmetric CD bond breaking in C<sub>2</sub>D<sub>2</sub> in an intense few-cycle laser field" *Chem. Phys. Lett.* **595–596**, 61-66 (2014).
6. E. Lötstedt, T. Kato and K. Yamanouchi, "D<sub>3</sub><sup>+</sup> and H<sub>3</sub><sup>+</sup> in intense laser fields studied with a quasiclassical model" *Phys. Rev. A* **85**, 053410 (2012).
7. E. Lötstedt, T. Kato and K. Yamanouchi, "Classical Dynamics of Laser-Driven D<sub>3</sub><sup>+</sup>" *Phys. Rev. Lett.* **106**, 203001 (2011).
8. B. Walker, B. Sheehy, L. F. DiMauro, P. Agostini, K. J. Schafer and K. C. Kulander, "Precision Measurement of Strong Field Double Ionization of Helium" *Phys. Rev. Lett.* **73**, 1227-1230 (1994).
9. Y. Furukawa, K. Hoshina, K. Yamanouchi and H. Nakano, "Ejection of triatomic hydrogen molecular ion from methanol in intense laser fields" *Chem. Phys. Lett.* **414**, 117-121 (2005).
10. T. Okino, Y. Furukawa, P. Liu, T. Ichikawa, R. Itakura, K. Hoshina, K. Yamanouchi and H. Nakano, "Coincidence momentum imaging of ejection of hydrogen molecular ions from methanol in intense laser fields" *Chem. Phys. Lett.* **419**, 223-227 (2006).
11. P. J. Ho, R. Panfili, S. Haan and J. Eberly, "Nonsequential double ionization as a completely classical photoelectric effect" *Phys. Rev. Lett.* **94**, 93002 (2005).

12. F. Mauger, C. Chandre and T. Uzer, "Strong field double ionization of H<sub>2</sub>: Insights from nonlinear dynamics" *Chem. Phys.* **366**, 64-70 (2009).
13. C. Kirschbaum and L. Wilets, "Classical many-body model for atomic collisions incorporating the Heisenberg and Pauli principles" *Phys. Rev. A* **21**, 834 (1980).
14. D. Wasson and S. Koonin, "Molecular-dynamics simulations of atomic ionization by strong laser fields" *Phys. Rev. A* **39**, 5676 (1989).
15. P. B. Lerner, K. J. LaGattuta and J. S. Cohen, "Ionization of helium by a short pulse of radiation: a fermi molecular-dynamics calculation" *Phys. Rev. A* **49**, 12-15 (1994).
16. J. S. Cohen, "Molecular effects on antiproton capture by H<sub>2</sub> and the states of  $\bar{p}p$  formed" *Phys. Rev. A* **56**, 3583 (1997).
17. J. S. Cohen, "Isotope effects on antiproton and muon capture by hydrogen and deuterium atoms and molecules" *Phys. Rev. A* **59**, 1160 (1999).
18. J. S. Cohen, "Enhancement of intense field ionization of Rydberg atoms by nonhydrogenic cores and quantum-mechanical tunnelling" *J. Phys. B: At. Mol. Opt. Phys.* **37**, 525 (2003).
19. J. S. Cohen, "Reactive collisions of atomic antihydrogen with the H<sub>2</sub> and H<sub>2</sub> molecules" *J. Phys. B: At. Mol. Opt. Phys.* **39**, 3561 (2006).
20. L. Wilets and J. S. Cohen, "Fermion molecular dynamics in atomic, molecular, and optical physics" *Contemp. Phys.* **39**, 163-175 (1998).
21. K. LaGattuta, "Behavior of H<sub>2</sub><sup>+</sup> and H<sub>2</sub> in strong laser fields simulated by fermion molecular dynamics" *Phys. Rev. A* **73**, 043404 (2006).
22. K. T. Taylor, J. S. Parker, D. Dundas, K. J. Meharg, B. J. S. Doherty, D. S. Murphy and J. F. McCann, "Multiphoton double ionization of atoms and molecules by FEL XUV light" *J. Electron Spectrosc.* **144-147**, 1191-1196 (2005).
23. S. Baier, C. Ruiz, L. Plaja and A. Becker, "Nonsequential double ionization of the hydrogen molecule in a few-cycle laser pulse" *Phys. Rev. A* **74**, 033405 (2006).
24. D. Shalashilin and M. Child, "Time dependent quantum propagation in phase space" *J. Chem. Phys.* **113**, 10028-10036 (2000).

25. D. V. Shalashilin and M. S. Child, "The phase space CCS approach to quantum and semiclassical molecular dynamics for high-dimensional systems" *Chem. Phys.* **304**, 103-120 (2004).
26. D. Shalashilin and M. Child, "Electronic energy levels with the help of trajectory-guided random grid of coupled wave packets. I. Six-dimensional simulation of H<sub>2</sub>" *J. Chem. Phys.* **122**, 224108 (2005).
27. D. Shalashilin and M. Child, "A version of diffusion Monte Carlo method based on random grids of coherent states. II. Six-dimensional simulation of electronic states of H<sub>2</sub>" *J. Chem. Phys.* **122**, 244109 (2005).
28. D. V. Shalashilin, M. S. Child and A. Kirrander, "Mechanisms of double ionization in strong laser field from simulation with Coupled Coherent States: Beyond reduced dimensionality models" *Chem. Phys.* **347**, 257-262 (2008).
29. D. V. Shalashilin and I. Burghardt, "Gaussian-based techniques for quantum propagation from the time-dependent variational principle: Formulation in terms of trajectories of coupled classical and quantum variables" *J. Chem. Phys.* **129**, 084104 (2008).
30. D. V. Shalashilin, "Quantum mechanics with the basis set guided by Ehrenfest trajectories: Theory and application to spin-boson model" *J. Chem. Phys.* **130**, 244101 (2009).
31. A. Kirrander and D. V. Shalashilin, "Quantum dynamics with fermion coupled coherent states: Theory and application to electron dynamics in laser fields" *Phys. Rev. A* **84**, 033406 (2011).
32. S. K. Reed, M. L. González-Martínez, J. Rubayo-Soneira and D. V. Shalashilin, "Cartesian coupled coherent states simulations: Ne<sub>n</sub>Br<sub>2</sub> dissociation as a test case" *J. Chem. Phys.* **134**, 054110-054110-12 (2011).
33. D. V. Shalashilin, "Multiconfigurational Ehrenfest approach to quantum coherent dynamics in large molecular systems" *Faraday Discuss.* **153**, 105-116 (2011).
34. K. Saita and D. V. Shalashilin, "On-the-fly ab initio molecular dynamics with multiconfigurational Ehrenfest method" *J. Chem. Phys.* **137**, 22A506-22A506-8 (2012).

35. H. Nakai, "Simultaneous determination of nuclear and electronic wave functions without Born–Oppenheimer approximation: Ab initio NO MO/HF theory" *Int. J. Quantum Chem.* **86**, 511-517 (2001).
36. H. Nakai, M. Hoshino, K. Miyamoto and S. Hyodo, "Elimination of translational and rotational motions in nuclear orbital plus molecular orbital theory" *J. Chem. Phys.* **122**, 164101 (2005).
37. H. Nakai, "Nuclear orbital plus molecular orbital theory: Simultaneous determination of nuclear and electronic wave functions without Born–Oppenheimer approximation" *Int. J. Quantum Chem.* **107**, 2849-2869 (2007).
38. M. Hoshino, H. Nishizawa and H. Nakai, "Rigorous non-Born-Oppenheimer theory: Combination of explicitly correlated Gaussian method and nuclear orbital plus molecular orbital theory" *J. Chem. Phys.* **135**, 024111 (2011).
39. H. Nishizawa, M. Hoshino, Y. Imamura and H. Nakai, "Evaluation of electron repulsion integral of the explicitly correlated Gaussian-nuclear orbital plus molecular orbital theory" *Chem. Phys. Lett.* **521**, 142-149 (2012).
40. H. Nishizawa, Y. Imamura, Y. Iwabata and H. Nakai, "Development of the explicitly correlated Gaussian-nuclear orbital plus molecular orbital theory: Incorporation of electron-electron correlation" *Chem. Phys. Lett.* **533** (2012).

## 2. Quantum dynamics with floating Gaussians and general formulations

### 2.1. General equations of motion (EOMs)

The EOMs are derived from the variational principle. In the non-relativistic quantum mechanics, the Lagrangian  $L$  is determined as

$$L = \left\langle \Psi \left| i\hbar \frac{\partial}{\partial t} - \hat{H} \right| \Psi \right\rangle , \quad (2-1)$$

where  $\hat{H}$  is the total Hamiltonian of the system,  $\Psi$  is the wave function of the system, and  $t$  is the time. The action  $S$  of the system is expressed as follows,

$$S = \int_{t_1}^{t_2} L dt , \quad (2-2)$$

and the EOMs are obtained from the condition of the principle of least action,

$$\delta S = 0 . \quad (2-3)$$

$\delta S$  is derived from Equation (2-2) as

$$\delta S = \int_{t_1}^{t_2} dt \left( \left\langle \Psi + \delta\Psi \left| i\hbar \frac{\partial}{\partial t} - \hat{H} \right| \Psi + \delta\Psi \right\rangle - \left\langle \Psi \left| i\hbar \frac{\partial}{\partial t} - \hat{H} \right| \Psi \right\rangle \right) \quad (2-4)$$

$$= \int_{t_1}^{t_2} dt \left( \left\langle \delta\Psi \left| i\hbar \frac{\partial}{\partial t} - \hat{H} \right| \Psi \right\rangle + \left\langle \Psi \left| i\hbar \frac{\partial}{\partial t} - \hat{H} \right| \delta\Psi \right\rangle \right) . \quad (2-5)$$

From integration by parts for  $t$ ,

$$\int_{t_1}^{t_2} dt \left\langle \Psi \left| i\hbar \frac{\partial}{\partial t} \right| \delta\Psi \right\rangle = \iiint dq \int_{t_1}^{t_2} dt \Psi^* i\hbar \frac{\partial}{\partial t} \delta\Psi \quad (2-6)$$

$$= \iiint dq \left( i\hbar [\Psi^* \delta\Psi]_{t_1}^{t_2} - \int_{t_1}^{t_2} dt \delta\Psi i\hbar \frac{\partial}{\partial t} \Psi^* \right) . \quad (2-7)$$

$\delta\Psi(t_1) = \delta\Psi(t_2) = 0$  as the boundary condition, then Equation (2-7) is formulated as

$$\begin{aligned} \int_{t_1}^{t_2} dt \left\langle \Psi \left| i\hbar \frac{\partial}{\partial t} \right| \delta\Psi \right\rangle &= - \iiint dq \int_{t_1}^{t_2} dt \delta\Psi i\hbar \frac{\partial}{\partial t} \Psi^* \\ &= \int_{t_1}^{t_2} dt \left\langle \Psi \left| -i\hbar \frac{\tilde{\partial}}{\partial t} \right| \delta\Psi \right\rangle , \end{aligned} \quad (2-8)$$

where  $\tilde{\partial}/\partial t$  denotes differentiation of the bra vector with respect to time. Therefore Equation (2-5) is derived from Equation (2-8) as

$$\delta S = \int dt \left\langle \delta\Psi \left| i\hbar \frac{\partial}{\partial t} - \hat{H} \right| \Psi \right\rangle + \left\langle \Psi \left| -i\hbar \frac{\tilde{\partial}}{\partial t} - \hat{H} \right| \delta\Psi \right\rangle = 0 , \quad (2-9)$$

where  $\tilde{\partial}/\partial t$  denotes differentiation of the ket vector with respect to time. Hence,

$$\begin{aligned} \langle \delta\Psi | \hat{H} | \Psi \rangle + \langle \Psi | \hat{H} | \delta\Psi \rangle &= \delta \langle \Psi | \hat{H} | \Psi \rangle \\ &= i\hbar (\langle \delta\Psi | \dot{\Psi} \rangle - \langle \dot{\Psi} | \delta\Psi \rangle) \end{aligned} \quad (2-10)$$

is satisfied. Equation (2-10) is rewritten as

$$\frac{\partial H}{\partial \xi_i} = i\hbar \left( \left\langle \frac{\partial \Psi}{\partial \xi_i^*} \middle| \dot{\Psi} \right\rangle - \left\langle \dot{\Psi} \middle| \frac{\partial \Psi}{\partial \xi_i} \right\rangle \right) = \sum_j c_{ij} \dot{\xi}_j , \quad (2-11)$$

where  $\{\xi_j\}$  are the parameters describing the dynamics of the Gaussian wave packets such as their positions and orbital momenta,  $H = \langle \Psi | \hat{H} | \Psi \rangle$ ,

$$c_{ij} = \frac{\partial Z_j}{\partial \xi_i} - \frac{\partial Z_i}{\partial \xi_j} , \quad (2-12)$$

and furthermore,

$$Z_j = \frac{i\hbar}{2} \left( \left\langle \Psi \middle| \frac{\partial \Psi}{\partial \xi_j} \right\rangle - \left\langle \frac{\partial \Psi}{\partial \xi_j^*} \middle| \Psi \right\rangle \right) . \quad (2-13)$$

As a notation,

$$\left\langle \frac{\partial \Psi}{\partial \xi_j^*} \middle| \Psi \right\rangle = \iiint dq \frac{\partial \Psi^*}{\partial \xi_j} \Psi , \quad (2-14)$$

and Equation (2-11) is not necessarily the same as the equation in the references<sup>1-3)</sup> on the complex conjugate of  $\xi_i$  in the bra. This is because we are assuming that the time-dependent variables are complex numbers. Here,

$$\frac{\partial Z_j}{\partial \xi_i} = \frac{i\hbar}{2} \left( \left\langle \frac{\partial \Psi}{\partial \xi_i^*} \middle| \frac{\partial \Psi}{\partial \xi_j} \right\rangle + \left\langle \Psi \middle| \frac{\partial}{\partial \xi_i} \frac{\partial \Psi}{\partial \xi_j} \right\rangle - \left\langle \frac{\partial \Psi}{\partial \xi_j^*} \middle| \frac{\partial \Psi}{\partial \xi_i} \right\rangle - \left\langle \frac{\partial}{\partial \xi_i^*} \frac{\partial \Psi}{\partial \xi_j^*} \middle| \Psi \right\rangle \right) , \quad (2-15)$$

$$\frac{\partial Z_i}{\partial \xi_j} = \frac{i\hbar}{2} \left( \left\langle \frac{\partial \Psi}{\partial \xi_j^*} \middle| \frac{\partial \Psi}{\partial \xi_i} \right\rangle + \left\langle \Psi \middle| \frac{\partial}{\partial \xi_j} \frac{\partial \Psi}{\partial \xi_i} \right\rangle - \left\langle \frac{\partial \Psi}{\partial \xi_i^*} \middle| \frac{\partial \Psi}{\partial \xi_j} \right\rangle - \left\langle \frac{\partial}{\partial \xi_j^*} \frac{\partial \Psi}{\partial \xi_i^*} \middle| \Psi \right\rangle \right) , \quad (2-16)$$

and  $\Psi$  is at least class  $C^2$ , then

$$\frac{\partial}{\partial \xi_i} \frac{\partial \Psi}{\partial \xi_j} = \frac{\partial}{\partial \xi_j} \frac{\partial \Psi}{\partial \xi_i} , \quad (2-17)$$

therefore the relationship of Equation (2-12) is satisfied.

Hence, the time variation of parameters in the wave function can be obtained solving Equation (2-11) as

$$\dot{\xi}_j = \sum_i (c^{-1})_{ji} \frac{\partial H}{\partial \xi_i} . \quad (2-18)$$

### 2.1.1. In the case of unnormalized wave function

When the wave function is not normalized, if this wave function is put  $\psi$  as

$$|\Psi\rangle = \frac{|\psi\rangle}{\sqrt{\langle\psi|\psi\rangle}}, \quad (2-19)$$

then, Equation (2-13) is written as

$$Z_j = \frac{i\hbar}{2} \left( \frac{1}{\langle\psi|\psi\rangle} \left\langle \psi \left| \frac{\partial\psi}{\partial\xi_j} \right. \right\rangle + \frac{\langle\psi|\psi\rangle}{\sqrt{\langle\psi|\psi\rangle}} \frac{\partial}{\partial\xi_j} \left( \frac{1}{\sqrt{\langle\psi|\psi\rangle}} \right) - \frac{1}{\langle\psi|\psi\rangle} \left\langle \frac{\partial\psi}{\partial\xi_j^*} \left| \psi \right. \right\rangle \right. \\ \left. - \frac{\partial}{\partial\xi_j} \left( \frac{1}{\sqrt{\langle\psi|\psi\rangle}} \right) \frac{\langle\psi|\psi\rangle}{\sqrt{\langle\psi|\psi\rangle}} \right) \quad (2-20)$$

$$= \frac{i\hbar}{2\langle\psi|\psi\rangle} \left( \left\langle \psi \left| \frac{\partial\psi}{\partial\xi_j} \right. \right\rangle - \left\langle \frac{\partial\psi}{\partial\xi_j^*} \left| \psi \right. \right\rangle \right). \quad (2-21)$$

## 2.2. Derivation of Integrals for Gaussians

In this section, integrals for Gaussians are derived. In CCS method, wave function is expanded with linear combination of floating Gaussians and integrals needed in the EOMs can be derived in analytical form. Against the Gaussians

$$\langle x|z^{(k)}\rangle = \left(\frac{\gamma}{\pi}\right)^{\frac{1}{4}} \exp\left(-\frac{\gamma}{2}(x - q^{(k)})^2 + \frac{i}{\hbar}p^{(k)}(x - q^{(k)}) + \frac{ip^{(k)}q^{(k)}}{2\hbar}\right), \quad (2-22)$$

the integrals for  $|z\rangle$  is derived. Here a  $M$ -dimensional Gaussian  $|Z\rangle$  is derived as

$$|Z\rangle = \prod_{k=1}^M |z^{(k)}\rangle, \quad (2-23)$$

as a product of 1-dimensional Gaussians  $|z^{(k)}\rangle$ . In present research, the dynamics on real 3D space will be considered and  $M = 3$ .

### 2.2.1. Overlap integral

First, overlap integral  $\langle z'|z\rangle$  is derived. In the case of 1 dimension,

$$\langle z'|z\rangle = \int_{-\infty}^{\infty} dx \left(\frac{\gamma'}{\pi}\right)^{\frac{1}{4}} \exp\left(-\frac{\gamma'}{2}(x - q')^2 + \frac{i}{\hbar}p'(x - q')\right) \\ + \frac{ip'q'}{2\hbar} \left(\frac{\gamma}{\pi}\right)^{\frac{1}{4}} \exp\left(-\frac{\gamma}{2}(x - q)^2 + \frac{i}{\hbar}p(x - q) + \frac{ipq}{2\hbar}\right). \quad (2-24)$$

Here,

$$\exp\left(-\frac{\gamma'}{2}(x-q')^2 - \frac{i}{\hbar}p'(x-q') - \frac{ip'q'}{2\hbar}\right) \exp\left(-\frac{\gamma}{2}(x-q)^2 + \frac{i}{\hbar}p(x-q) + \frac{ipq}{2\hbar}\right) \quad (2-25)$$

$$= \exp\left(-\frac{\gamma'+\gamma}{2}x^2 + (\gamma q + \gamma'q')x - \left(\frac{\gamma}{2}q^2 + \frac{\gamma'}{2}q'^2\right) + \frac{i}{\hbar}(p-p')x + \frac{ip'q'}{\hbar} - \frac{ipq}{\hbar} - \frac{ip'q'}{2\hbar} + \frac{ipq}{2\hbar}\right) \quad (2-26)$$

$$= \exp\left(-\frac{\gamma'+\gamma}{2}x^2 + \left[(\gamma q + \gamma'q') + \frac{i}{\hbar}(p-p')\right]x - \left(\frac{\gamma}{2}q^2 + \frac{\gamma'}{2}q'^2\right) - \frac{i}{2\hbar}(pq - p'q')\right) \quad (2-27)$$

$$= \exp\left(-\frac{\gamma'+\gamma}{2}\left(x - \frac{1}{\gamma'+\gamma}\left[(\gamma q + \gamma'q') + \frac{i}{\hbar}(p-p')\right]\right)^2 + \frac{1}{2(\gamma'+\gamma)}\left[(\gamma q + \gamma'q') + \frac{i}{\hbar}(p-p')\right]^2 - \frac{1}{2}[\gamma q^2 + \gamma'q'^2] - \frac{i}{2\hbar}(pq - p'q')\right). \quad (2-28)$$

If we use a label of complex number

$$z = \frac{\gamma^{\frac{1}{2}}q + i\hbar^{-1}\gamma^{-\frac{1}{2}}p}{\sqrt{2}}, \quad (2-29)$$

we can derive as

$$q = (2\gamma)^{-\frac{1}{2}}(z + z^*) \quad (2-30)$$

$$p = -i\hbar\left(\frac{\gamma}{2}\right)^{\frac{1}{2}}(z - z^*) \quad (2-31)$$

$$pq = \frac{-i\hbar}{2}(z^2 - z^{*2}) \quad (2-32)$$

$$p'q = \frac{\hbar}{2i}\sqrt{\frac{\gamma'}{\gamma}}(z + z^*)(z' - z'^*) \quad (2-33)$$

$$pq' = \frac{\hbar}{2i} \sqrt{\frac{\gamma}{\gamma'}} (z' + z'^*) (z - z^*) , \quad (2-34)$$

and

$$(\gamma q + \gamma' q') + \frac{i}{\hbar} (p - p')$$

$$= \left(\frac{\gamma}{2}\right)^{\frac{1}{2}} [(z + z^*) + (z - z^*)] + \left(\frac{\gamma'}{2}\right)^{\frac{1}{2}} [(z' + z'^*) - (z' - z'^*)] \quad (2-35)$$

$$= \sqrt{2\gamma} z + \sqrt{2\gamma'} z'^* \quad (2-36)$$

$$\begin{aligned} \therefore \frac{1}{2(\gamma' + \gamma)} \left[ (\gamma q + \gamma' q') + \frac{i}{\hbar} (p - p') \right]^2 &= \frac{1}{(\gamma' + \gamma)} (\sqrt{\gamma} z + \sqrt{\gamma'} z'^*)^2 \\ &= \frac{1}{(\gamma' + \gamma)} (\gamma z^2 + \gamma' z'^{*2} + 2\sqrt{\gamma\gamma'} z z'^*) \end{aligned} \quad (2-37)$$

$$\gamma q^2 + \gamma' q'^2 = \frac{1}{2} [(z + z^*)^2 + (z' + z'^*)^2] \quad (2-38)$$

$$\frac{i}{\hbar} (pq - p'q') = \frac{1}{2} [z^2 - z^{*2} - z'^2 + z'^{*2}] \quad (2-39)$$

$$\begin{aligned} \therefore \gamma q^2 + \gamma' q'^2 + \frac{i}{\hbar} (pq - p'q') \\ = \frac{1}{2} [z^2 + z^{*2} + z'^2 + z'^{*2} + 2zz^* + 2z'z'^* + z^2 - z^{*2} - z'^2 + z'^{*2}] \end{aligned} \quad (2-40)$$

$$= \frac{1}{2} [2z^2 + 2z'^{*2} + 2zz^* + 2z'z'^*] \quad (2-41)$$

$$\begin{aligned} \frac{1}{2(\gamma' + \gamma)} \left[ (\gamma q + \gamma' q') + \frac{i}{\hbar} (p - p') \right]^2 - \frac{1}{2} [\gamma q^2 + \gamma' q'^2] - \frac{i}{2\hbar} (pq - p'q') \\ = \frac{1}{(\gamma' + \gamma)} (\gamma z^2 + \gamma' z'^{*2} + 2\sqrt{\gamma\gamma'} z z'^*) - \frac{1}{2} [z^2 + z'^{*2} + zz^* + z'z'^*] \end{aligned} \quad (2-42)$$

$$= \frac{\gamma - \gamma'}{2(\gamma' + \gamma)} (z^2 - z'^{*2}) + \frac{2\sqrt{\gamma\gamma'}}{(\gamma' + \gamma)} z z'^* - \frac{1}{2} [zz^* + z'z'^*] . \quad (2-43)$$

When we consider about generalized form of

$$\begin{aligned} \int_{-\infty}^{\infty} dx (C(x - q)^2 + D(x - q) + E) \exp(-A(x - q)^2 + B) \\ = C \exp(B) \int_{-\infty}^{\infty} dx (x - q)^2 \exp(-A(x - q)^2) \end{aligned} \quad (2-44)$$

$$\begin{aligned}
& + D \exp(B) \int_{-\infty}^{\infty} dx (x - q) \exp(-A(x - q)^2) \\
& + E \exp(B) \int_{-\infty}^{\infty} dx \exp(-A(x - q)^2)
\end{aligned}$$

If we put  $y = \sqrt{A}(x - q)$ , then  $dy = \sqrt{A}dx$  and

$$\int_{-\infty}^{\infty} dx \exp(-A(x - q)^2) = A^{-\frac{1}{2}} \int_{-\infty}^{\infty} \exp(-y^2) dy = \left(\frac{\pi}{A}\right)^{\frac{1}{2}} \quad (2-45)$$

$$\int_{-\infty}^{\infty} (x - q) dx \exp(-A(x - q)^2) = 0 \quad (2-46)$$

$$\begin{aligned}
\therefore \int_{-\infty}^{\infty} dx (C(x - q)^2 + D(x - q) + E) \exp(-A(x - q)^2 + B) \\
= \exp(B) \left[ C \frac{1}{2} A^{-\frac{3}{2}} \sqrt{\pi} + E A^{-\frac{1}{2}} \sqrt{\pi} \right]. \quad (2-47)
\end{aligned}$$

By comparing Equation (2-28) with Equations (2-43) and (2-47),

$$A = \frac{\gamma' + \gamma}{2} \quad (2-48)$$

$$B = \frac{\gamma - \gamma'}{2(\gamma' + \gamma)} (z^2 - z'^{*2}) + \frac{2\sqrt{\gamma\gamma'}}{(\gamma' + \gamma)} zz'^* - \frac{1}{2} [zz^* + z'z'^*]. \quad (2-49)$$

Hence 1 dimensional  $\langle z'|z \rangle$  is

$$\begin{aligned}
\langle z'|z \rangle = \left( \frac{\gamma'}{\pi} \right)^{\frac{1}{4}} \left( \frac{\gamma}{\pi} \right)^{\frac{1}{4}} \left( \frac{\gamma' + \gamma}{2} \right)^{-\frac{1}{2}} \sqrt{\pi} \exp \left( \frac{\gamma - \gamma'}{2(\gamma' + \gamma)} (z^2 - z'^{*2}) + \frac{2\sqrt{\gamma\gamma'}}{(\gamma' + \gamma)} zz'^* \right. \\
\left. - \frac{1}{2} [zz^* + z'z'^*] \right) \quad (2-50)
\end{aligned}$$

$$\begin{aligned}
= \gamma'^{\frac{1}{4}} \gamma^{\frac{1}{4}} \left( \frac{\gamma' + \gamma}{2} \right)^{-\frac{1}{2}} \exp \left( \frac{\gamma - \gamma'}{2(\gamma' + \gamma)} (z^2 - z'^{*2}) + \frac{2\sqrt{\gamma\gamma'}}{(\gamma' + \gamma)} zz'^* \right. \\
\left. - \frac{1}{2} [zz^* + z'z'^*] \right). \quad (2-51)
\end{aligned}$$

For the case of  $M$  dimension, it can be obtained as a product of 1D cases, then 3 dimensional  $\langle z'|z \rangle$  is derived as

$$\langle z'|z\rangle = \gamma'^{\frac{3}{4}}\gamma^{\frac{3}{4}}\left(\frac{\gamma'+\gamma}{2}\right)^{-\frac{3}{2}} \exp\left(\frac{\gamma-\gamma'}{2(\gamma'+\gamma)}(z^2-z'^{*2}) + \frac{2\sqrt{\gamma'}}{(\gamma'+\gamma)}zz'^{*} - \frac{1}{2}[zz^* + z'z'^*]\right). \quad (2-52)$$

### 2.2.2. Kinetic integral

Next, the integral for the operation of Laplacian is derived. In the same way as the overlap integral, if we consider the 1D case,

$$\langle z'|\Delta|z\rangle = \int_{-\infty}^{\infty} dx \left(\frac{\gamma'}{\pi}\right)^{\frac{1}{4}} \exp\left(-\frac{\gamma'}{2}(x-q')^2 + \frac{i}{\hbar}p'(x-q') + \frac{ip'q'}{2\hbar}\right)^* \nabla^2 \left(\frac{\gamma}{\pi}\right)^{\frac{1}{4}} \exp\left(-\frac{\gamma}{2}(x-q)^2 + \frac{i}{\hbar}p(x-q) + \frac{ipq}{2\hbar}\right). \quad (2-53)$$

Here

$$\begin{aligned} & \left(\frac{\gamma'}{\pi}\right)^{\frac{1}{4}} \exp\left(-\frac{\gamma'}{2}(x-q')^2 + \frac{i}{\hbar}p'(x-q') + \frac{ip'q'}{2\hbar}\right)^* \nabla^2 \left(\frac{\gamma}{\pi}\right)^{\frac{1}{4}} \exp\left(-\frac{\gamma}{2}(x-q)^2 + \frac{i}{\hbar}p(x-q) + \frac{ipq}{2\hbar}\right) \\ &= \left(\frac{\gamma'}{\pi}\right)^{\frac{1}{4}} \left(\frac{\gamma}{\pi}\right)^{\frac{1}{4}} \int_{-\infty}^{\infty} dx \exp\left(-\frac{\gamma'}{2}(x-q')^2 + \frac{i}{\hbar}p'(x-q') + \frac{ip'q'}{2\hbar}\right)^* \left\{ \left[ -\gamma(x-q) + \frac{i}{\hbar}p \right]^2 - \gamma \right\} \exp\left(-\frac{\gamma}{2}(x-q)^2 + \frac{i}{\hbar}p(x-q) + \frac{ipq}{2\hbar}\right). \end{aligned} \quad (2-54)$$

If we put

$$\tilde{n} = \frac{1}{\gamma'+\gamma} \left[ (\gamma q + \gamma' q') + \frac{i}{\hbar}(p-p') \right], \quad (2-55)$$

then,

$$= \frac{1}{(\gamma'+\gamma)\sqrt{2}} \left[ \left( \sqrt{\gamma}(z+z^*) + \sqrt{\gamma'}(z'+z'^*) \right) + \left( \sqrt{\gamma}(z-z^*) - \sqrt{\gamma'}(z'-z'^*) \right) \right] \quad (2-56)$$

$$= \frac{\sqrt{2}}{(\gamma' + \gamma)} (z\sqrt{\gamma} + z'^*\sqrt{\gamma'}) \quad (2-57)$$

and Equation (2-54) is

$$\begin{aligned} & \left\{ \gamma^2(x - q)^2 - \frac{2i}{\hbar} p\gamma(x - q) - \frac{p^2}{\hbar^2} - \gamma \right\} \\ & = \gamma^2(x - \tilde{n})^2 - 2\gamma^2 \left[ (q - \tilde{n}) + \frac{i}{\gamma\hbar} p \right] (x - \tilde{n}) + \left\{ \gamma(q - \tilde{n}) + \frac{i}{\hbar} p \right\}^2 - \gamma, \end{aligned} \quad (2-58)$$

then, each coefficient in Equation (2-47) is

$$A = \frac{\gamma' + \gamma}{2}, \quad (2-59)$$

$$B = \frac{\gamma - \gamma'}{2(\gamma' + \gamma)} (z^2 - z'^{*2}) + \frac{2\sqrt{\gamma\gamma'}}{(\gamma' + \gamma)} zz'^* - \frac{1}{2} [zz^* + z'z'^*], \quad (2-60)$$

$$C = \gamma^2, \quad (2-61)$$

$$E = \left\{ \gamma(q - \tilde{n}) + \frac{i}{\hbar} p \right\}^2 - \gamma \quad (2-62)$$

$$= \left\{ \gamma \left( (2\gamma)^{-\frac{1}{2}} (z + z^*) - \frac{\sqrt{2}}{(\gamma' + \gamma)} (z\sqrt{\gamma} + z'^*\sqrt{\gamma'}) \right) + \left( \frac{\gamma}{2} \right)^{\frac{1}{2}} (z - z^*) \right\}^2 - \gamma \quad (2-63)$$

$$= \frac{\gamma}{2} \left\{ 2z - \frac{2\sqrt{\gamma} (z\sqrt{\gamma} + z'^*\sqrt{\gamma'})}{(\gamma' + \gamma)} \right\}^2 - \gamma = \frac{\gamma}{2} \left\{ \frac{2\gamma'}{(\gamma' + \gamma)} z - \frac{2\sqrt{\gamma\gamma'}}{(\gamma' + \gamma)} z'^* \right\}^2 - \gamma, \quad (2-64)$$

therefore,

$$\langle z' | \Delta | z \rangle = \gamma \langle z' | z \rangle \left[ \frac{1}{2} \left\{ \frac{2\gamma'}{(\gamma' + \gamma)} z - \frac{2\sqrt{\gamma\gamma'}}{(\gamma' + \gamma)} z'^* \right\}^2 - \frac{\gamma'}{(\gamma' + \gamma)} \right]. \quad (2-65)$$

In the case of 3D, in the same way as the overlap integral,

$$\langle z' | \Delta | z \rangle = \gamma \langle z' | z \rangle \left[ \frac{1}{2} \left\{ \frac{2\gamma'}{(\gamma' + \gamma)} z - \frac{2\sqrt{\gamma\gamma'}}{(\gamma' + \gamma)} z'^* \right\}^2 - \frac{3\gamma'}{(\gamma' + \gamma)} \right]. \quad (2-66)$$

### 2.2.3. Coulomb integral

In this section, a Coulomb integral between 2 particles as Equation (2-67) is derived.

$$\langle z_2' | \langle z_1' | \frac{1}{|r_1 - r_2|} | z_1 \rangle | z_2 \rangle \quad (2-67)$$

This formula of Gaussian integral can be integrated with Fourier transformation<sup>4)</sup>. In this case, if we put

$$\tilde{n}_i = \frac{\sqrt{2}}{(\gamma_i' + \gamma_i)} \left( z_i'^* \sqrt{\gamma_i'} + z_i \sqrt{\gamma_i} \right), \quad (2-68)$$

$$\tilde{n} = \tilde{n}_1 - \tilde{n}_2, \quad (2-69)$$

$$\rho = \sqrt{\tilde{n} \cdot \tilde{n}} = \sqrt{\tilde{n}^2}. \quad (2-70)$$

Then,

$$\begin{aligned} & \langle z_2' | \langle z_1' | \frac{1}{|r_1 - r_2|} | z_1 \rangle | z_2 \rangle \\ &= \langle z_1' | z_1 \rangle \langle z_2' | z_2 \rangle \frac{1}{\rho} \operatorname{erf} \left( \rho \sqrt{\frac{\left( \frac{\gamma_1'}{2} + \frac{\gamma_1}{2} \right) \left( \frac{\gamma_2'}{2} + \frac{\gamma_2}{2} \right)}{\left( \frac{\gamma_1'}{2} + \frac{\gamma_1}{2} + \frac{\gamma_2'}{2} + \frac{\gamma_2}{2} \right)}} \right). \end{aligned} \quad (2-71)$$

These results were validated by comparison with numerical integrations using expressions of Equations (2-24), (2-53) and (2-67). Calculation of hundreds of thousands of times with Monte Carlo integral resulted in agreement with upper 3 digits of calculation against the analytical forms.

### 2.3. Optimization methods

Through above discussions, we can obtain the quantum dynamics along the EOMs. In this section, we will consider about how to get the ground state and approaches for optimization.

#### 2.3.1. Gradient descent method (GDM)

The usual way for optimization is gradient descent. We can know the analytical form of the integral of Hamiltonian  $\frac{\partial H}{\partial x}$ , then the integral of Hamiltonian can be optimized to a local minimum through the gradient descent.

In usual gradient descent,  $H$  is defined on  $\mathbb{R}^n \rightarrow \mathbb{R}$  and with a small  $\alpha$ ,  $H$  can be optimized through iterations as

$$x_{i+1} = x_i - \alpha \frac{\partial H}{\partial x_i}. \quad (2-72)$$

However, in the present research  $H(x)$  is defined on  $\mathbb{C}^n \rightarrow \mathbb{C}$  and the usual gradient descent cannot be adopted and needs to be improved.

For a small  $d$ ,

$$H(x + d) = H(x) + \frac{\partial H}{\partial x} \cdot d . \quad (2-73)$$

Here if  $d$  is put with  $\beta > 0, \beta \in \mathbb{R}$  as

$$d = -\beta \left( \frac{\partial H}{\partial x} \right)^* , \quad (2-74)$$

then,

$$H(x + d) = H(x) - \beta \frac{\partial H}{\partial x} \cdot \left( \frac{\partial H}{\partial x} \right)^* = H(x) - \beta \left| \frac{\partial H}{\partial x} \right|^2 , \quad (2-75)$$

so if  $x$  is set properly to satisfy  $H(x + d)$  and  $H(x)$  to be real,

$$\beta \left| \frac{\partial H}{\partial x} \right|^2 \in \mathbb{R} \wedge \beta \left| \frac{\partial H}{\partial x} \right|^2 \geq 0 \quad (2-76)$$

$$\therefore H(x + d) \leq H(x) . \quad (2-77)$$

Hence, through iterations of

$$x_{i+1} = x_i - \beta \left( \frac{\partial H}{\partial x_i} \right)^* , \quad (2-78)$$

the optimization of  $H$  can be achieved.

### 2.3.2. Imaginary time propagation (ITP) method

GDM is the simple method for the optimization but the convergence speed is not necessarily fast. In present research, the formulations are for time propagation and we can use the imaginary time propagation method for the optimization. It was suggested that the imaginary time propagation may avoid the problem of a convergence to a local minimum not to a global minimum<sup>5)</sup>.

The imaginary time  $\tau$  is defined as

$$\tau = it . \quad (2-79)$$

When we assume a vibrational component of  $e^{-i\omega t}$  in the wave function, this component is expressed as

$$e^{-i\omega t} = e^{-\omega \tau} \quad (2-80)$$

replacing the real time  $t$  by the imaginary time  $\tau$ . In that case, equation (2-80) will be dumped exponentially as  $e^{-\omega \tau} \rightarrow 0$  in  $\tau \rightarrow \infty$ .

The EOMs for the imaginary time is expressed from equation (2-18) as

$$\frac{d\xi_j}{d\tau} = \frac{d\xi_j}{dit} = -i \sum_i (c^{-1})_{ji} \frac{\partial H}{\partial \xi_i} . \quad (2-81)$$

By imaginary time propagating this EOMs, the wave function can be converged to the ground state.

## References

1. D. Rowe, A. Ryman and G. Rosensteel, "Many-body quantum mechanics as a symplectic dynamical system" *Phys. Rev. A* **22**, 2362 (1980).
2. J. Broeckhove, L. Lathouwers, E. Kesteloot and P. Van Leuven, "On the equivalence of time-dependent variational principles" *Chem. Phys. Lett.* **149**, 547-550 (1988).
3. P. Kramer, "A review of the time-dependent variational principle" *J. Phys.: Conf. Ser.* **99**, 012009 (2008).
4. A. Szabo and N. S. Ostlund, in *Modern quantum chemistry : introduction to advanced electronic structure theory* (Dover Publications, 1996).
5. C. Lin and A. A. Demkov, "Efficient and stable orbital-searching algorithm for the configuration interaction method and its application to quantum impurity problems" *Phys. Rev. B* **90**, 235122 (2014).

### 3. Theory for application to H<sub>2</sub> molecule

In this chapter, we will consider the application of general theory in Chapter 1 to H<sub>2</sub> molecule. We will treat the electron-nuclear wave function and the problem is 4-particle system.

#### 3.1. Total wave function

##### 3.1.1. Expression of wave function with 4 orbital functions

In the present research, nuclei are treated in the same way as electrons, and the wave function of the system is represented as

$$|\Psi\rangle = |A\rangle|B\rangle \quad (3-1)$$

in a product form of  $|A\rangle, |B\rangle$  where  $|A\rangle$  is the Slater determinant of electrons and  $|B\rangle$  is the Slater determinant of nuclei. Here they are treated in singlet configurations and their spatial parts are written by the spatial orbital of each particle as

$$[\text{Spatial part of } |A\rangle] = \frac{|z_1\rangle|z_2\rangle + |z_2\rangle|z_1\rangle}{\sqrt{2(\langle z_1|z_1\rangle\langle z_2|z_2\rangle + \langle z_1|z_2\rangle\langle z_2|z_1\rangle)}} \quad (3-2)$$

$$[\text{Spatial part of } |B\rangle] = \frac{|w_1\rangle|w_2\rangle + |w_2\rangle|w_1\rangle}{\sqrt{2(\langle w_1|w_1\rangle\langle w_2|w_2\rangle + \langle w_1|w_2\rangle\langle w_2|w_1\rangle)}} \quad (3-3)$$

where  $|z_1\rangle, |z_2\rangle$  are spatial orbitals of electron 1, 2, and  $|w_1\rangle, |w_2\rangle$  are spatial orbitals of nuclear 1, 2.

The total Hamiltonian is integrated with this  $\Psi$  as follows.

$$\begin{aligned} & \langle \Psi | \hat{H} | \Psi \rangle \\ &= \frac{1}{4(\langle z_1|z_1\rangle\langle z_2|z_2\rangle + \langle z_1|z_2\rangle\langle z_2|z_1\rangle)(\langle w_1|w_1\rangle\langle w_2|w_2\rangle + \langle w_1|w_2\rangle\langle w_2|w_1\rangle)} \\ & (\langle w_2|\langle w_1|\langle z_2|\langle z_1|\hat{H}|z_1\rangle|z_2\rangle|w_1\rangle|w_2\rangle + \langle w_1|\langle w_2|\langle z_2|\langle z_1|\hat{H}|z_1\rangle|z_2\rangle|w_1\rangle|w_2\rangle \\ & + \langle w_1|\langle w_2|\langle z_1|\langle z_2|\hat{H}|z_1\rangle|z_2\rangle|w_1\rangle|w_2\rangle + \langle w_2|\langle w_1|\langle z_1|\langle z_2|\hat{H}|z_1\rangle|z_2\rangle|w_1\rangle|w_2\rangle \\ & + \langle w_2|\langle w_1|\langle z_2|\langle z_1|\hat{H}|z_1\rangle|z_2\rangle|w_2\rangle|w_1\rangle + \langle w_1|\langle w_2|\langle z_2|\langle z_1|\hat{H}|z_1\rangle|z_2\rangle|w_2\rangle|w_1\rangle \\ & + \langle w_1|\langle w_2|\langle z_1|\langle z_2|\hat{H}|z_1\rangle|z_2\rangle|w_2\rangle|w_1\rangle + \langle w_2|\langle w_1|\langle z_1|\langle z_2|\hat{H}|z_1\rangle|z_2\rangle|w_2\rangle|w_1\rangle \\ & + \langle w_2|\langle w_1|\langle z_2|\langle z_1|\hat{H}|z_2\rangle|z_1\rangle|w_1\rangle|w_2\rangle + \langle w_1|\langle w_2|\langle z_2|\langle z_1|\hat{H}|z_2\rangle|z_1\rangle|w_1\rangle|w_2\rangle \\ & + \langle w_1|\langle w_2|\langle z_1|\langle z_2|\hat{H}|z_2\rangle|z_1\rangle|w_1\rangle|w_2\rangle + \langle w_2|\langle w_1|\langle z_1|\langle z_2|\hat{H}|z_2\rangle|z_1\rangle|w_1\rangle|w_2\rangle \end{aligned} \quad (3-4)$$

$$\begin{aligned}
& + \langle w_2 | \langle w_1 | \langle z_2 | \langle z_1 | \hat{H} | z_2 \rangle | z_1 \rangle | w_2 \rangle | w_1 \rangle + \langle w_1 | \langle w_2 | \langle z_2 | \langle z_1 | \hat{H} | z_2 \rangle | z_1 \rangle | w_2 \rangle | w_1 \rangle \\
& + \langle w_1 | \langle w_2 | \langle z_1 | \langle z_2 | \hat{H} | z_2 \rangle | z_1 \rangle | w_2 \rangle | w_1 \rangle + \langle w_2 | \langle w_1 | \langle z_1 | \langle z_2 | \hat{H} | z_2 \rangle | z_1 \rangle | w_2 \rangle | w_1 \rangle
\end{aligned}$$

$\hat{H}$  is symmetric against the exchange of  $z_1, z_2$ , that is

$$\langle z_2 | \langle z_1 | \hat{H} | z_1 \rangle | z_2 \rangle = \langle z_1 | \langle z_2 | \hat{H} | z_2 \rangle | z_1 \rangle , \quad (3-5)$$

$$\langle z_1 | \langle z_2 | \hat{H} | z_1 \rangle | z_2 \rangle = \langle z_2 | \langle z_1 | \hat{H} | z_2 \rangle | z_1 \rangle , \quad (3-6)$$

using this relationship to Equation (3-4),

$$\begin{aligned}
& \langle \Psi | \hat{H} | \Psi \rangle \\
& = \frac{1}{2(\langle z_1 | z_1 \rangle \langle z_2 | z_2 \rangle + \langle z_1 | z_2 \rangle \langle z_2 | z_1 \rangle)} (\langle w_1 | w_1 \rangle \langle w_2 | w_2 \rangle + \langle w_1 | w_2 \rangle \langle w_2 | w_1 \rangle) \\
& (\langle w_2 | \langle w_1 | \langle z_2 | \langle z_1 | \hat{H} | z_1 \rangle | z_2 \rangle | w_1 \rangle | w_2 \rangle + \langle w_1 | \langle w_2 | \langle z_2 | \langle z_1 | \hat{H} | z_1 \rangle | z_2 \rangle | w_1 \rangle | w_2 \rangle \\
& + \langle w_1 | \langle w_2 | \langle z_1 | \langle z_2 | \hat{H} | z_1 \rangle | z_2 \rangle | w_1 \rangle | w_2 \rangle + \langle w_2 | \langle w_1 | \langle z_1 | \langle z_2 | \hat{H} | z_1 \rangle | z_2 \rangle | w_1 \rangle | w_2 \rangle \\
& + \langle w_2 | \langle w_1 | \langle z_2 | \langle z_1 | \hat{H} | z_1 \rangle | z_2 \rangle | w_2 \rangle | w_1 \rangle + \langle w_1 | \langle w_2 | \langle z_2 | \langle z_1 | \hat{H} | z_1 \rangle | z_2 \rangle | w_2 \rangle | w_1 \rangle \\
& \quad + \langle w_1 | \langle w_2 | \langle z_1 | \langle z_2 | \hat{H} | z_1 \rangle | z_2 \rangle | w_2 \rangle | w_1 \rangle \\
& \quad + \langle w_2 | \langle w_1 | \langle z_1 | \langle z_2 | \hat{H} | z_1 \rangle | z_2 \rangle | w_2 \rangle | w_1 \rangle)
\end{aligned} \quad (3-7)$$

and also  $\hat{H}$  is symmetric against the exchange of  $w_1, w_2$ ,

$$\langle w_2 | \langle w_1 | \hat{H} | w_1 \rangle | w_2 \rangle = \langle w_1 | \langle w_2 | \hat{H} | w_2 \rangle | w_1 \rangle , \quad (3-8)$$

$$\langle w_1 | \langle w_2 | \hat{H} | w_1 \rangle | w_2 \rangle = \langle w_2 | \langle w_1 | \hat{H} | w_2 \rangle | w_1 \rangle , \quad (3-9)$$

then using this relationship to Equation (3-7),

$$\begin{aligned}
& \langle \Psi | \hat{H} | \Psi \rangle \\
& = \frac{1}{(\langle z_1 | z_1 \rangle \langle z_2 | z_2 \rangle + \langle z_1 | z_2 \rangle \langle z_2 | z_1 \rangle)} (\langle w_1 | w_1 \rangle \langle w_2 | w_2 \rangle + \langle w_1 | w_2 \rangle \langle w_2 | w_1 \rangle) \\
& (\langle w_2 | \langle w_1 | \langle z_2 | \langle z_1 | \hat{H} | z_1 \rangle | z_2 \rangle | w_1 \rangle | w_2 \rangle + \langle w_1 | \langle w_2 | \langle z_2 | \langle z_1 | \hat{H} | z_1 \rangle | z_2 \rangle | w_1 \rangle | w_2 \rangle \\
& \quad + \langle w_1 | \langle w_2 | \langle z_1 | \langle z_2 | \hat{H} | z_1 \rangle | z_2 \rangle | w_1 \rangle | w_2 \rangle \\
& \quad + \langle w_2 | \langle w_1 | \langle z_1 | \langle z_2 | \hat{H} | z_1 \rangle | z_2 \rangle | w_1 \rangle | w_2 \rangle)
\end{aligned} \quad (3-10)$$

### 3.1.2. Expression of each orbital with Gaussians

Next, each orbital is expressed by linear combination of total number  $M$  of Gaussian bases  $|G_m\rangle$  as follows,

$$|z_1\rangle = \sum_m \mu_m^{z_1} |G_m\rangle , \quad (3-11)$$

$$|z_2\rangle = \sum_m \mu_m^{z_2} |G_m\rangle, \quad (3-12)$$

$$|w_1\rangle = \sum_m \mu_m^{w_1} |G_m\rangle, \quad (3-13)$$

$$|w_2\rangle = \sum_m \mu_m^{w_2} |G_m\rangle, \quad (3-14)$$

where  $\mu^i$  is the column vector of  $M \times 1$  and this is the orbital coefficient of the each particle  $i$  expressing the weight of Gaussian bases in the orbital.  $|G_m\rangle$  is expressed in the form of CCS as

$$\langle \mathbf{r} | G_m \rangle = \left( \frac{\gamma_m}{\pi} \right)^{\frac{3}{4}} \exp \left( -\frac{\gamma_m}{2} (\mathbf{r} - \mathbf{q}_m(t))^2 + \frac{i}{\hbar} \mathbf{p}_m(t) (\mathbf{r} - \mathbf{q}_m(t)) + \frac{i \mathbf{p}_m(t) \mathbf{q}_m(t)}{2\hbar} \right). \quad (3-15)$$

in the 3-dimensional space.

### 3.1.3. Expression of total Hamiltonian

In the case of H<sub>2</sub> molecule, total Hamiltonian is expressed as

$$\begin{aligned} \hat{H} = & -\frac{1}{2} \left( \Delta_{e_1} + \Delta_{e_2} + \frac{\Delta_{p_1}}{m_p} + \frac{\Delta_{p_2}}{m_p} \right) - \frac{1}{|\mathbf{r}_{e_1} - \mathbf{r}_{p_1}|} - \frac{1}{|\mathbf{r}_{e_2} - \mathbf{r}_{p_1}|} \\ & - \frac{1}{|\mathbf{r}_{e_1} - \mathbf{r}_{p_2}|} \\ & - \frac{1}{|\mathbf{r}_{e_2} - \mathbf{r}_{p_2}|} + \frac{1}{|\mathbf{r}_{e_1} - \mathbf{r}_{e_2}|} + \frac{1}{|\mathbf{r}_{p_1} - \mathbf{r}_{p_2}|} + (\mathbf{r}_{e_1} + \mathbf{r}_{e_2} - \mathbf{r}_{p_1} - \mathbf{r}_{p_2}) \cdot \mathbf{E}(t) \end{aligned} \quad (3-16)$$

in atomic unit.  $e_1$  and  $e_2$  are symbols which represent electrons, and  $p_1$  and  $p_2$  are for nuclei. In the present research, the nuclei are also treated quantum mechanically, so the total Hamiltonian includes all terms for four particles in H<sub>2</sub> molecule. The effect of laser field is involved as a time-dependent electric field  $\mathbf{E}(t)$  in length gauge.

## 3.2. Expression of each integral

The integral of total Hamiltonian  $H$  can be obtained in the analytical form and it is needed to derive analytical forms of integrals in  $H$ .

### 3.2.1. Overlap integral

The overlap integral is written as follows,

$$\langle z_1 | z_1 \rangle = \sum_n \mu_n^{z_1} \left( \sum_m \mu_m^{z_1*} \langle G_m | \right) | G_n \rangle = \sum_{m,n} \mu_m^{z_1*} \mu_n^{z_1} \langle G_m | G_n \rangle \quad (3-17)$$

$$\langle z_2 | z_1 \rangle = \sum_n \mu_n^{z_1} \left( \sum_m \mu_m^{z_2*} \langle G_m | \right) | G_n \rangle = \sum_{m,n} \mu_m^{z_2*} \mu_n^{z_1} \langle G_m | G_n \rangle \quad (3-18)$$

and if we use identifier  $i, j$  for each particle

$$\langle i | j \rangle = \sum_n \mu_n^j \left( \sum_m \mu_m^i \langle G_m | \right) | G_n \rangle = \sum_{m,n} \mu_m^i \mu_n^j \langle G_m | G_n \rangle . \quad (3-19)$$

If the matrix  $S$  of  $M \times M$  is determined as

$$(S)_{mn} = \langle G_m | G_n \rangle \quad (3-20)$$

$$= \gamma_m^{\frac{3}{4}} \gamma_n^{\frac{3}{4}} \left( \frac{\gamma_m + \gamma_n}{2} \right)^{-\frac{3}{2}} \exp \left( \frac{\gamma_n - \gamma_m}{2(\gamma_m + \gamma_n)} (z_n^2 - z_m^{*2}) + \frac{2\sqrt{\gamma_n \gamma_m}}{(\gamma_m + \gamma_n)} z_n z_m^* - \frac{1}{2} [z_n z_n^* + z_m z_m^*] \right) \quad (3-21)$$

Equation (3-18) can be expressed as

$$\langle i | j \rangle = \mu^i S \mu^j . \quad (3-22)$$

### 3.2.2. Kinetic integral

Next, the kinetic integral will be discussed. For example,

$$\langle z_2 | \langle z_1 | \Delta_{x_1} | z_1 \rangle | z_2 \rangle = \langle z_2 | z_2 \rangle \sum_n \mu_n^{z_1} \left( \sum_m \mu_m^{z_1*} \langle G_m | \right) \Delta | G_n \rangle \quad (3-23)$$

$$= \langle z_2 | z_2 \rangle \sum_{m,n} \mu_m^{z_1*} \mu_n^{z_1} \langle G_m | G_n \rangle \gamma_n \left[ \frac{1}{2} \left\{ \frac{2\gamma_m}{(\gamma_m + \gamma_n)} z_n - \frac{2\sqrt{\gamma_n \gamma_m}}{(\gamma_m + \gamma_n)} z_m^* \right\}^2 - \frac{3\gamma_m}{(\gamma_m + \gamma_n)} \right] \quad (3-24)$$

If we put the matrix  $R$  of  $M \times M$  as

$$(R)_{mn} = \gamma_n \left[ \frac{1}{2} \left\{ \frac{2\gamma_m}{(\gamma_m + \gamma_n)} z_n - \frac{2\sqrt{\gamma_n \gamma_m}}{(\gamma_m + \gamma_n)} z_m^* \right\}^2 - \frac{3\gamma_m}{(\gamma_m + \gamma_n)} \right] \quad (3-25)$$

and the matrix  $K$  of  $M \times M$  as

$$K = S \circ R \quad (3-26)$$

where operator  $\circ$  means multiplication of matrices against each element like as

$$(A \circ B)_{mn} = a_{mn} \times b_{mn} , \quad (3-27)$$

which is called Hadamard product. Then, the kinetic integral can be expressed as

$$\langle i|\Delta|j\rangle = \mu^{i*} K \mu^j . \quad (3-28)$$

### 3.2.3. Coulomb integral

Integral for Coulomb interaction is generally expressed as

$$\langle z_2|\langle z_1|\frac{1}{|r_1 - r_2|}|z_1'\rangle|z_2'\rangle . \quad (3-29)$$

By putting as

$$\tilde{n}_{mn} = \frac{\sqrt{2}}{(\gamma_m + \gamma_n)} (g_n \sqrt{\gamma_n} + g_m^* \sqrt{\gamma_m}) , \quad (3-30)$$

$$\tilde{n}_{mnij} = \tilde{n}_{mn} - \tilde{n}_{ij} , \quad (3-31)$$

$$\rho_{mnij} = \sqrt{\tilde{n}_{mnij} \cdot \tilde{n}_{mnij}} = \sqrt{\tilde{n}_{mnij}^2} , \quad (3-32)$$

where the number of bases is  $M$  and  $m, n, i, j \leq M$ . Then

Eq.(3-29)

$$= \sum_{m,n,i,j} \mu_m^{z_1^*} \mu_n^{z_1'} \mu_i^{z_2^*} \mu_j^{z_2'} \langle G_m|G_n\rangle \langle G_i|G_j\rangle \frac{1}{\rho_{mnij}} \operatorname{erf} \left( \rho_{mnij} \sqrt{\frac{(\frac{\gamma_m}{2} + \frac{\gamma_n}{2}) (\frac{\gamma_i}{2} + \frac{\gamma_j}{2})}{(\frac{\gamma_m}{2} + \frac{\gamma_n}{2} + \frac{\gamma_i}{2} + \frac{\gamma_j}{2})}} \right) \quad (3-33)$$

Here  $M \times M \times M \times M$  tensor  $P$  is put as

$$(P)_{mnij} = \frac{1}{\rho_{mnij}} \operatorname{erf} \left( \rho_{mnij} \sqrt{\frac{(\frac{\gamma_m}{2} + \frac{\gamma_n}{2}) (\frac{\gamma_i}{2} + \frac{\gamma_j}{2})}{(\frac{\gamma_m}{2} + \frac{\gamma_n}{2} + \frac{\gamma_i}{2} + \frac{\gamma_j}{2})}} \right) , \quad (3-34)$$

and

$$\mu^{11'} = (\mu^{z_1'} \mu^{z_1^*})^t , \quad (3-35)$$

$$\mu^{22'} = (\mu^{z_2'} \mu^{z_2*})^t , \quad (3-36)$$

and  $M \times M \times M \times M$  tensor  $C$  is put as

$$C = S \circ_{mn} (S \circ_{ij} P_{::ij})_{mn::} \quad (3-37)$$

where  $P_{::ij}$  means  $M \times M$  dimension matrix  $D$  such as

$$(D)_{mn} = (P)_{mnij} , \quad (3-38)$$

and a operator  $\circ_{ij}$  means the execution of  $\circ$  against all  $i,j$ . For example, the procedure of tensor  $E = S \circ_{ij} P_{::ij}$  is expressed with a pseudo code like as,

for i=1 to M

for j=1 to M

$$E(:, :, i, j) = S \circ P(:, :, i, j);$$

end

end

$\circ_{mn}$  is determined in the same way. Then Equation (3-29) is expressed as

$$\langle z_2 | \langle z_1 | \frac{1}{|r_1 - r_2|} | z_1' \rangle | z_2' \rangle = \sum_{m,n,i,j} (\mu^{22'} \circ_{mn} (\mu^{11'} \circ_{ij} C_{::ij})_{mn::})_{mnij} . \quad (3-39)$$

### 3.2.4. Integral for laser field

Integral for electric field is expressed as

$$\langle z_2 | \langle z_1 | r_1 \cdot E | z_1' \rangle | z_2' \rangle = \langle z_2 | z_2' \rangle \sum_{m,n} \mu_m^{z_1*} \mu_n^{z_1'} \langle G_m | G_n \rangle \tilde{n}_{mn} \cdot E . \quad (3-40)$$

Then if we put  $M \times M$  matrix  $\tilde{N}$  as

$$(\tilde{N})_{mn} = \tilde{n}_{mn} \cdot E , \quad (3-41)$$

and

$$L = S \circ N , \quad (3-42)$$

then integral for electric field is expressed with

$$\langle z_1 | r_1 \cdot E | z_1' \rangle = \mu^{z_1*} L \mu^{z_1'} . \quad (3-43)$$

### 3.3. Differential of integral of Hamiltonian with each parameter

To obtain  $\partial H / \partial \xi_i$ , it is needed to derive

$$\frac{\partial H}{\partial \xi_i} = \frac{\partial}{\partial \xi_i} \langle \Psi | \hat{H} | \Psi \rangle . \quad (3-44)$$

From Equation (3-10), Equation (3-44) is formulated as

$$\begin{aligned} & \frac{\partial}{\partial \xi_i} \langle \Psi | \hat{H} | \Psi \rangle \\ &= \left( \frac{\partial}{\partial \xi_i} \frac{1}{(\langle z_1 | z_1 \rangle \langle z_2 | z_2 \rangle + \langle z_1 | z_2 \rangle \langle z_2 | z_1 \rangle) (\langle w_1 | w_1 \rangle \langle w_2 | w_2 \rangle + \langle w_1 | w_2 \rangle \langle w_2 | w_1 \rangle)} \right) \\ & \times (\langle w_2 | \langle w_1 | \langle z_2 | \langle z_1 | \hat{H} | z_1 \rangle | z_2 \rangle | w_1 \rangle | w_2 \rangle + \langle w_1 | \langle w_2 | \langle z_2 | \langle z_1 | \hat{H} | z_1 \rangle | z_2 \rangle | w_1 \rangle | w_2 \rangle \\ & + \langle w_1 | \langle w_2 | \langle z_1 | \langle z_2 | \hat{H} | z_1 \rangle | z_2 \rangle | w_1 \rangle | w_2 \rangle + \langle w_2 | \langle w_1 | \langle z_1 | \langle z_2 | \hat{H} | z_1 \rangle | z_2 \rangle | w_1 \rangle | w_2 \rangle) \\ & + \frac{1}{(\langle z_1 | z_1 \rangle \langle z_2 | z_2 \rangle + \langle z_1 | z_2 \rangle \langle z_2 | z_1 \rangle) (\langle w_1 | w_1 \rangle \langle w_2 | w_2 \rangle + \langle w_1 | w_2 \rangle \langle w_2 | w_1 \rangle)} \\ & \times \frac{\partial}{\partial \xi_i} (\langle w_2 | \langle w_1 | \langle z_2 | \langle z_1 | \hat{H} | z_1 \rangle | z_2 \rangle | w_1 \rangle | w_2 \rangle + \langle w_1 | \langle w_2 | \langle z_2 | \langle z_1 | \hat{H} | z_1 \rangle | z_2 \rangle | w_1 \rangle | w_2 \rangle \\ & + \langle w_1 | \langle w_2 | \langle z_1 | \langle z_2 | \hat{H} | z_1 \rangle | z_2 \rangle | w_1 \rangle | w_2 \rangle + \langle w_2 | \langle w_1 | \langle z_1 | \langle z_2 | \hat{H} | z_1 \rangle | z_2 \rangle | w_1 \rangle | w_2 \rangle) . \end{aligned} \quad (3-45)$$

To express Equation (3-45), it is easier way to obtain the next element generally as

$$\begin{aligned} & \frac{\partial}{\partial \xi_i} \langle w_2 | \langle w_1 | \langle z_2 | \langle z_1 | \hat{H} | z_1' \rangle | z_2' \rangle | w_1' \rangle | w_2' \rangle \\ &= -\frac{1}{2} \left( \frac{\partial}{\partial \xi_i} \langle w_1 | w_1' \rangle \langle w_2 | w_2' \rangle + \langle w_1 | w_1' \rangle \frac{\partial}{\partial \xi_i} \langle w_2 | w_2' \rangle \right) (\langle z_2 | z_2' \rangle \langle z_1 | \Delta | z_1' \rangle \\ & \quad + \langle z_1 | z_1' \rangle \langle z_2 | \Delta | z_2' \rangle) \\ & - \frac{1}{2m_p} \left( \frac{\partial}{\partial \xi_i} \langle z_1 | z_1' \rangle \langle z_2 | z_2' \rangle + \langle z_1 | z_1' \rangle \frac{\partial}{\partial \xi_i} \langle z_2 | z_2' \rangle \right) (\langle w_2 | w_2' \rangle \langle w_1 | \Delta | w_1' \rangle \\ & \quad + \langle w_1 | w_1' \rangle \langle w_2 | \Delta | w_2' \rangle) \\ & - \left( \frac{\partial}{\partial \xi_i} \langle w_2 | w_2' \rangle \langle z_2 | z_2' \rangle + \langle w_2 | w_2' \rangle \frac{\partial}{\partial \xi_i} \langle z_2 | z_2' \rangle \right) \langle w_1 | \langle z_1 | \frac{1}{|r_1 - r_2|} | z_1' \rangle | w_1' \rangle \\ & - \left( \frac{\partial}{\partial \xi_i} \langle w_2 | w_2' \rangle \langle z_1 | z_1' \rangle + \langle w_2 | w_2' \rangle \frac{\partial}{\partial \xi_i} \langle z_1 | z_1' \rangle \right) \langle w_1 | \langle z_2 | \frac{1}{|r_1 - r_2|} | z_2' \rangle | w_1' \rangle \\ & - \left( \frac{\partial}{\partial \xi_i} \langle w_1 | w_1' \rangle \langle z_2 | z_2' \rangle + \langle w_1 | w_1' \rangle \frac{\partial}{\partial \xi_i} \langle z_2 | z_2' \rangle \right) \langle w_2 | \langle z_1 | \frac{1}{|r_1 - r_2|} | z_1' \rangle | w_2' \rangle \\ & - \left( \frac{\partial}{\partial \xi_i} \langle w_1 | w_1' \rangle \langle z_1 | z_1' \rangle + \langle w_1 | w_1' \rangle \frac{\partial}{\partial \xi_i} \langle z_1 | z_1' \rangle \right) \langle w_2 | \langle z_2 | \frac{1}{|r_1 - r_2|} | z_2' \rangle | w_2' \rangle \end{aligned} \quad (3-46)$$

$$\begin{aligned}
& + \left( \frac{\partial}{\partial \xi_i} \langle w_1 | w_1' \rangle \langle w_2 | w_2' \rangle \right. \\
& \quad \left. + \langle w_1 | w_1' \rangle \frac{\partial}{\partial \xi_i} \langle w_2 | w_2' \rangle \right) \langle z_2 | \langle z_1 | \frac{1}{|r_1 - r_2|} | z_1' \rangle | z_2' \rangle \\
& + \left( \frac{\partial}{\partial \xi_i} \langle z_1 | z_1' \rangle \langle z_2 | z_2' \rangle + \langle z_1 | z_1' \rangle \frac{\partial}{\partial \xi_i} \langle z_2 | z_2' \rangle \right) \langle w_2 | \langle w_1 | \frac{1}{|r_1 - r_2|} | w_1' \rangle | w_2' \rangle \\
& + \left( \frac{\partial}{\partial \xi_i} \langle w_1 | w_1' \rangle \langle w_2 | w_2' \rangle + \langle w_1 | w_1' \rangle \frac{\partial}{\partial \xi_i} \langle w_2 | w_2' \rangle \right) (\langle z_2 | z_2' \rangle \langle z_1 | r \cdot E | z_1' \rangle \\
& \quad + \langle z_1 | z_1' \rangle \langle z_2 | r \cdot E | z_2' \rangle) \\
& - \left( \frac{\partial}{\partial \xi_i} \langle z_1 | z_1' \rangle \langle z_2 | z_2' \rangle + \langle z_1 | z_1' \rangle \frac{\partial}{\partial \xi_i} \langle z_2 | z_2' \rangle \right) (\langle w_2 | w_2' \rangle \langle w_1 | r \cdot E | w_1' \rangle \\
& \quad + \langle w_1 | w_1' \rangle \langle w_2 | r \cdot E | w_2' \rangle) \\
& - \frac{1}{2} \langle w_1 | w_1' \rangle \langle w_2 | w_2' \rangle \left( \frac{\partial}{\partial \xi_i} \langle z_2 | z_2' \rangle \langle z_1 | \Delta | z_1' \rangle + \langle z_2 | z_2' \rangle \frac{\partial}{\partial \xi_i} \langle z_1 | \Delta | z_1' \rangle \right. \\
& \quad \left. + \frac{\partial}{\partial \xi_i} \langle z_1 | z_1' \rangle \langle z_2 | \Delta | z_2' \rangle + \langle z_1 | z_1' \rangle \frac{\partial}{\partial \xi_i} \langle z_2 | \Delta | z_2' \rangle \right) \\
& - \frac{1}{2m_p} \langle z_1 | z_1' \rangle \langle z_2 | z_2' \rangle \left( \frac{\partial}{\partial \xi_i} \langle w_2 | w_2' \rangle \langle w_1 | \Delta | w_1' \rangle + \langle w_2 | w_2' \rangle \frac{\partial}{\partial \xi_i} \langle w_1 | \Delta | w_1' \rangle \right. \\
& \quad \left. + \frac{\partial}{\partial \xi_i} \langle w_1 | w_1' \rangle \langle w_2 | \Delta | w_2' \rangle + \langle w_1 | w_1' \rangle \frac{\partial}{\partial \xi_i} \langle w_2 | \Delta | w_2' \rangle \right) \\
& - \langle w_2 | w_2' \rangle \langle z_2 | z_2' \rangle \frac{\partial}{\partial \xi_i} \langle w_1 | \langle z_1 | \frac{1}{|r_1 - r_2|} | z_1' \rangle | w_1' \rangle \\
& \quad - \langle w_2 | w_2' \rangle \langle z_1 | z_1' \rangle \frac{\partial}{\partial \xi_i} \langle w_1 | \langle z_2 | \frac{1}{|r_1 - r_2|} | z_2' \rangle | w_1' \rangle \\
& - \langle w_1 | w_1' \rangle \langle z_2 | z_2' \rangle \frac{\partial}{\partial \xi_i} \langle w_2 | \langle z_1 | \frac{1}{|r_1 - r_2|} | z_1' \rangle | w_2' \rangle \\
& \quad - \langle w_1 | w_1' \rangle \langle z_1 | z_1' \rangle \frac{\partial}{\partial \xi_i} \langle w_2 | \langle z_2 | \frac{1}{|r_1 - r_2|} | z_2' \rangle | w_2' \rangle \\
& + \langle w_1 | w_1' \rangle \langle w_2 | w_2' \rangle \frac{\partial}{\partial \xi_i} \langle z_2 | \langle z_1 | \frac{1}{|r_1 - r_2|} | z_1' \rangle | z_2' \rangle \\
& \quad + \langle z_1 | z_1' \rangle \langle z_2 | z_2' \rangle \frac{\partial}{\partial \xi_i} \langle w_2 | \langle w_1 | \frac{1}{|r_1 - r_2|} | w_1' \rangle | w_2' \rangle . \\
& + \langle w_1 | w_1' \rangle \langle w_2 | w_2' \rangle \left( \frac{\partial}{\partial \xi_i} \langle z_2 | z_2' \rangle \langle z_1 | r \cdot E | z_1' \rangle + \langle z_2 | z_2' \rangle \frac{\partial}{\partial \xi_i} \langle z_1 | r \cdot E | z_1' \rangle \right. \\
& \quad \left. + \frac{\partial}{\partial \xi_i} \langle z_1 | z_1' \rangle \langle z_2 | r \cdot E | z_2' \rangle + \langle z_1 | z_1' \rangle \frac{\partial}{\partial \xi_i} \langle z_2 | r \cdot E | z_2' \rangle \right)
\end{aligned}$$

$$-\langle z_1|z_1'\rangle\langle z_2|z_2'\rangle\left(\frac{\partial}{\partial\xi_i}\langle w_2|w_2'\rangle\langle w_1|r\cdot E|w_1'\rangle+\langle w_2|w_2'\rangle\frac{\partial}{\partial\xi_i}\langle w_1|r\cdot E|w_1'\rangle\right. \\ \left.+\frac{\partial}{\partial\xi_i}\langle w_1|w_1'\rangle\langle w_2|r\cdot E|w_2'\rangle+\langle w_1|w_1'\rangle\frac{\partial}{\partial\xi_i}\langle w_2|r\cdot E|w_2'\rangle\right)$$

Then we need to obtain further details of differential by  $\xi_i$  and it is shown in the next section.

### 3.3.1. Differential by Gaussian label $g_x^i$

#### 3.3.1.1. Overlap integral

From differential of Equation (3-23),

$$\frac{\partial}{\partial g_x^i}\langle i|j\rangle=\mu^{i*}\frac{\partial S}{\partial g_x^i}\mu^j, \quad (3-47)$$

and term  $\partial S/\partial g_x^i$  is obtained putting  $M \times M$  matrix  $A, B$  as

$$\frac{\partial S}{\partial g_x^i}=A+B, \quad (3-48)$$

where,

$$(A)_{mn}=\begin{cases} \langle G_m|G_n\rangle\left(\frac{\gamma_n-\gamma_m}{(\gamma_m+\gamma_n)}g_x^n+\frac{2\sqrt{\gamma_n\gamma_m}}{(\gamma_m+\gamma_n)}g_x^{m*}-\frac{1}{2}g_x^{n*}\right) & (\text{when } n=i) \\ 0 & (\text{when } n\neq i) \end{cases}, \quad (3-49)$$

$$(B)_{mn}=\begin{cases} \langle G_m|G_n\rangle\left(-\frac{1}{2}g_x^{m*}\right) & (\text{when } m=i) \\ 0 & (\text{when } m\neq i) \end{cases}. \quad (3-50)$$

In a similar way,  $\partial S/\partial g_x^{i*}$  is obtained with  $M \times M$  matrix  $C, D$  as

$$\frac{\partial S}{\partial g_x^{i*}}=C+D \quad (3-51)$$

where,

$$(C)_{mn}=\begin{cases} \langle G_m|G_n\rangle\left(-\frac{1}{2}g_x^n\right) & (\text{when } n=i) \\ 0 & (\text{when } n\neq i) \end{cases}, \quad (3-52)$$

$$(D)_{mn}=\begin{cases} \langle G_m|G_n\rangle\left(\frac{\gamma_m-\gamma_n}{(\gamma_m+\gamma_n)}g_x^{m*}+\frac{2\sqrt{\gamma_n\gamma_m}}{(\gamma_m+\gamma_n)}g_x^n-\frac{1}{2}g_x^m\right) & (\text{when } m=i) \\ 0 & (\text{when } m\neq i) \end{cases}. \quad (3-53)$$

### 3.3.1.2. Kinetic integral

Differential of  $K$  is formulated with Hadamard product operator  $\circ$  from the product rule as

$$\frac{\partial K}{\partial g_x^i} = \frac{\partial S}{\partial g_x^i} \circ R + S \circ \frac{\partial R}{\partial g_x^i} \quad (3-54)$$

where,

$$\left( \frac{\partial R}{\partial g_x^i} \right)_{mn} = \begin{cases} \frac{2\gamma_m \gamma_n}{(\gamma_m + \gamma_n)} \left\{ \frac{2\gamma_m}{(\gamma_m + \gamma_n)} g_x^n - \frac{2\sqrt{\gamma_n \gamma_m}}{(\gamma_m + \gamma_n)} g_x^{m*} \right\} & (\text{when } n = i) \\ 0 & (\text{when } n \neq i) \end{cases}, \quad (3-55)$$

$$\left( \frac{\partial R}{\partial g_x^{i*}} \right)_{mn} = \begin{cases} -\frac{2\gamma_n \sqrt{\gamma_n \gamma_m}}{(\gamma_m + \gamma_n)} \left\{ \frac{2\gamma_m}{(\gamma_m + \gamma_n)} g_x^n - \frac{2\sqrt{\gamma_n \gamma_m}}{(\gamma_m + \gamma_n)} g_x^{m*} \right\} & (\text{when } m = i) \\ 0 & (\text{when } m \neq i) \end{cases}. \quad (3-56)$$

### 3.3.1.3. Electric field integral

Differential of  $L$  is expressed in similar way with  $K$  as

$$\frac{\partial L}{\partial g_x^i} = \frac{\partial S}{\partial g_x^i} \circ \tilde{N} + S \circ \frac{\partial \tilde{N}}{\partial g_x^i} \quad (3-57)$$

where,

$$\left( \frac{\partial \tilde{N}}{\partial g_x^i} \right)_{mn} = \begin{cases} \frac{\sqrt{2\gamma_n}}{(\gamma_m + \gamma_n)} E_x & (\text{when } n = i) \\ 0 & (\text{when } n \neq i) \end{cases}, \quad (3-58)$$

### 3.3.1.4. Coulomb integral

Differential of  $C$  is derived from Equation (3-38) as

$$\begin{aligned} \frac{\partial C}{\partial g_x^t} = & \frac{\partial S}{\partial g_x^t} \circ_{mn} (S \circ_{ij} P_{::ij})_{mn::} + S \circ_{mn} \left( \frac{\partial S}{\partial g_x^t} \circ_{ij} P_{::ij} \right)_{mn::} \\ & + S \circ_{mn} \left( S \circ_{ij} \left( \frac{\partial P}{\partial g_x^t} \right)_{::ij} \right)_{mn::}. \end{aligned} \quad (3-59)$$

First we obtain  $\partial P / \partial g_x^t$ . Putting  $\gamma_{all}$  as

$$\gamma_{all} = \frac{\left( \frac{\gamma_m}{2} + \frac{\gamma_n}{2} \right) \left( \frac{\gamma_i}{2} + \frac{\gamma_j}{2} \right)}{\left( \frac{\gamma_m}{2} + \frac{\gamma_n}{2} + \frac{\gamma_i}{2} + \frac{\gamma_j}{2} \right)}, \quad (3-60)$$

$\partial P / \partial g_x^i$  is expressed from Equation (3-34) as

$$\begin{aligned} & \frac{\partial}{\partial g_x^t} \left( \frac{1}{\rho_{mnij}} \operatorname{erf}(\sqrt{\gamma_{all}} \rho_{mnij}) \right) \\ &= \frac{1}{\rho_{mnij}} \frac{\partial}{\partial g_x^t} \operatorname{erf}(\sqrt{\gamma_{all}} \rho_{mnij}) + \operatorname{erf}(\sqrt{\gamma_{all}} \rho_{mnij}) \frac{\partial}{\partial g_x^t} \frac{1}{\rho_{mnij}} , \end{aligned} \quad (3-61)$$

and

$$\frac{\partial}{\partial g_x^t} \operatorname{erf}(\sqrt{\gamma_{all}} \rho_{mnij}) = \frac{2}{\sqrt{\pi}} \exp(-\gamma_{all} \rho_{mnij}^2) \frac{\partial}{\partial g_x^t} \sqrt{\gamma_{all}} \rho_{mnij} , \quad (3-62)$$

$$\frac{\partial}{\partial g_x^t} \rho_{mnij} = \frac{\partial}{\partial g_x^t} \sqrt{\tilde{n}_{mnij}^2} = \frac{1}{2} \frac{1}{\sqrt{\tilde{n}_{mnij}^2}} \frac{\partial \tilde{n}_{mnij}^2}{\partial g_x^t} , \quad (3-63)$$

$$\frac{\partial \tilde{n}_{mnij}^2}{\partial g_x^t} = 2 \tilde{n}_x^{mnij} \frac{\partial \tilde{n}_x^{mnij}}{\partial g_x^t} , \quad (3-64)$$

$$\therefore \frac{\partial}{\partial g_x^t} \rho_{mnij} = \frac{\tilde{n}_x^{mnij}}{\rho_{mnij}} \frac{\partial \tilde{n}_x^{mnij}}{\partial g_x^t} , \quad (3-65)$$

$$\therefore \frac{\partial}{\partial g_x^t} \operatorname{erf}(\sqrt{\gamma_{all}} \rho_{mnij}) = \frac{2}{\sqrt{\pi}} \frac{\sqrt{\gamma_{all}}}{\rho_{mnij}^2} \exp(-\gamma_{all} \rho_{mnij}^2) \tilde{n}_x^{mnij} \frac{\partial \tilde{n}_x^{mnij}}{\partial g_x^t} . \quad (3-66)$$

By the way

$$\frac{\partial}{\partial g_x^t} \frac{1}{\rho_{mnij}} = - \frac{1}{\rho_{mnij}^2} \frac{\partial}{\partial g_x^t} \rho_{mnij} = - \frac{\tilde{n}_x^{mnij}}{\rho_{mnij}^3} \frac{\partial \tilde{n}_x^{mnij}}{\partial g_x^t} , \quad (3-67)$$

and if we put

$$(F)_{mnij} = \frac{2}{\sqrt{\pi}} \frac{\sqrt{\gamma_{all}}}{\rho_{mnij}^2} \exp(-\gamma_{all} \rho_{mnij}^2) - \frac{1}{\rho_{mnij}^3} \operatorname{erf}(\sqrt{\gamma_{all}} \rho_{mnij}) , \quad (3-68)$$

$$(N)_{mnij} = \tilde{n}_x^{mnij} \frac{\partial \tilde{n}_x^{mnij}}{\partial g_x^t} , \quad (3-69)$$

then from Equations (3-61), (3-68) and (3-69),

$$\frac{\partial P}{\partial g_x^t} = F \circ N , \quad (3-70)$$

where,

$$(N)_{mnij} = \begin{cases} \frac{\tilde{n}_x^{mnij} \sqrt{2\gamma_n}}{(\gamma_m + \gamma_n)} & (\text{when } n = t) \\ \frac{-\tilde{n}_x^{mnij} \sqrt{2\gamma_j}}{(\gamma_i + \gamma_j)} & (\text{when } j = t) \\ \tilde{n}_x^{mnij} \left[ \frac{\sqrt{2\gamma_t}}{(\gamma_m + \gamma_t)} - \frac{\sqrt{2\gamma_t}}{(\gamma_i + \gamma_t)} \right] & (\text{when } n = j = t) \\ 0 & (\text{the others}) \end{cases} \quad (3-71)$$

Differential by  $g_x^{i*}$  is obtained in similar way putting  $(N)_{mnij}$  as

$$(N)_{mnij} = \tilde{n}_x^{mnij} \frac{\partial \tilde{n}_x^{mnij}}{\partial g_x^{t*}}, \quad (3-72)$$

where,

$$(N)_{mnij} = \begin{cases} \frac{\tilde{n}_x^{mnij} \sqrt{2\gamma_m}}{(\gamma_m + \gamma_n)} & (\text{when } m = t) \\ \frac{-\tilde{n}_x^{mnij} \sqrt{2\gamma_i}}{(\gamma_i + \gamma_j)} & (\text{when } i = t) \\ \tilde{n}_x^{mnij} \left[ \frac{\sqrt{2\gamma_t}}{(\gamma_m + \gamma_t)} - \frac{\sqrt{2\gamma_t}}{(\gamma_i + \gamma_t)} \right] & (\text{when } m = i = t) \\ 0 & (\text{the others}) \end{cases} . \quad (3-73)$$

### 3.3.2. Differential by orbital coefficients

Next, differential by orbital coefficient  $\mu_l^i$  is obtained. For different particle identifier  $z_f$  and  $z_d$ , each differential by  $l$ -th elements of  $\mu^{z_d}$  and  $\mu^{z_f*}$  is derived as

$$\frac{\partial}{\partial \mu_l^{z_d}} \langle z_f | z_d \rangle = \mu^{z_f*} S \frac{\partial \mu^{z_d}}{\partial \mu_l^{z_d}}, \quad (3-74)$$

$$\frac{\partial}{\partial \mu_l^{z_f*}} \langle z_f | z_d \rangle = \frac{\partial \mu^{z_f*}}{\partial \mu_l^{z_f*}} S \mu^{z_d}, \quad (3-75)$$

$$\frac{\partial}{\partial \mu_l^{z_d}} \langle z_f | \Delta | z_d \rangle = \mu^{z_f*} K \frac{\partial \mu^{z_d}}{\partial \mu_l^{z_d}}, \quad (3-76)$$

$$\frac{\partial}{\partial \mu_l^{z_f*}} \langle z_f | \Delta | z_d \rangle = \frac{\partial \mu^{z_f*}}{\partial \mu_l^{z_f*}} K \mu^{z_d}, \quad (3-77)$$

$$\frac{\partial}{\partial \mu_l^{z_d}} \langle z_f | r \cdot E | z_d \rangle = \mu^{z_f^*} L \frac{\partial \mu^{z_d}}{\partial \mu_l^{z_d}} , \quad (3-78)$$

$$\frac{\partial}{\partial \mu_l^{z_f^*}} \langle z_f | r \cdot E | z_d \rangle = \frac{\partial \mu^{z_f^*}}{\partial \mu_l^{z_f^*}} L \mu^{z_d} , \quad (3-79)$$

$$\frac{\partial}{\partial \mu_l^{z_d'}} \langle z_x | \langle z_y | \frac{1}{|r_1 - r_2|} | z_d' \rangle | z_z' \rangle = \sum_{m,n,i,j} \left( \mu^{xz'} \circ_{mn} \left( \frac{\partial \mu^{yd'}}{\partial \mu_l^{z_d'}} \circ_{ij} C_{::ij} \right)_{mn::} \right)_{mni j} , \quad (3-80)$$

where,

$$\frac{\partial}{\partial \mu_l^{z_d'}} \mu^{yd'} = \left( \frac{\partial}{\partial \mu_l^{z_d'}} \mu^{z_d'} \mu^{zy^*} \right)^t , \quad (3-81)$$

In similar ways,

$$\frac{\partial}{\partial \mu_l^{z_d'}} \langle z_x | \langle z_y | \frac{1}{|r_1 - r_2|} | z_z' \rangle | z_d' \rangle = \sum_{m,n,i,j} \left( \frac{\partial \mu^{xd'}}{\partial \mu_l^{z_d'}} \circ_{mn} (\mu^{yz'} \circ_{ij} C_{::ij})_{mn::} \right)_{mni j} , \quad (3-82)$$

$$\frac{\partial}{\partial \mu_l^{z_y^*}} \langle z_x | \langle z_y | \frac{1}{|r_1 - r_2|} | z_d' \rangle | z_z' \rangle = \sum_{m,n,i,j} \left( \mu^{xz'} \circ_{mn} \left( \frac{\partial \mu^{yd'}}{\partial \mu_l^{z_y^*}} \circ_{ij} C_{::ij} \right)_{mn::} \right)_{mni j} , \quad (3-83)$$

$$\frac{\partial}{\partial \mu_l^{z_x^*}} \langle z_x | \langle z_y | \frac{1}{|r_1 - r_2|} | z_z' \rangle | z_d' \rangle = \sum_{m,n,i,j} \left( \frac{\partial \mu^{xd'}}{\partial \mu_l^{z_x^*}} \circ_{mn} (\mu^{yz'} \circ_{ij} C_{::ij})_{mn::} \right)_{mni j} . \quad (3-84)$$

### 3.4. Derivation of $c_{ij}$

To solve equations of motion Equation (2-11), one needs to derive  $c_{ij}$  and  $\partial H / \partial \xi_i$ . When  $|\psi\rangle$  in Equation (2-19) is put as

$$|\psi\rangle = |A\rangle |B\rangle , \quad (3-85)$$

$$|A\rangle = |z_1\rangle |z_2\rangle + |z_2\rangle |z_1\rangle , \quad (3-86)$$

$$|B\rangle = |w_1\rangle |w_2\rangle + |w_2\rangle |w_1\rangle , \quad (3-87)$$

then, for a variable  $\xi_i$  in the wave function  $|\psi\rangle$ ,

$$\left\langle \psi \left| \frac{\partial \psi}{\partial \xi_i} \right. \right\rangle = \left. \frac{\partial \langle \psi(\xi_i') | \psi(\xi_i) \rangle}{\partial \xi_i} \right|_{\xi_i' = \xi_i} \quad (3-88)$$

$$= \left. \left\{ \frac{\partial}{\partial \xi_i} 4(\langle w_2' | \langle w_1' | \langle z_2' | \langle z_1' | | z_1 \rangle | z_2 \rangle | w_1 \rangle | w_2 \rangle \right. \right. \\ \left. \left. + \langle w_1' | \langle w_2' | \langle z_2' | \langle z_1' | | z_1 \rangle | z_2 \rangle | w_1 \rangle | w_2 \rangle \right. \right. \\ \left. \left. + \langle w_2' | \langle w_1' | \langle z_1' | \langle z_2' | | z_1 \rangle | z_2 \rangle | w_1 \rangle | w_2 \rangle \right. \right. \\ \left. \left. + \langle w_1' | \langle w_2' | \langle z_1' | \langle z_2' | | z_1 \rangle | z_2 \rangle | w_1 \rangle | w_2 \rangle \right) \right|_{\xi_i' = \xi_i} \quad (3-89)$$

$$= 4 \frac{\partial}{\partial \xi_i} \left\{ (\langle z_1' | z_1 \rangle \langle z_2' | z_2 \rangle + \langle z_2' | z_1 \rangle \langle z_1' | z_2 \rangle) (\langle w_1' | w_1 \rangle \langle w_2' | w_2 \rangle \right. \\ \left. + \langle w_2' | w_1 \rangle \langle w_1' | w_2 \rangle) \right\} \Big|_{\xi_i' = \xi_i} , \quad (3-90)$$

where,

$$|\psi(\xi_i')\rangle = |A'\rangle |B'\rangle , \quad (3-91)$$

$$|A'\rangle = |z_1'\rangle |z_2'\rangle + |z_2'\rangle |z_1'\rangle , \quad (3-92)$$

$$|B'\rangle = |w_1'\rangle |w_2'\rangle + |w_2'\rangle |w_1'\rangle , \quad (3-93)$$

and  $\psi(\xi_i')$  means the wave function  $\psi$  where  $\xi_i$  is replaced by  $\xi_i'$  such as

$$\psi(\xi_i) = \psi(\xi_1, \xi_2, \dots, \xi_i, \dots, \xi_n) , \psi(\xi_i') = \psi(\xi_1, \xi_2, \dots, \xi_i', \dots, \xi_n) . \quad (3-94)$$

By distinguishing  $\xi_i$  and  $\xi_i'$ , it is able to express Equation (3-88) in simple form. In similar ways,  $|z_1'\rangle$ ,  $|z_2'\rangle$ ,  $|w_1'\rangle$ , and  $|w_2'\rangle$  mean  $\xi_i$  in them is replaced by  $\xi_i'$  respectively.

If the label of the Gaussian basis

$$z_{tx} = \frac{\gamma_t \frac{1}{2} q_x + i \hbar^{-1} \gamma_t^{-\frac{1}{2}} p_x}{\sqrt{2}} \quad (3-95)$$

is selected as one of time-dependent variables in the wave function, using

$$\left( \frac{\partial \vec{S}}{\partial z_{tx}} \right)_{mn} \Big|_{z_{tx}' = z_{tx}} \\ = \begin{cases} \langle G_m | G_n \rangle \left( \frac{\gamma_n - \gamma_m}{(\gamma_m + \gamma_n)} z_{nx} + \frac{2\sqrt{\gamma_n \gamma_m}}{(\gamma_m + \gamma_n)} z_{m^* x} - \frac{1}{2} z_{n^* x} \right) & (\text{when } n = t) \\ 0 & (\text{when } n \neq t) \end{cases} \quad (3-96)$$

$$\left( \frac{\partial \vec{S}}{\partial z_{tx}} \right)_{mn} \Big|_{z_{tx}' = z_{tx}} = \begin{cases} \langle G_m | G_n \rangle \left( -\frac{1}{2} z_{m^* x} \right) & (\text{when } m = t) \\ 0 & (\text{when } m \neq t) \end{cases} \quad (3-97)$$

$$\check{S} = \left( \frac{\partial \check{S}}{\partial z_{tx}} \right)_{mn} \Big|_{z_{tx}'=z_{tx}} - \left( \frac{\partial \check{S}}{\partial z_{tx}'} \right)_{mn} \Big|_{z_{tx}'=z_{tx}} \quad (3-98)$$

it can be derived as

$$\begin{aligned} \left\langle \psi \left| \frac{\partial \psi}{\partial z_{tx}} \right. \right\rangle - \left\langle \frac{\partial \psi}{\partial z_{tx}} \left| \psi \right. \right\rangle &= G_{tx} \\ &= 4\{(\mu^{z_1*} \check{S} \mu^{z_1} \langle z_2 | z_2 \rangle + \langle z_1 | z_1 \rangle \mu^{z_2*} \check{S} \mu^{z_2} + \mu^{z_2*} \check{S} \mu^{z_1} \langle z_1 | z_2 \rangle \\ &\quad + \langle z_2 | z_1 \rangle \mu^{z_1*} \check{S} \mu^{z_2}) (\langle w_1 | w_1 \rangle \langle w_2 | w_2 \rangle + \langle w_2 | w_1 \rangle \langle w_1 | w_2 \rangle) \\ &\quad + (\langle z_1 | z_1 \rangle \langle z_2 | z_2 \rangle + \langle z_2 | z_1 \rangle \langle z_1 | z_2 \rangle) (\mu^{w_1*} \check{S} \mu^{w_1} \langle w_2 | w_2 \rangle + \langle w_1 | w_1 \rangle \mu^{w_2*} \check{S} \mu^{w_2} \\ &\quad + \mu^{w_2*} \check{S} \mu^{w_1} \langle w_1 | w_2 \rangle + \langle w_2 | w_1 \rangle \mu^{w_1*} \check{S} \mu^{w_2})\} \end{aligned} \quad (3-99)$$

If the coefficient of the orbitals  $\mu_i^{z_1}$  is chosen as the variable, then

$$\left\langle \psi \left| \frac{\partial \psi}{\partial \mu_i^{z_1}} \right. \right\rangle - \left\langle \frac{\partial \psi}{\partial \mu_i^{z_1}} \left| \psi \right. \right\rangle = \left\langle \psi \left| \frac{\partial \psi}{\partial \mu_i^{z_1}} \right. \right\rangle = U_t^{z_1} \quad (3-100)$$

$$\begin{aligned} &= 4 \left( \mu^{z_1*} S \frac{\partial \mu^{z_1}}{\partial \mu_i^{z_1}} \langle z_2 | z_2 \rangle + \langle z_1 | z_2 \rangle \mu^{z_2*} S \frac{\partial \mu^{z_1}}{\partial \mu_i^{z_1}} \right) (\langle w_1 | w_1 \rangle \langle w_2 | w_2 \rangle \\ &\quad + \langle w_2 | w_1 \rangle \langle w_1 | w_2 \rangle) \end{aligned} \quad (3-101)$$

In the same way, for the other particles,

$$\begin{aligned} \left\langle \psi \left| \frac{\partial \psi}{\partial \mu_i^{z_1}} \right. \right\rangle &= 4 \left( \mu^{z_1*} S \frac{\partial \mu^{z_1}}{\partial \mu_i^{z_1}} \langle z_2 | z_2 \rangle + \langle z_1 | z_2 \rangle \mu^{z_2*} S \frac{\partial \mu^{z_1}}{\partial \mu_i^{z_1}} \right) (\langle w_1 | w_1 \rangle \langle w_2 | w_2 \rangle \\ &\quad + \langle w_2 | w_1 \rangle \langle w_1 | w_2 \rangle) \end{aligned} \quad (3-102)$$

$$\begin{aligned} \left\langle \psi \left| \frac{\partial \psi}{\partial \mu_i^{z_2}} \right. \right\rangle &= 4 \left( \langle z_1 | z_1 \rangle \mu^{z_2*} S \frac{\partial \mu^{z_2}}{\partial \mu_i^{z_2}} + \mu^{z_1*} S \frac{\partial \mu^{z_2}}{\partial \mu_i^{z_2}} \langle z_2 | z_1 \rangle \right) (\langle w_1 | w_1 \rangle \langle w_2 | w_2 \rangle \\ &\quad + \langle w_2 | w_1 \rangle \langle w_1 | w_2 \rangle) \end{aligned} \quad (3-103)$$

$$\begin{aligned} \left\langle \psi \left| \frac{\partial \psi}{\partial \mu_i^{w_1}} \right. \right\rangle &= 4(\langle z_1 | z_1 \rangle \langle z_2 | z_2 \rangle + \langle z_2 | z_1 \rangle \langle z_1 | z_2 \rangle) \left( \mu^{w_1*} S \frac{\partial \mu^{w_1}}{\partial \mu_i^{w_1}} \langle w_2 | w_2 \rangle \right. \\ &\quad \left. + \langle w_1 | w_2 \rangle \mu^{w_2*} S \frac{\partial \mu^{w_1}}{\partial \mu_i^{w_1}} \right) \end{aligned} \quad (3-104)$$

$$\begin{aligned} \left\langle \psi \left| \frac{\partial \psi}{\partial \mu_i^{w_1}} \right. \right\rangle &= 4(\langle z_1 | z_1 \rangle \langle z_2 | z_2 \rangle + \langle z_2 | z_1 \rangle \langle z_1 | z_2 \rangle) \left( \langle w_1 | w_1 \rangle \mu^{w_2*} S \frac{\partial \mu^{w_2}}{\partial \mu_i^{w_2}} \right. \\ &\quad \left. + \mu^{w_1*} S \frac{\partial \mu^{w_2}}{\partial \mu_i^{w_2}} \langle w_2 | w_1 \rangle \right) \end{aligned} \quad (3-105)$$

A differential of  $Z_j$  by a conjugate variable is invariable from (2-21) like as

$$\left\{ \frac{i\hbar}{2\langle\psi|\psi\rangle} \left( \left\langle \psi \left| \frac{\partial\psi}{\partial\xi_j} \right\rangle - \left\langle \frac{\partial\psi}{\partial\xi_j^*} \left| \psi \right\rangle \right) \right\}^* = \frac{-i\hbar}{2\langle\psi|\psi\rangle} \left( \left\langle \frac{\partial\psi}{\partial\xi_j} \left| \psi \right\rangle - \left\langle \psi \left| \frac{\partial\psi}{\partial\xi_j^*} \right\rangle \right) \right) \quad (3-106)$$

$$= \frac{i\hbar}{2\langle\psi|\psi\rangle} \left( \left\langle \psi \left| \frac{\partial\psi}{\partial\xi_j^*} \right\rangle - \left\langle \frac{\partial\psi}{\partial\xi_j} \left| \psi \right\rangle \right) \right). \quad (3-107)$$

$Z_j$  for the variables of the label of the Gaussian basis or the coefficient of the orbitals can be derived analytically from  $G_{t_x}$  or  $U_t^i$ .

### 3.4.1. Differential of $G_{t_x}$

Here we put

$$\check{S}(z_{t_x}) = S \circ \check{G}(z_{t_x}) = S \circ \left( \check{G}(z_{t_x}) - \vec{G}(z_{t_x}) \right) \quad (3-108)$$

$$\check{G}(z_{t_x}) = \begin{cases} \left( \frac{\gamma_n - \gamma_m}{(\gamma_m + \gamma_n)} z_{n_x} + \frac{2\sqrt{\gamma_n\gamma_m}}{(\gamma_m + \gamma_n)} z_{m_x}^* - \frac{1}{2} z_{n_x}^* \right) & (\text{when } n = t) \\ 0 & (\text{when } n \neq t) \end{cases} \quad (3-109)$$

$$\vec{G}(z_{t_x}) = \begin{cases} \left( -\frac{1}{2} z_{m_x}^* \right) & (\text{when } m = t) \\ 0 & (\text{when } m \neq t) \end{cases} \quad (3-110)$$

#### 3.4.1.1. Differential by $z_{t_x}$

First, the differential of  $G_{t_x}$  by  $z_{t_x}$  is considered.

$$\frac{\partial\check{S}(z_{t_x})}{\partial z_{t_x}} = \frac{\partial S}{\partial z_{t_x}} \circ \check{G}(z_{t_x}) + S \circ \frac{\partial\check{G}(z_{t_x})}{\partial z_{t_x}} \quad (3-111)$$

$$\frac{\partial\check{G}(z_{t_x})}{\partial z_{t_x}} = \frac{\partial\check{G}(z_{t_x})}{\partial z_{t_x}} - \frac{\partial\vec{G}(z_{t_x})}{\partial z_{t_x}} \quad (3-112)$$

$$\left( \frac{\partial\check{G}(z_{t_x})}{\partial z_{t_x}} \right)_{mn} = \begin{cases} \frac{\gamma_n - \gamma_m}{\gamma_m + \gamma_n} & (\text{when } n = t) \\ 0 & (\text{when } n \neq t) \end{cases} \quad (3-113)$$

$$\left( \frac{\partial\vec{G}(z_{t_x})}{\partial z_{t_x}} \right)_{mn} = 0 \quad (3-114)$$

$$\therefore \frac{\partial\check{G}(z_{t_x})}{\partial z_{t_x}} = \frac{\partial\check{G}(z_{t_x})}{\partial z_{t_x}} \quad (3-115)$$

and

$$\begin{aligned}
& \frac{\partial}{\partial z_{tx}} \left( \left\langle \psi \left| \frac{\partial \psi}{\partial z_{tx}} \right\rangle - \left\langle \frac{\partial \psi}{\partial z_{tx}} \left| \psi \right\rangle \right) \right. \\
&= 4 \left( \mu^{z_1^*} \check{S} \mu^{z_1} \mu^{z_2^*} \frac{\partial S}{\partial z_{tx}} \mu^{z_2} + \mu^{z_1^*} \frac{\partial S}{\partial z_{tx}} \mu^{z_1} \mu^{z_2^*} \check{S} \mu^{z_2} \right. \\
&\quad + \mu^{z_2^*} \check{S} \mu^{z_1} \mu^{z_1^*} \frac{\partial S}{\partial z_{tx}} \mu^{z_2} \\
&\quad \left. + \mu^{z_2^*} \frac{\partial S}{\partial z_{tx}} \mu^{z_1} \mu^{z_1^*} \check{S} \mu^{z_2} \right) (\langle w_1 | w_1 \rangle \langle w_2 | w_2 \rangle \\
&\quad + \langle w_2 | w_1 \rangle \langle w_1 | w_2 \rangle) \\
&+ 4 \left( \mu^{z_1^*} \frac{\partial \check{S}}{\partial z_{tx}} \mu^{z_1} \langle z_2 | z_2 \rangle + \langle z_1 | z_1 \rangle \mu^{z_2^*} \frac{\partial \check{S}}{\partial z_{tx}} \mu^{z_2} + \mu^{z_2^*} \frac{\partial \check{S}}{\partial z_{tx}} \mu^{z_1} \langle z_1 | z_2 \rangle \right. \\
&\quad \left. + \langle z_2 | z_1 \rangle \mu^{z_1^*} \frac{\partial \check{S}}{\partial z_{tx}} \mu^{z_2} \right) (\langle w_1 | w_1 \rangle \langle w_2 | w_2 \rangle \\
&\quad + \langle w_2 | w_1 \rangle \langle w_1 | w_2 \rangle) \\
&+ 4 (\mu^{z_1^*} \check{S} \mu^{z_1} \langle z_2 | z_2 \rangle + \langle z_1 | z_1 \rangle \mu^{z_2^*} \check{S} \mu^{z_2} + \mu^{z_2^*} \check{S} \mu^{z_1} \langle z_1 | z_2 \rangle \\
&\quad + \langle z_2 | z_1 \rangle \mu^{z_1^*} \check{S} \mu^{z_2}) \left( \mu^{w_1^*} \frac{\partial S}{\partial z_{tx}} \mu^{w_1} \langle w_2 | w_2 \rangle \right. \\
&\quad + \langle w_1 | w_1 \rangle \mu^{w_2^*} \frac{\partial S}{\partial z_{tx}} \mu^{w_2} + \mu^{w_2^*} \frac{\partial S}{\partial z_{tx}} \mu^{w_1} \langle w_1 | w_2 \rangle \\
&\quad \left. + \langle w_2 | w_1 \rangle \mu^{w_1^*} \frac{\partial S}{\partial z_{tx}} \mu^{w_2} \right) \\
&+ 4 (\langle z_1 | z_1 \rangle \langle z_2 | z_2 \rangle + \langle z_2 | z_1 \rangle \langle z_1 | z_2 \rangle) \left( \mu^{w_1^*} \check{S} \mu^{w_1} \mu^{w_2^*} \frac{\partial S}{\partial z_{tx}} \mu^{w_2} \right. \\
&\quad + \mu^{w_1^*} \frac{\partial S}{\partial z_{tx}} \mu^{w_1} \mu^{w_2^*} \check{S} \mu^{w_2} + \mu^{w_2^*} \check{S} \mu^{w_1} \mu^{w_1^*} \frac{\partial S}{\partial z_{tx}} \mu^{w_2} \\
&\quad \left. + \mu^{w_2^*} \frac{\partial S}{\partial z_{tx}} \mu^{w_1} \mu^{w_1^*} \check{S} \mu^{w_2} \right) \\
&+ 4 (\langle z_1 | z_1 \rangle \langle z_2 | z_2 \rangle + \langle z_2 | z_1 \rangle \langle z_1 | z_2 \rangle) \left( \mu^{w_1^*} \frac{\partial \check{S}}{\partial z_{tx}} \mu^{w_1} \langle w_2 | w_2 \rangle \right. \\
&\quad + \langle w_1 | w_1 \rangle \mu^{w_2^*} \frac{\partial \check{S}}{\partial z_{tx}} \mu^{w_2} + \mu^{w_2^*} \frac{\partial \check{S}}{\partial z_{tx}} \mu^{w_1} \langle w_1 | w_2 \rangle \\
&\quad \left. + \langle w_2 | w_1 \rangle \mu^{w_1^*} \frac{\partial \check{S}}{\partial z_{tx}} \mu^{w_2} \right)
\end{aligned} \tag{3-116}$$

$$\begin{aligned}
& +4(\mu^{w_1*} \check{S} \mu^{w_1} \langle w_2 | w_2 \rangle + \langle w_1 | w_1 \rangle \mu^{w_2*} \check{S} \mu^{w_2} + \mu^{w_2*} \check{S} \mu^{w_1} \langle w_1 | w_2 \rangle \\
& \quad + \langle w_2 | w_1 \rangle \mu^{w_1*} \check{S} \mu^{w_2}) \\
& \left( \mu^{z_1*} \frac{\partial S}{\partial z_{t_x}} \mu^{z_1} \langle z_2 | z_2 \rangle + \langle z_1 | z_1 \rangle \mu^{z_2*} \frac{\partial S}{\partial z_{t_x}} \mu^{z_2} + \mu^{z_2*} \frac{\partial S}{\partial z_{t_x}} \mu^{z_1} \langle z_1 | z_2 \rangle \right. \\
& \quad \left. + \langle z_2 | z_1 \rangle \mu^{z_1*} \frac{\partial S}{\partial z_{t_x}} \mu^{z_2} \right)
\end{aligned}$$

### 3.4.1.2. Differential with other z

The differential of  $G_{t_x}$  by  $z_{t_y}$  which belongs to axis y instead of axis x,  $z_{s_x}$  and  $z_{s_y}$  which belong to s instead of axis t are considered here.

$$\frac{\partial \check{G}(z_{t_x})}{\partial z_{t_y}} = 0 \quad (3-117)$$

$$\therefore \frac{\partial \check{S}(z_{t_x})}{\partial z_{t_y}} = \frac{\partial S}{\partial z_{t_y}} \circ \check{G}(z_{t_x}) \quad (3-118)$$

In similar ways,

$$\frac{\partial \check{S}(z_{t_x})}{\partial z_{s_x}} = \frac{\partial S}{\partial z_{s_x}} \circ \check{G}(z_{t_x}) \quad (3-119)$$

$$\frac{\partial \check{S}(z_{t_x})}{\partial z_{s_y}} = \frac{\partial S}{\partial z_{s_y}} \circ \check{G}(z_{t_x}) \quad (3-120)$$

Then differential of  $G_{t_x}$  are similar in Equation (3-116).

### 3.4.1.3. Differential by orbital coefficients

The differential of  $G_{t_x}$  by orbital coefficients  $\mu^i$  are like as

$$\frac{\partial}{\partial \mu^{z_1}} \left( \left\langle \psi \left| \frac{\partial \psi}{\partial z_{t_x}} \right. \right\rangle - \left\langle \frac{\partial \psi}{\partial z_{t_x}} \left| \psi \right. \right\rangle \right) \quad (3-121)$$

$$\begin{aligned}
&= 4 \left( \mu^{z_1*} \check{S} \frac{\partial \mu^{z_1}}{\partial \mu^{z_1_l}} \langle z_2|z_2 \rangle + \mu^{z_1*} S \frac{\partial \mu^{z_1}}{\partial \mu^{z_1_l}} \mu^{z_2*} \check{S} \mu^{z_2} + \langle z_1|z_2 \rangle \mu^{z_2*} \check{S} \frac{\partial \mu^{z_1}}{\partial \mu^{z_1_l}} \right. \\
&\quad \left. + \mu^{z_1*} \check{S} \mu^{z_2} \mu^{z_2*} S \frac{\partial \mu^{z_1}}{\partial \mu^{z_1_l}} \right) (\langle w_1|w_1 \rangle \langle w_2|w_2 \rangle \\
&\quad + \langle w_1|w_2 \rangle \langle w_2|w_1 \rangle) \\
&+ 4 \left( \mu^{z_1*} S \frac{\partial \mu^{z_1}}{\partial \mu^{z_1_l}} \langle z_2|z_2 \rangle + \mu^{z_2*} S \frac{\partial \mu^{z_1}}{\partial \mu^{z_1_l}} \langle z_1|z_2 \rangle \right) (\mu^{w_1*} \check{S} \mu^{w_1} \langle w_2|w_2 \rangle \\
&\quad + \langle w_1|w_1 \rangle \mu^{w_2*} \check{S} \mu^{w_2} + \langle w_1|w_2 \rangle \mu^{w_2*} \check{S} \mu^{w_1} \\
&\quad + \mu^{w_1*} \check{S} \mu^{w_2} \langle w_2|w_1 \rangle) \\
&\frac{\partial}{\partial \mu^{z_2_l}} \left( \left\langle \psi \left| \frac{\partial \psi}{\partial z_{t_x}} \right. \right\rangle - \left\langle \frac{\partial \psi}{\partial z_{t_x}} \left| \psi \right. \right\rangle \right) \\
&= 4 \left( \mu^{z_1*} \check{S} \mu^{z_1} \mu^{z_2*} S \frac{\partial \mu^{z_2}}{\partial \mu^{z_2_l}} + \langle z_1|z_1 \rangle \mu^{z_2*} \check{S} \frac{\partial \mu^{z_2}}{\partial \mu^{z_2_l}} + \mu^{z_1*} S \frac{\partial \mu^{z_2}}{\partial \mu^{z_2_l}} \mu^{z_2*} \check{S} \mu^{z_1} \right. \\
&\quad \left. + \mu^{z_1*} \check{S} \frac{\partial \mu^{z_2}}{\partial \mu^{z_2_l}} \langle z_2|z_1 \rangle \right) (\langle w_1|w_1 \rangle \langle w_2|w_2 \rangle \\
&\quad + \langle w_1|w_2 \rangle \langle w_2|w_1 \rangle) \\
&+ 4 \left( \langle z_1|z_1 \rangle \mu^{z_2*} S \frac{\partial \mu^{z_2}}{\partial \mu^{z_2_l}} + \mu^{z_1*} S \frac{\partial \mu^{z_2}}{\partial \mu^{z_2_l}} \langle z_2|z_1 \rangle \right) (\mu^{w_1*} \check{S} \mu^{w_1} \langle w_2|w_2 \rangle \\
&\quad + \langle w_1|w_1 \rangle \mu^{w_2*} \check{S} \mu^{w_2} + \langle w_1|w_2 \rangle \mu^{w_2*} \check{S} \mu^{w_1} \\
&\quad + \mu^{w_1*} \check{S} \mu^{w_2} \langle w_2|w_1 \rangle)
\end{aligned} \tag{3-122}$$

For  $\mu^{w_1}$  and  $\mu^{w_2}$ ,  $z$  and  $w$  are permuted in Equation (3-121) and (3-122).

### 3.4.2. Differential of $U_t^i$

#### 3.4.2.1. Differential by $z_{t_x}$

Differential of  $U_t^i$  is considered in the similar way as

$$\begin{aligned}
&\frac{\partial}{\partial z_{t_x}} \left( \left\langle \psi \left| \frac{\partial \psi}{\partial \mu^{z_1_l}} \right. \right\rangle - \left\langle \frac{\partial \psi}{\partial \mu^{z_1_l}} \left| \psi \right. \right\rangle \right) \\
&= 4 \left( \mu^{z_1*} \frac{\partial S}{\partial z_{t_x}} \frac{\partial \mu^{z_1}}{\partial \mu^{z_1_l}} \langle z_2|z_2 \rangle + \mu^{z_1*} S \frac{\partial \mu^{z_1}}{\partial \mu^{z_1_l}} \mu^{z_2*} \frac{\partial S}{\partial z_{t_x}} \mu^{z_2} \right. \\
&\quad \left. + \mu^{z_2*} \frac{\partial S}{\partial z_{t_x}} \frac{\partial \mu^{z_1}}{\partial \mu^{z_1_l}} \langle z_1|z_2 \rangle + \mu^{z_2*} S \frac{\partial \mu^{z_1}}{\partial \mu^{z_1_l}} \mu^{z_1*} \frac{\partial S}{\partial z_{t_x}} \mu^{z_2} \right)
\end{aligned} \tag{3-123}$$

$$\begin{aligned}
& (\langle w_1|w_1\rangle\langle w_2|w_2\rangle + \langle w_2|w_1\rangle\langle w_1|w_2\rangle) \\
& + 4 \left( \mu^{z_1^*} S \frac{\partial \mu^{z_1}}{\partial \mu^{z_{1l}}} \langle z_2|z_2\rangle + \mu^{z_2^*} S \frac{\partial \mu^{z_1}}{\partial \mu^{z_{1l}}} \langle z_1|z_2\rangle \right) \\
& \quad \left( \mu^{w_1^*} \frac{\partial S}{\partial z_{tx}} \mu^{w_1} \langle w_2|w_2\rangle + \langle w_1|w_1\rangle \mu^{w_2^*} \frac{\partial S}{\partial z_{tx}} \mu^{w_2} \right. \\
& \quad \left. + \mu^{w_2^*} \frac{\partial S}{\partial z_{tx}} \mu^{w_1} \langle w_1|w_2\rangle + \langle w_2|w_1\rangle \mu^{w_1^*} \frac{\partial S}{\partial z_{tx}} \mu^{w_2} \right) \\
& \frac{\partial}{\partial z_{tx}} \left( \left\langle \psi \left| \frac{\partial \psi}{\partial \mu^{z_{2l}}} \right. \right\rangle - \left\langle \frac{\partial \psi}{\partial \mu^{z_{2l}}} \left| \psi \right. \right\rangle \right) \\
& = 4 \left( \mu^{z_1^*} \frac{\partial S}{\partial z_{tx}} \mu^{z_1} \mu^{z_2^*} S \frac{\partial \mu^{z_2}}{\partial \mu^{z_{2l}}} + \langle z_1|z_1\rangle \mu^{z_2^*} \frac{\partial S}{\partial z_{tx}} \frac{\partial \mu^{z_2}}{\partial \mu^{z_{2l}}} \right. \\
& \quad \left. + \mu^{z_2^*} \frac{\partial S}{\partial z_{tx}} \mu^{z_1} \mu^{z_1^*} S \frac{\partial \mu^{z_2}}{\partial \mu^{z_{2l}}} + \langle z_2|z_1\rangle \mu^{z_1^*} \frac{\partial S}{\partial z_{tx}} \frac{\partial \mu^{z_2}}{\partial \mu^{z_{2l}}} \right) \\
& \quad (\langle w_1|w_1\rangle\langle w_2|w_2\rangle + \langle w_2|w_1\rangle\langle w_1|w_2\rangle) \tag{3-124} \\
& + 4 \left( \langle z_1|z_1\rangle \mu^{z_2^*} S \frac{\partial \mu^{z_2}}{\partial \mu^{z_{2l}}} + \langle z_2|z_1\rangle \mu^{z_1^*} S \frac{\partial \mu^{z_2}}{\partial \mu^{z_{2l}}} \right) \\
& \quad \left( \mu^{w_1^*} \frac{\partial S}{\partial z_{tx}} \mu^{w_1} \langle w_2|w_2\rangle + \langle w_1|w_1\rangle \mu^{w_2^*} \frac{\partial S}{\partial z_{tx}} \mu^{w_2} \right. \\
& \quad \left. + \mu^{w_2^*} \frac{\partial S}{\partial z_{tx}} \mu^{w_1} \langle w_1|w_2\rangle + \langle w_2|w_1\rangle \mu^{w_1^*} \frac{\partial S}{\partial z_{tx}} \mu^{w_2} \right)
\end{aligned}$$

For  $\mu^{w_1}$  and  $\mu^{w_2}$ ,  $z$  and  $w$  are permuted in Equations (3-123) and (3-124).

### 3.4.2.2. Differential by orbital coefficients

The differential by orbital coefficients is expressed against different identifiers  $t$ ,  $s$  like as

$$\frac{\partial}{\partial \mu^{z_{1t}}} \left\langle \psi \left| \frac{\partial \psi}{\partial \mu^{z_{1t}}} \right. \right\rangle - \left\langle \frac{\partial \psi}{\partial \mu^{z_{1t}}} \left| \psi \right. \right\rangle = 0 \tag{3-125}$$

$$= \frac{\partial}{\partial \mu^{z_{1s}}} \left\langle \psi \left| \frac{\partial \psi}{\partial \mu^{z_{1t}}} \right. \right\rangle - \left\langle \frac{\partial \psi}{\partial \mu^{z_{1t}}} \left| \psi \right. \right\rangle \tag{3-126}$$

$$\begin{aligned}
& \frac{\partial}{\partial \mu^{z_2}_s} \left\langle \psi \left| \frac{\partial \psi}{\partial \mu^{z_1}_t} \right\rangle - \left\langle \frac{\partial \psi}{\partial \mu^{z_1}_t} \left| \psi \right\rangle \right. \\
&= 4 \left( \mu^{z_1*} S \frac{\partial \mu^{z_1}}{\partial \mu^{z_1}_t} \mu^{z_2*} S \frac{\partial \mu^{z_2}}{\partial \mu^{z_2}_s} \right. \\
&\quad \left. + \mu^{z_2*} S \frac{\partial \mu^{z_1}}{\partial \mu^{z_1}_t} \mu^{z_1*} S \frac{\partial \mu^{z_2}}{\partial \mu^{z_2}_s} \right) (\langle w_1 | w_1 \rangle \langle w_2 | w_2 \rangle \\
&\quad + \langle w_2 | w_1 \rangle \langle w_1 | w_2 \rangle)
\end{aligned} \tag{3-127}$$

$$\begin{aligned}
& \frac{\partial}{\partial \mu^{w_1}_s} \left\langle \psi \left| \frac{\partial \psi}{\partial \mu^{z_1}_t} \right\rangle - \left\langle \frac{\partial \psi}{\partial \mu^{z_1}_t} \left| \psi \right\rangle \right. \\
&= 4 \left( \mu^{z_1*} S \frac{\partial \mu^{z_1}}{\partial \mu^{z_1}_t} \langle z_2 | z_2 \rangle + \mu^{z_2*} S \frac{\partial \mu^{z_1}}{\partial \mu^{z_1}_t} \langle z_1 | z_2 \rangle \right) \left( \mu^{w_1*} S \frac{\partial \mu^{w_1}}{\partial \mu^{w_1}_s} \langle w_2 | w_2 \rangle \right. \\
&\quad \left. + \mu^{w_2*} S \frac{\partial \mu^{w_1}}{\partial \mu^{w_1}_s} \langle w_1 | w_2 \rangle \right)
\end{aligned} \tag{3-128}$$

$$\begin{aligned}
& \frac{\partial}{\partial \mu^{w_2}_s} \left\langle \psi \left| \frac{\partial \psi}{\partial \mu^{z_1}_t} \right\rangle - \left\langle \frac{\partial \psi}{\partial \mu^{z_1}_t} \left| \psi \right\rangle \right. \\
&= 4 \left( \mu^{z_1*} S \frac{\partial \mu^{z_1}}{\partial \mu^{z_1}_t} \langle z_2 | z_2 \rangle + \mu^{z_2*} S \frac{\partial \mu^{z_1}}{\partial \mu^{z_1}_t} \langle z_1 | z_2 \rangle \right) \left( \langle w_1 | w_1 \rangle \mu^{w_2*} S \frac{\partial \mu^{w_2}}{\partial \mu^{w_2}_s} \right. \\
&\quad \left. + \langle w_2 | w_1 \rangle \mu^{w_1*} S \frac{\partial \mu^{w_2}}{\partial \mu^{w_2}_s} \right)
\end{aligned} \tag{3-129}$$

Differentials of  $U_t^{z_2}, U_t^{w_1}, U_t^{w_2}$  are derived in the similar way.

### 3.4.3. Differential of $G_{t_x}$ by conjugate variables

#### 3.4.3.1. Differential by $z^*$

Next, the differential of  $G_{t_x}$  by conjugate variables is considered as

$$\frac{\partial \check{S}(z_{t_x})}{\partial z_{t_x}^*} = \frac{\partial S}{\partial z_{t_x}^*} \circ \check{G}(z_{t_x}) + S \circ \frac{\partial \check{G}(z_{t_x})}{\partial z_{t_x}^*} \tag{3-130}$$

$$\frac{\partial \check{G}(z_{t_x})}{\partial z_{t_x}^*} = \frac{\partial \tilde{G}(z_{t_x})}{\partial z_{t_x}^*} - \frac{\partial \vec{G}(z_{t_x})}{\partial z_{t_x}^*} \tag{3-131}$$

$$\left(\frac{\partial \check{G}(z_{tx})}{\partial z_{tx}^*}\right)_{mn} = \begin{cases} -\frac{1}{2} & (\text{when } n = t, n \neq m) \\ \frac{2\sqrt{\gamma_n \gamma_m}}{(\gamma_m + \gamma_n)} - \frac{1}{2} & (\text{when } n = t = m) \\ 0 & (\text{when } n \neq t) \end{cases} \quad (3-132)$$

$$\left(\frac{\partial \vec{G}(z_{tx})}{\partial z_{tx}^*}\right)_{mn} = \begin{cases} -\frac{1}{2} & (\text{when } m = t) \\ 0 & (\text{when } m \neq t) \end{cases} \quad (3-133)$$

and for other identifiers

$$\frac{\partial \check{S}(z_{tx})}{\partial z_{ty}^*} = \frac{\partial S}{\partial z_{ty}^*} \circ \check{G}(z_{tx}) + S \circ \frac{\partial \check{G}(z_{tx})}{\partial z_{ty}^*} \quad (3-134)$$

$$\frac{\partial \check{G}(z_{tx})}{\partial z_{ty}^*} = 0 \quad (3-135)$$

$$\therefore \frac{\partial \check{S}(z_{tx})}{\partial z_{ty}^*} = \frac{\partial S}{\partial z_{ty}^*} \circ \check{G}(z_{tx}) \quad (3-136)$$

$$\frac{\partial \check{S}(z_{tx})}{\partial z_{sx}^*} = \frac{\partial S}{\partial z_{sx}^*} \circ \check{G}(z_{tx}) + S \circ \frac{\partial \check{G}(z_{tx})}{\partial z_{sx}^*} \quad (3-137)$$

$$\left(\frac{\partial \check{G}(z_{tx})}{\partial z_{sx}^*}\right)_{mn} = \begin{cases} \frac{2\sqrt{\gamma_n \gamma_m}}{(\gamma_m + \gamma_n)} & (\text{when } n = t, m = s) \\ 0 & (\text{when } n \neq t) \end{cases} \quad (3-138)$$

$$\left(\frac{\partial \vec{G}(z_{tx})}{\partial z_{sx}^*}\right)_{mn} = 0 \quad (3-139)$$

$$\frac{\partial \check{S}(z_{tx})}{\partial z_{sy}^*} = \frac{\partial S}{\partial z_{sy}^*} \circ \check{G}(z_{tx}) \quad (3-140)$$

Total expression of differential is the same as Equation (3-116).

### 3.4.3.2. Differential by orbital coefficients

The differential by orbital coefficients is expressed as

$$\begin{aligned}
& \frac{\partial}{\partial \mu^{z_1 l^*}} \left( \left\langle \psi \left| \frac{\partial \psi}{\partial z_{t_x}} \right. \right\rangle - \left\langle \frac{\partial \psi}{\partial z_{t_x}} \left| \psi \right. \right\rangle \right) \\
&= 4 \left( \frac{\partial \mu^{z_1^*}}{\partial \mu^{z_1 l^*}} \check{S} \mu^{z_1} \langle z_2 | z_2 \rangle + \frac{\partial \mu^{z_1^*}}{\partial \mu^{z_1 l^*}} S \mu^{z_1} \mu^{z_2^*} \check{S} \mu^{z_2} + \mu^{z_2^*} \check{S} \mu^{z_1} \frac{\partial \mu^{z_1^*}}{\partial \mu^{z_1 l^*}} S \mu^{z_2} \right. \\
&\quad \left. + \langle z_2 | z_1 \rangle \frac{\partial \mu^{z_1^*}}{\partial \mu^{z_1 l^*}} \check{S} \mu^{z_2} \right) (\langle w_1 | w_1 \rangle \langle w_2 | w_2 \rangle) \\
&\quad + \langle w_2 | w_1 \rangle \langle w_1 | w_2 \rangle \\
&+ 4 \left( \frac{\partial \mu^{z_1^*}}{\partial \mu^{z_1 l^*}} S \mu^{z_1} \langle z_2 | z_2 \rangle + \langle z_2 | z_1 \rangle \frac{\partial \mu^{z_1^*}}{\partial \mu^{z_1 l^*}} S \mu^{z_2} \right) (\mu^{w_1^*} \check{S} \mu^{w_1} \langle w_2 | w_2 \rangle \\
&\quad + \langle w_1 | w_1 \rangle \mu^{w_2^*} \check{S} \mu^{w_2} + \mu^{w_2^*} \check{S} \mu^{w_1} \langle w_1 | w_2 \rangle \\
&\quad + \langle w_2 | w_1 \rangle \mu^{w_1^*} \check{S} \mu^{w_2})
\end{aligned} \tag{3-141}$$

$$\begin{aligned}
& \frac{\partial}{\partial \mu^{z_2 l^*}} \left( \left\langle \psi \left| \frac{\partial \psi}{\partial z_{t_x}} \right. \right\rangle - \left\langle \frac{\partial \psi}{\partial z_{t_x}} \left| \psi \right. \right\rangle \right) \\
&= 4 \left( \mu^{z_1^*} \check{S} \mu^{z_1} \frac{\partial \mu^{z_2^*}}{\partial \mu^{z_2 l^*}} S \mu^{z_2} + \langle z_1 | z_1 \rangle \frac{\partial \mu^{z_2^*}}{\partial \mu^{z_2 l^*}} \check{S} \mu^{z_2} + \frac{\partial \mu^{z_2^*}}{\partial \mu^{z_2 l^*}} \check{S} \mu^{z_1} \langle z_1 | z_2 \rangle \right. \\
&\quad \left. + \frac{\partial \mu^{z_2^*}}{\partial \mu^{z_2 l^*}} S \mu^{z_1} \mu^{z_1^*} \check{S} \mu^{z_2} \right) (\langle w_1 | w_1 \rangle \langle w_2 | w_2 \rangle) \\
&\quad + \langle w_2 | w_1 \rangle \langle w_1 | w_2 \rangle \\
&+ 4 \left( \langle z_1 | z_1 \rangle \frac{\partial \mu^{z_2^*}}{\partial \mu^{z_2 l^*}} S \mu^{z_2} + \frac{\partial \mu^{z_2^*}}{\partial \mu^{z_2 l^*}} S \mu^{z_1} \langle z_1 | z_2 \rangle \right) (\mu^{w_1^*} \check{S} \mu^{w_1} \langle w_2 | w_2 \rangle \\
&\quad + \langle w_1 | w_1 \rangle \mu^{w_2^*} \check{S} \mu^{w_2} + \mu^{w_2^*} \check{S} \mu^{w_1} \langle w_1 | w_2 \rangle \\
&\quad + \langle w_2 | w_1 \rangle \mu^{w_1^*} \check{S} \mu^{w_2})
\end{aligned} \tag{3-142}$$

For  $\mu^{w_1}$  and  $\mu^{w_2}$ ,  $z$  and  $w$  are permuted in Equations (3-141) and (3-142).

### 3.4.4. Differential of $U_t^i$ by orbital coefficients

#### 3.4.4.1. Differential by $z_{t_x}^*$

Differential of  $U_t^i$  by orbital coefficients is derived in the same way like as

$$\frac{\partial}{\partial z_{t_x}^*} \left( \left\langle \psi \left| \frac{\partial \psi}{\partial \mu^{z_1 l^*}} \right. \right\rangle - \left\langle \frac{\partial \psi}{\partial \mu^{z_1 l^*}} \left| \psi \right. \right\rangle \right) \tag{3-143}$$

$$\begin{aligned}
&= 4 \left( \mu^{z_1^*} \frac{\partial S}{\partial z_{t_x}^*} \frac{\partial \mu^{z_1}}{\partial \mu^{z_{1l}}} \langle z_2 | z_2 \rangle + \mu^{z_1^*} S \frac{\partial \mu^{z_1}}{\partial \mu^{z_{1l}}} \mu^{z_2^*} \frac{\partial S}{\partial z_{t_x}^*} \mu^{z_2} \right. \\
&\quad \left. + \mu^{z_2^*} \frac{\partial S}{\partial z_{t_x}^*} \frac{\partial \mu^{z_1}}{\partial \mu^{z_{1l}}} \langle z_1 | z_2 \rangle + \mu^{z_2^*} S \frac{\partial \mu^{z_1}}{\partial \mu^{z_{1l}}} \mu^{z_1^*} \frac{\partial S}{\partial z_{t_x}^*} \mu^{z_2} \right) \\
&\quad (\langle w_1 | w_1 \rangle \langle w_2 | w_2 \rangle + \langle w_2 | w_1 \rangle \langle w_1 | w_2 \rangle) \\
&+ 4 \left( \mu^{z_1^*} S \frac{\partial \mu^{z_1}}{\partial \mu^{z_{1l}}} \langle z_2 | z_2 \rangle + \mu^{z_2^*} S \frac{\partial \mu^{z_1}}{\partial \mu^{z_{1l}}} \langle z_1 | z_2 \rangle \right) \\
&\quad \left( \mu^{w_1^*} \frac{\partial S}{\partial z_{t_x}^*} \mu^{w_1} \langle w_2 | w_2 \rangle + \langle w_1 | w_1 \rangle \mu^{w_2^*} \frac{\partial S}{\partial z_{t_x}^*} \mu^{w_2} \right. \\
&\quad \left. + \mu^{w_2^*} \frac{\partial S}{\partial z_{t_x}^*} \mu^{w_1} \langle w_1 | w_2 \rangle + \langle w_2 | w_1 \rangle \mu^{w_1^*} \frac{\partial S}{\partial z_{t_x}^*} \mu^{w_2} \right) \\
&\frac{\partial}{\partial z_{t_x}} \left( \left\langle \psi \left| \frac{\partial \psi}{\partial \mu^{z_{2l}}} \right. \right\rangle - \left\langle \frac{\partial \psi}{\partial \mu^{z_{2l}}} \left| \psi \right. \right\rangle \right) \\
&= 4 \left( \mu^{z_1^*} \frac{\partial S}{\partial z_{t_x}^*} \mu^{z_1} \mu^{z_2^*} S \frac{\partial \mu^{z_2}}{\partial \mu^{z_{2l}}} + \langle z_1 | z_1 \rangle \mu^{z_2^*} \frac{\partial S}{\partial z_{t_x}^*} \frac{\partial \mu^{z_2}}{\partial \mu^{z_{2l}}} \right. \\
&\quad \left. + \mu^{z_2^*} \frac{\partial S}{\partial z_{t_x}^*} \mu^{z_1} \mu^{z_1^*} S \frac{\partial \mu^{z_2}}{\partial \mu^{z_{2l}}} + \langle z_2 | z_1 \rangle \mu^{z_1^*} \frac{\partial S}{\partial z_{t_x}^*} \frac{\partial \mu^{z_2}}{\partial \mu^{z_{2l}}} \right) \\
&\quad (\langle w_1 | w_1 \rangle \langle w_2 | w_2 \rangle + \langle w_2 | w_1 \rangle \langle w_1 | w_2 \rangle) \tag{3-144} \\
&+ 4 \left( \langle z_1 | z_1 \rangle \mu^{z_2^*} S \frac{\partial \mu^{z_2}}{\partial \mu^{z_{2l}}} + \langle z_2 | z_1 \rangle \mu^{z_1^*} S \frac{\partial \mu^{z_2}}{\partial \mu^{z_{2l}}} \right) \\
&\quad \left( \mu^{w_1^*} \frac{\partial S}{\partial z_{t_x}^*} \mu^{w_1} \langle w_2 | w_2 \rangle + \langle w_1 | w_1 \rangle \mu^{w_2^*} \frac{\partial S}{\partial z_{t_x}^*} \mu^{w_2} \right. \\
&\quad \left. + \mu^{w_2^*} \frac{\partial S}{\partial z_{t_x}^*} \mu^{w_1} \langle w_1 | w_2 \rangle + \langle w_2 | w_1 \rangle \mu^{w_1^*} \frac{\partial S}{\partial z_{t_x}^*} \mu^{w_2} \right)
\end{aligned}$$

For  $\mu^{w_1}$  and  $\mu^{w_2}$ ,  $z$  and  $w$  are permuted in Equations (3-143) and (3-144).

#### 3.4.4.2. Differential by orbital coefficients

The differential by orbital coefficients is expressed as

$$\begin{aligned}
& \frac{\partial}{\partial \mu^{z_1}_s^*} \left( \left\langle \psi \left| \frac{\partial \psi}{\partial \mu^{z_1}_t} \right\rangle - \left\langle \frac{\partial \psi}{\partial \mu^{z_1}_t} \left| \psi \right\rangle \right) \\
&= 4 \left( \frac{\partial \mu^{z_1^*}}{\partial \mu^{z_1}_s} S \frac{\partial \mu^{z_1}}{\partial \mu^{z_1}_t} \langle z_2 | z_2 \rangle + \frac{\partial \mu^{z_1^*}}{\partial \mu^{z_1}_s} S \mu^{z_2} \mu^{z_2^*} S \frac{\partial \mu^{z_1}}{\partial \mu^{z_1}_t} \right) (\langle w_1 | w_1 \rangle \langle w_2 | w_2 \rangle \\
&\quad + \langle w_1 | w_2 \rangle \langle w_2 | w_1 \rangle) \tag{3-145}
\end{aligned}$$

$$\begin{aligned}
& \frac{\partial}{\partial \mu^{z_2}_s^*} \left( \left\langle \psi \left| \frac{\partial \psi}{\partial \mu^{z_1}_t} \right\rangle - \left\langle \frac{\partial \psi}{\partial \mu^{z_1}_t} \left| \psi \right\rangle \right) \\
&= 4 \left( \mu^{z_1^*} S \frac{\partial \mu^{z_1}}{\partial \mu^{z_1}_t} \frac{\partial \mu^{z_2^*}}{\partial \mu^{z_2}_s} S \mu^{z_2} \right. \\
&\quad \left. + \langle z_1 | z_2 \rangle \frac{\partial \mu^{z_2^*}}{\partial \mu^{z_2}_s} S \frac{\partial \mu^{z_1}}{\partial \mu^{z_1}_t} \right) (\langle w_1 | w_1 \rangle \langle w_2 | w_2 \rangle \\
&\quad + \langle w_1 | w_2 \rangle \langle w_2 | w_1 \rangle) \tag{3-146}
\end{aligned}$$

$$\begin{aligned}
& \frac{\partial}{\partial \mu^{w_1}_s^*} \left( \left\langle \psi \left| \frac{\partial \psi}{\partial \mu^{z_1}_t} \right\rangle - \left\langle \frac{\partial \psi}{\partial \mu^{z_1}_t} \left| \psi \right\rangle \right) \\
&= 4 \left( \mu^{z_1^*} S \frac{\partial \mu^{z_1}}{\partial \mu^{z_1}_t} \langle z_2 | z_2 \rangle + \langle z_1 | z_2 \rangle \mu^{z_2^*} S \frac{\partial \mu^{z_1}}{\partial \mu^{z_1}_t} \right) \left( \frac{\partial \mu^{w_1^*}}{\partial \mu^{w_1}_s} S \mu^{w_1} \langle w_2 | w_2 \rangle \right. \\
&\quad \left. + \frac{\partial \mu^{w_1^*}}{\partial \mu^{w_1}_s} S \mu^{w_2} \langle w_2 | w_1 \rangle \right) \tag{3-147}
\end{aligned}$$

$$\begin{aligned}
& \frac{\partial}{\partial \mu^{w_2}_s^*} \left( \left\langle \psi \left| \frac{\partial \psi}{\partial \mu^{z_1}_t} \right\rangle - \left\langle \frac{\partial \psi}{\partial \mu^{z_1}_t} \left| \psi \right\rangle \right) \\
&= 4 \left( \mu^{z_1^*} S \frac{\partial \mu^{z_1}}{\partial \mu^{z_1}_t} \langle z_2 | z_2 \rangle + \langle z_1 | z_2 \rangle \mu^{z_2^*} S \frac{\partial \mu^{z_1}}{\partial \mu^{z_1}_t} \right) \left( \langle w_1 | w_1 \rangle \frac{\partial \mu^{w_2^*}}{\partial \mu^{w_2}_s} S \mu^{w_2} \right. \\
&\quad \left. + \langle w_1 | w_2 \rangle \frac{\partial \mu^{w_2^*}}{\partial \mu^{w_2}_s} S \mu^{w_1} \right) \tag{3-148}
\end{aligned}$$

These ways of formulations are the same when  $s = t$ . Differentials of  $U_t^{z_2}, U_t^{w_1}, U_t^{w_2}$  are also derived in the similar way.

#### 4. Ground state of H<sub>2</sub> molecule

In this chapter, the simulation results for H<sub>2</sub> molecule using the theory in Chapter 1 will be shown and discussed. A flow chart of the simulation is shown in Figure 4-1. First I will show results of optimization to ground-state of electron-nuclear wave function of H<sub>2</sub> molecule. Next the vibrational period of molecule at ground-state will be discussed.

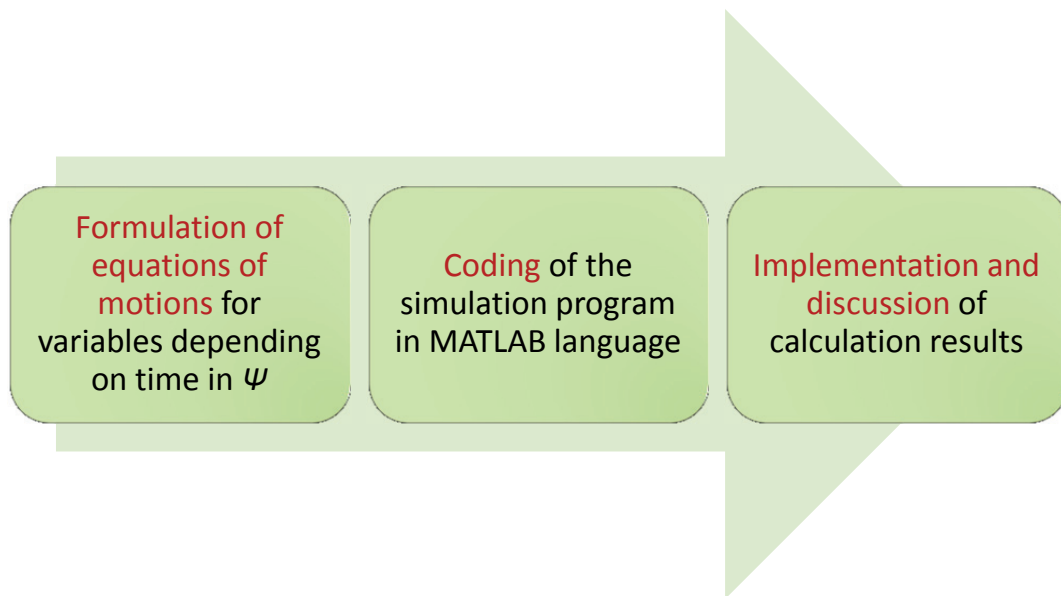


**Figure 4-1** The flow chart of the simulation. Formulation of equations of motions was shown in Chapter 2 and 3. I coded the simulation program along the formulae in MATLAB language. Then the Implementation and discussion of calculation results will be shown in this chapter and next chapter.

#### 4.1. Optimization to ground-state

##### 4.1.1. Gradient descent

##### 4.1.1.1. Case of $M = 4$

First, the number of Gaussians  $M$  is set 4 to assign one basis to each particle to consider the simplest case. For initial value sets, the widths of Gaussian  $\gamma$  are set as

$$\gamma = (0.7 \quad 0.7 \quad 30 \quad 30) . \quad (4-1)$$

The initial positions of Gaussians  $q$  are

$$q = \begin{pmatrix} 0.7 & -0.7 & 0.7 & -0.7 \\ 0 & 0 & 0 & 0 \\ 0 & 0 & 0 & 0 \end{pmatrix}, \quad (4-2)$$

and the initial momenta of Gaussians  $p$  are

$$p = \begin{pmatrix} 0 & 0 & 0 & 0 \\ 0 & 0 & 0 & 0 \\ 0 & 0 & 0 & 0 \end{pmatrix}. \quad (4-3)$$

where in Equations (4-2) and (4-3) rows are related to the number of Gaussians and columns are related to spatial coordinates  $x, y$  and  $z$ .

Orbital coefficients of 4 particles are set as

$$\mu^{z_1} = (1 \ 0 \ 0 \ 0)^t, \quad (4-4)$$

$$\mu^{z_2} = (0 \ 1 \ 0 \ 0)^t, \quad (4-5)$$

$$\mu^{w_1} = (0 \ 0 \ 1 \ 0)^t, \quad (4-6)$$

$$\mu^{w_2} = (0 \ 0 \ 0 \ 1)^t. \quad (4-7)$$

Figure 4-2 shows the variation of total energy with orbital coefficients fixed through the iterations of GDM optimizing the label of the complex number  $z$  of Gaussians. Here the total energy is converged to  $H = -0.9414$  a.u.

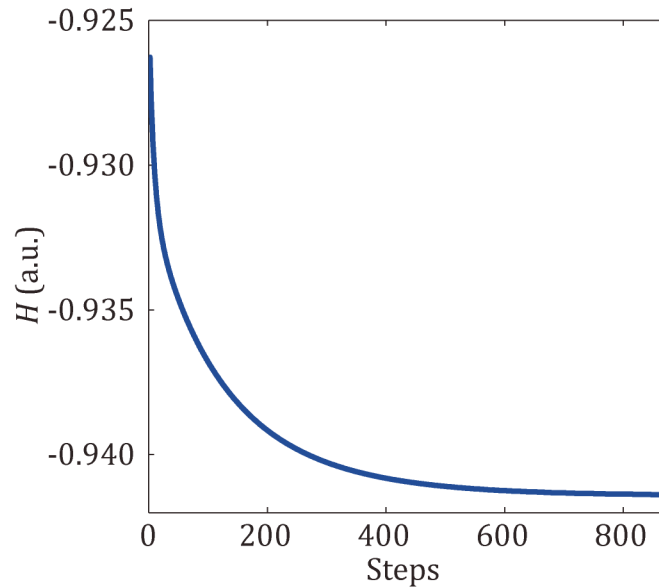


**Figure 4-2** The variation of total energy at  $M = 4$  for steps of gradient descent

### optimization.

After the optimization, the positions of Gaussians  $q$  are

$$q = \begin{pmatrix} 0.6857 & -0.6857 & 0.7932 & -0.7932 \\ 0 & 0 & 0 & 0 \\ 0 & 0 & 0 & 0 \end{pmatrix}, \quad (4-8)$$

and the momenta of Gaussians  $p$  are

$$p = \begin{pmatrix} 0 & 0 & 0 & 0 \\ 0 & 0 & 0 & 0 \\ 0 & 0 & 0 & 0 \end{pmatrix}. \quad (4-9)$$

where the width of optimization step  $\beta$  in Equation (2-74) was 0.1.

#### 4.1.1.2. Case of $M = 10$

Next, the number of Gaussians  $M$  is set 10 to assign one basis to one proton and 4 bases to one electron. For initial value sets, the widths of Gaussian  $\gamma$  are set as

$$\gamma = (0.64 \quad 18 \quad 0.16 \quad 2.7 \quad 0.64 \quad 18 \quad 0.16 \quad 2.7 \quad 60 \quad 60). \quad (4-10)$$

where the widths for electrons are selected to match with those of 6-31G basis set.

The initial positions of Gaussians  $q$  are

$$q = \begin{pmatrix} 0.691 & 0.691 & 0.691 & 0.691 & -0.691 & -0.691 & -0.691 & -0.691 & 0.7 & -0.7 \\ 0 & 0 & 0 & 0 & 0 & 0 & 0 & 0 & 0 & 0 \\ 0 & 0 & 0 & 0 & 0 & 0 & 0 & 0 & 0 & 0 \end{pmatrix} \quad (4-11)$$

and the initial momenta of Gaussians  $p$  are

$$p = \begin{pmatrix} 0 & 0 & 0 & 0 & 0 & 0 & 0 & 0 & 0 & 0 \\ 0 & 0 & 0 & 0 & 0 & 0 & 0 & 0 & 0 & 0 \\ 0 & 0 & 0 & 0 & 0 & 0 & 0 & 0 & 0 & 0 \end{pmatrix} \quad (4-12)$$

where in Equations (4-11) and (4-12) rows are related to the number of Gaussians and columns are related to spatial coordinates  $x$ ,  $y$  and  $z$ .

Orbital coefficients of 4 particles are set as

$$\mu^{z_1} = (0.8 \quad 0.06 \quad 0.3 \quad 0.2 \quad 0.05 \quad 0 \quad 0 \quad 0 \quad 0 \quad 0)^t \quad (4-13)$$

$$\mu^{z_2} = (0.05 \quad 0 \quad 0 \quad 0 \quad 0.8 \quad 0.06 \quad 0.3 \quad 0.2 \quad 0 \quad 0)^t \quad (4-14)$$

$$\mu^{w_1} = (0 \quad 0 \quad 1 \quad 0)^t \quad (4-15)$$

$$\mu^{w_2} = (0 \quad 0 \quad 1)^t \quad (4-16)$$

For this initial value set, the total energy was

$$H = -1.0346 \text{ a. u. .} \quad (4-17)$$

For these initial values, parameters were optimized with GDM except for widths  $\gamma$ .

After the optimization, the positions of Gaussians  $q$  are

$$q = \begin{pmatrix} 0.6469 & 0.6905 & 0.6680 & 0.6524 & -0.6469 & -0.6905 & -0.6680 & -0.6524 & 0.7072 & -0.7072 \\ 0 & 0 & 0 & 0 & 0 & 0 & 0 & 0 & 0 & 0 \\ 0 & 0 & 0 & 0 & 0 & 0 & 0 & 0 & 0 & 0 \end{pmatrix} \quad (4-18)$$

and the momenta of Gaussians  $p$  are

$$p = \begin{pmatrix} 0 & 0 & 0 & 0 & 0 & 0 & 0 & 0 & 0 & 0 \\ 0 & 0 & 0 & 0 & 0 & 0 & 0 & 0 & 0 & 0 \\ 0 & 0 & 0 & 0 & 0 & 0 & 0 & 0 & 0 & 0 \end{pmatrix}. \quad (4-19)$$

Orbital coefficients of 4 particles after optimization are

$$\mu^{z_1} = (0.7793 \quad 0.0381 \quad 0.2702 \quad 0.2993 \quad 0.0281 \quad 0.0102 \quad -0.0208 \quad 0.0617 \quad -0.0014 \quad 0.0009)^t \quad (4-20)$$

$$\mu^{z_2} = (0.0281 \quad 0.0102 \quad -0.0208 \quad 0.0617 \quad 0.7793 \quad 0.0381 \quad 0.2702 \quad 0.2993 \quad 0.0009 \quad -0.0014)^t \quad (4-21)$$

$$\mu^{w_1} = (-0.0001 \quad 0.0229 \quad -0.0002 \quad 0.0075 \quad -0.0002 \quad 0.0002 \quad -0.0000 \quad -0.0011 \quad 0.9997 \quad 0.0000)^t \quad (4-22)$$

$$\mu^{w_2} = (-0.0002 \quad 0.0002 \quad -0.0000 \quad -0.0011 \quad -0.0001 \quad 0.0229 \quad -0.0002 \quad 0.0075 \quad 0.0000 \quad 0.9997)^t \quad (4-23)$$

The total energy was optimized to

$$H = -1.0649 \text{ a. u.} \quad (4-24)$$

where the width of optimization step  $\beta$  in Equation (2-74) was 0.05. The end condition of the optimization was when the norm of gradients of parameter is less than 0.01 but the convergence was slow near this norm. Then the optimization was stopped before the end condition was satisfied.

## 4.1.2. Imaginary time propagation

### 4.1.2.1. With orbital coefficients fixed

#### 4.1.2.1.1. Case of $M = 4$

First, the number of Gaussians  $M$  is set 4 in the same way as GDM. Orbital coefficients are fixed through the time propagation in this section. Initial values are set in the same values as GDM case.

Figure 4-3 shows the time variation of total energy with orbital coefficients fixed through the ITP optimizing the label of the complex number  $z$  of Gaussians in the same way as GDM. Here the total energy is converged to  $H = -0.9414$  a.u. Figure 4-4 shows variations of the center positions of the Gaussian bases. The red lines represent

the positions of the Gaussian bases of the nuclei and the blue lines represent the positions of electrons. The Gaussian bases were set symmetrically with respect to  $x = 0$  on the  $x$ -axis. We can see that the motions of protons are slower than that of electrons and electrons are converging to their ground-state against the positions of protons at that time and after that moving synchronously with protons.

After the optimization, the positions of Gaussians  $q$  are

$$q = \begin{pmatrix} 0.6921 & -0.6921 & 0.7993 & -0.7993 \\ 0 & 0 & 0 & 0 \\ 0 & 0 & 0 & 0 \end{pmatrix}, \quad (4-25)$$

and the momenta of Gaussians  $p$  are

$$p = \begin{pmatrix} 0 & 0 & 0 & 0 \\ 0 & 0 & 0 & 0 \\ 0 & 0 & 0 & 0 \end{pmatrix}. \quad (4-26)$$

The values of Equation (4-25) are slightly different from those of GDM in Equation (4-8) and this would be the optimization of GDM was not completely converged yet.

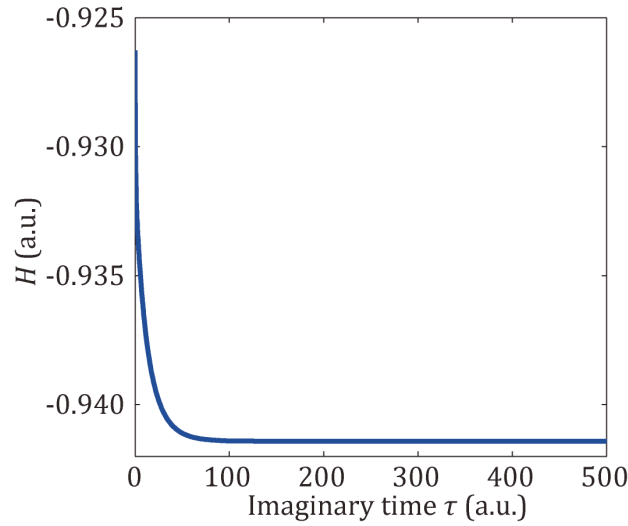


**Figure 4-3** The time variation of total energy at  $M = 4$  for imaginary time propagation.

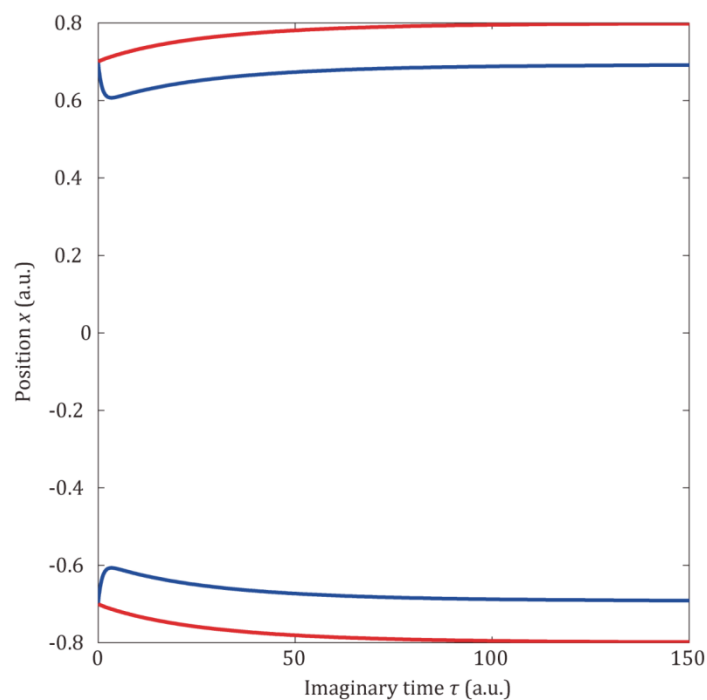


**Figure 4-4 Variations of the center positions of Gaussian bases developed for imaginary time at  $M = 4$ . The red lines represent the bases of the nuclei and the blue lines represent the bases of electrons.**

Figure 4-5 shows the comparison of calculation time of GDM and ITP. For GDM, the steps in Figure 4-2 were normalized by total calculation time assuming that the calculation time for each step was the same. For ITP the calculation time was treated in the same way. Figure 4-6 shows the comparison of difference of total energy and convergence value in the log scale. Here the convergence speed is faster in ITP but the order of the convergence speed was the same in GDM and ITP. Straight lines in Figure 4-6 indicate that the convergence speed against the calculation time was in the exponential order.

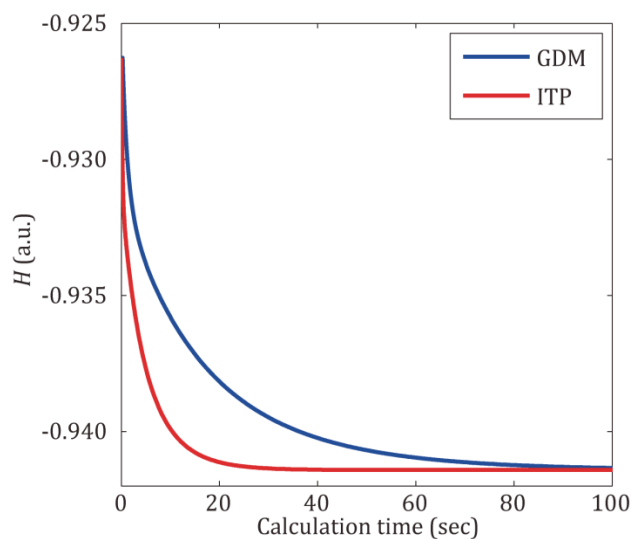


**Figure 4-5 Comparison of total energy against calculation time of GDM and ITP.**

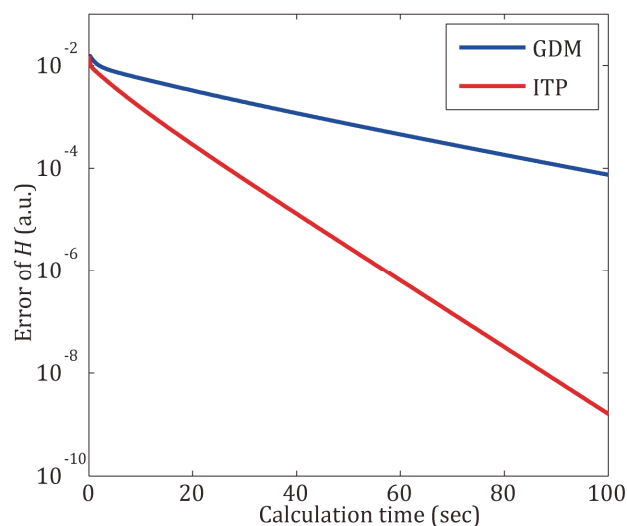


**Figure 4-6 Comparison of difference of total energy and convergence value against calculation time of GDM and ITP in the log scale.**

#### 4.1.2.1.2. Case of $M = 10$

In the optimization of ITP at  $M = 10$ , the values after the GDM optimization in Equations (4-18) to (4-23) are set as initial values for this optimization. In this section the orbital coefficients are fixed and the complex number label  $z$  of Gaussians are optimized. The time variations of the center positions of the Gaussian bases at this ITP iteration are shown in Figure 4-7.

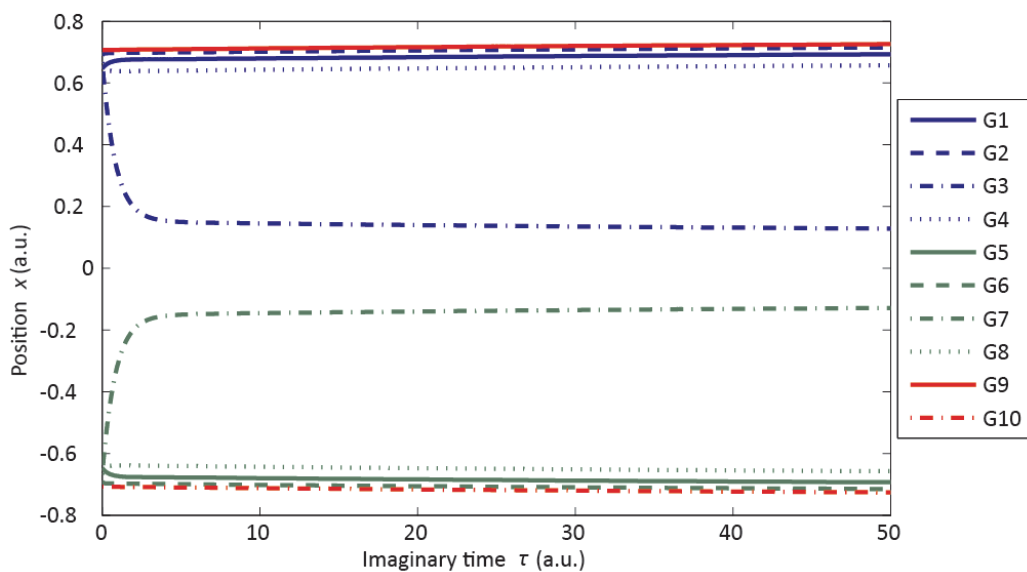


**Figure 4-7 Variations of the center positions of Gaussian bases developed for imaginary time. 10 bases were used for the system and set symmetrically with respect to  $x = 0$  on the  $x$ -axis.**

The convergence profile of the total energy in ITP is shown in Figure 4-8.  $H$  decreases towards  $-1.0665$  a. u.

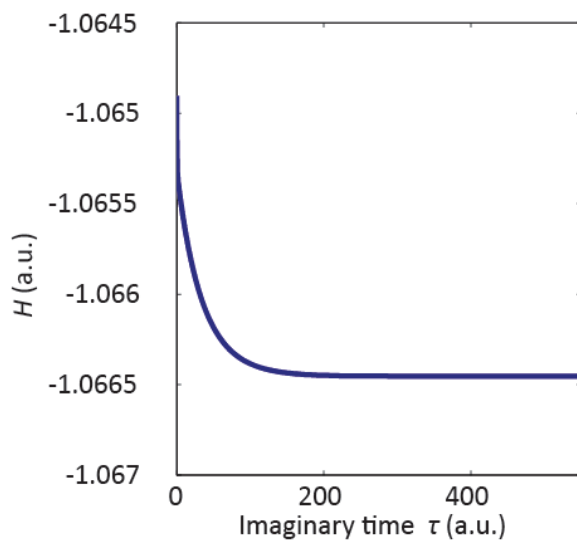


**Figure 4-8 The time variation of total energy at  $M = 10$  for imaginary time propagation.**

#### 4.1.2.2. With orbital coefficients varied

In above sections, the optimization with orbital coefficients fixed was discussed and in this section the orbital coefficients are also optimized. Initial values are set at the values after optimization in section 4.1.2.1.2 and the number of basis is reduced to  $M=9$ . The reduced bases are G3 and G7 of width  $\gamma = 0.16$  in Figure 4-7 and they are united to one basis of width  $\gamma = 0.16$  locating on  $x = 0$ . This is because the optimization will be failed down without removing these two bases. If the orbital coefficients are allowed to be varied in optimization, G3 and G7 will come close to  $x = 0$  and eventually the tensor  $c_{ij}$  in Equation (2-12) will get irreversible because bases of the same widths locate at the same place and the rank of  $c_{ij}$  is not enough. Then we cannot solve the EOMs Equation (2-18) and the calculation breaks down. To avoid this singularity, the two Gaussians are united to one.

The time variations of the center positions of the Gaussian bases at this ITP iteration are shown in Figure 4-9. the protonic and electronic Gaussians are optimized in different time scale. In the same way as the optimizations of ITP above, the electronic Gaussians are optimized within 10 a.u. to the electronic ground state and moving slowly with nuclear Gaussians. These different time scales originate from physical difference of mass for protons and electrons. The effect of difference of mass also appears in the time scale of dynamics for imaginary time.

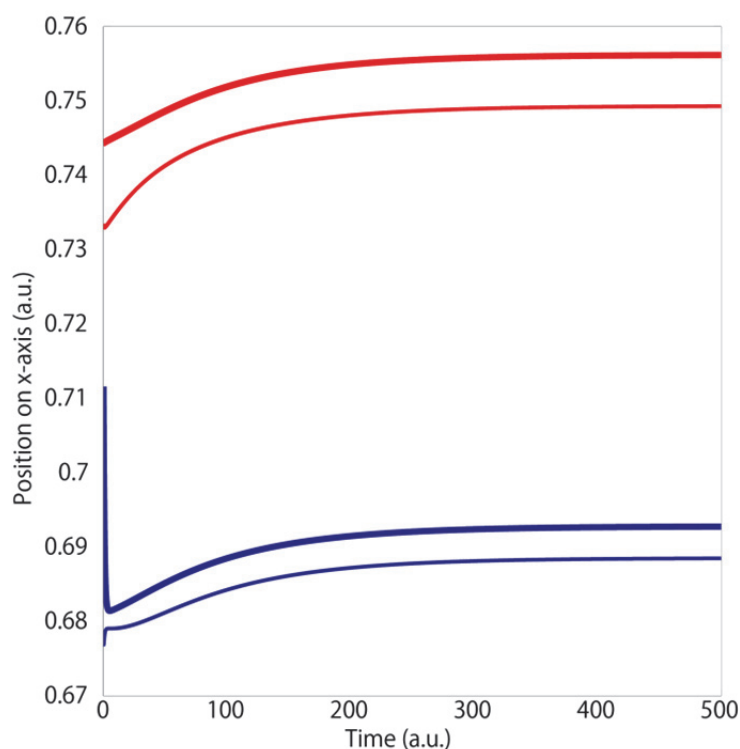


**Figure 4-9 Variations of the center positions of Gaussian bases developed for imaginary time. 9 bases were used for the system and set symmetrically with respect to  $x = 0$  on the  $x$ -axis. The region of  $x$ -axis between 0.67 and 0.76 a.u. is expanded on the figure and 4 bases are shown here. Another basis for electron locates at  $x = 0$ . Red lines represent nuclear bases and blue lines represent electronic bases.**

The detail of coefficients of the orbitals after this ITP optimization and related positions on  $x$ -axis and width  $\gamma$  are shown in Table 4-1. The coefficients of the orbitals and center positions of Gaussians are optimized through the ITP iteration and  $\gamma$  is fixed.

The convergence profile of the total energy in ITP is shown in Figure 4-10. The total energy was converged to  $-1.0684$  a.u. at  $\tau = 500$  a.u. from  $-1.0665$  a.u. in section 4.1.2.1.2. Figure 4-11 shows 2-dimensional density maps of protons and electrons of the electron-nuclear wave function after the optimization. We can see the keen separated peaks for protons and density like broad crowd for electrons. The EOMs are totally symmetric for electrons and protons except for the mass, so the

difference of mass is inducing the different structures for electrons and protons.

Figure 4-12 shows the additional information of the 1-dimensional density map of protons. There is a previous work<sup>1)</sup> indicating the 1D density map of nuclei of H<sub>2</sub> by NOMO/HF method for the optimizing calculation of the static ground state. By comparing these results, we can see the same density map structure. This indicates that the ITP optimization from the time-dependent EOMs results at the consistent state with that from the ground state calculation by optimization method for static state with NOMO/HF method.

**Table 4-1 Detail of the values of the orbital coefficients, position, and widths of nine Gaussians after optimization at Figure 4-9**

	electron1	electron2	proton1	proton2	Position on x axis	Width y
<b>G1</b>	1	0.020706	0.010425	-0.00223	0.6927	0.64
<b>G2</b>	0.040195	0.017089	0.287161	-0.00064	0.7493	18
<b>G3</b>	0.357373	0.357373	-0.00205	-0.00205	0	0.16
<b>G4</b>	0.404203	0.050135	-0.02962	0.002468	0.6885	2.7
<b>G5</b>	0.020706	1	-0.00223	0.010425	-0.6927	0.64
<b>G6</b>	0.017089	0.040195	-0.00064	0.287161	-0.7493	18
<b>G7</b>	0.050135	0.404203	0.002468	-0.02962	-0.6885	2.7
<b>G8</b>	-0.00034	-0.00088	1	0.000142	0.7562	60
<b>G9</b>	-0.00088	-0.00034	0.000142	1	-0.7562	60

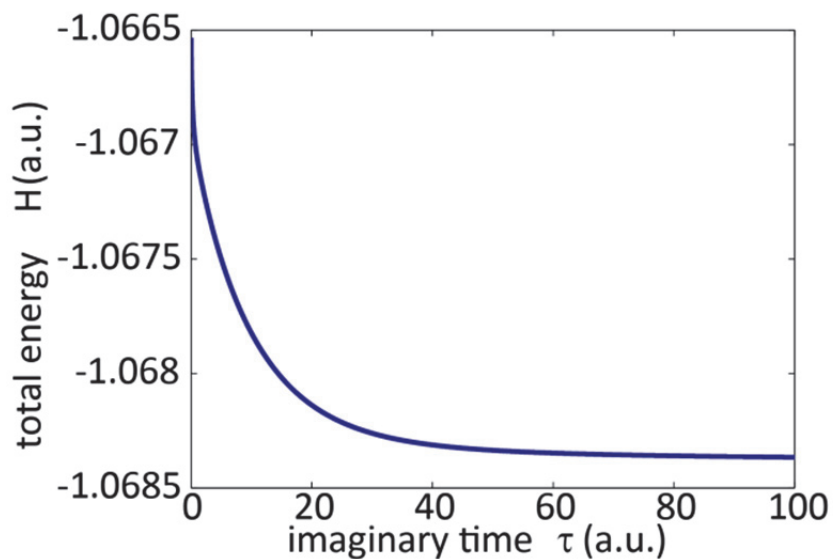


Figure 4-10 Variation of the total energy  $H = \langle \Psi | \hat{H} | \Psi \rangle$  in imaginary time. The total energy converges towards the energy of the electron-nuclear ground state.

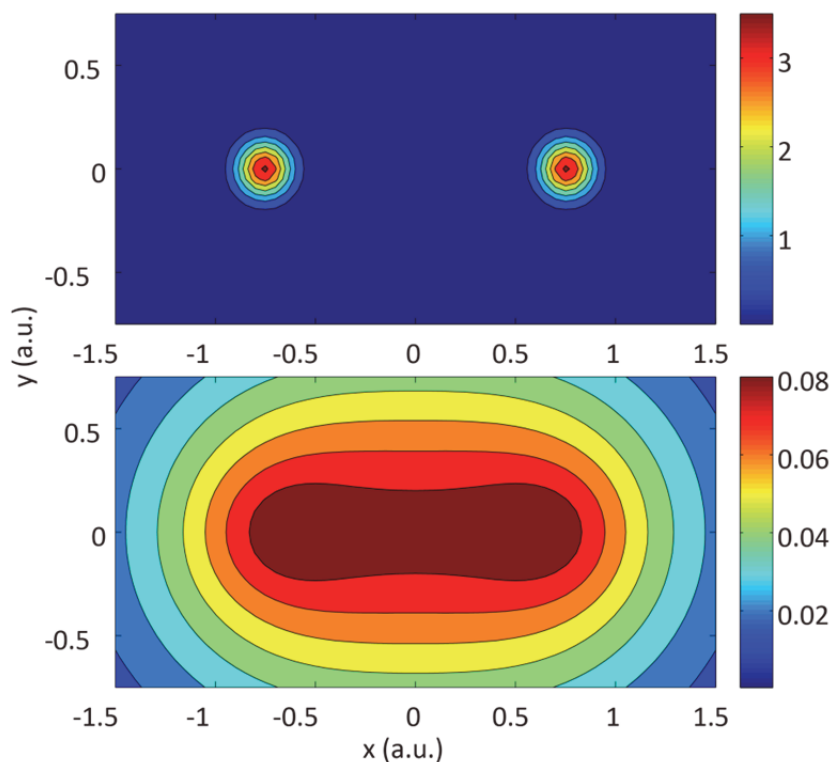
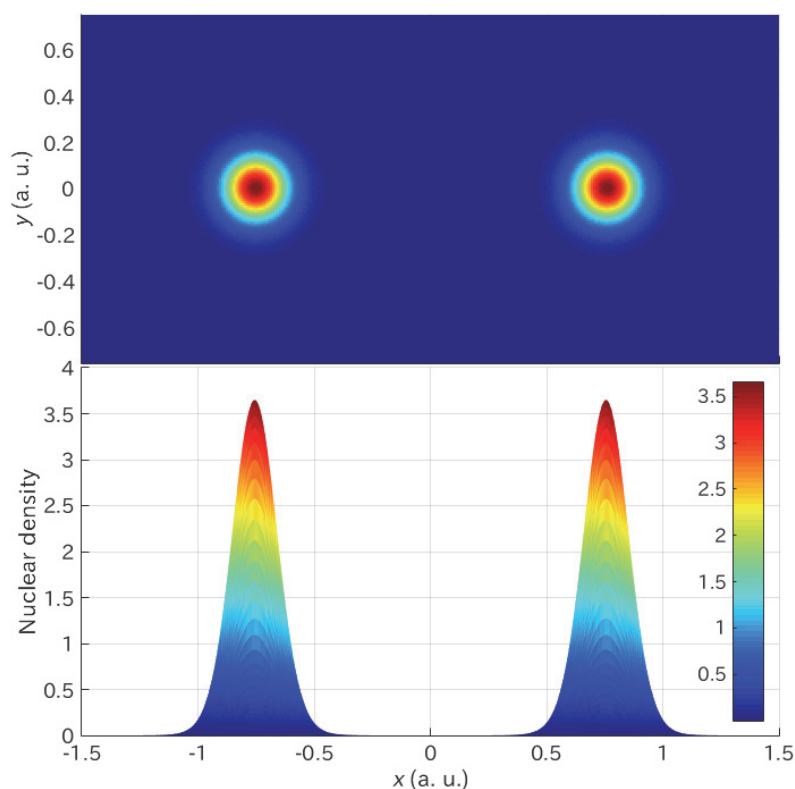


Figure 4-11 2-dimensional density maps of protons and electrons of the optimized electron-nuclear wave function. The upper row shows 2D density of nuclei and the lower row shows 2D density of electrons.



**Figure 4-12 2-dimensional and 1-dimensional density maps of protons of the optimized electron-nuclear wave function. The upper row shows 2D density of nuclei and the lower row shows 1D density of nuclei.**

### 4.1.3. Discussion for ground-state wave function

In section 4.1.2.1, the ground-state energy was obtained  $H = -0.9414$  a.u. for  $M = 4$  case and  $H = -1.0665$  a.u. for  $M = 10$  case. In aspect of variational principle, the total energy should be smaller for larger number of parameters and these values are reflecting this principle. Compared to those cases, in section 4.1.2.2 the orbital coefficients are allowed to be varied. In that case, the total energy is  $H = -1.0684$  a.u. for  $M = 9$  case. Even the number of bases decreased but the energy gets further smaller. It suggests that the  $M = 10$  is not large number enough for the energy optimization and allowing orbital coefficients to change the energy can be more optimized with less number of Gaussians. However, in Born-Openheimer

approximation the energy of H<sub>2</sub> molecule is obtained as  $H = -1.174$  a.u.<sup>2)</sup> and this value is smaller than that we obtained in this study. The difference of energy between wave function under Born-Oppenheimer approximation and electron-nuclear wave function should be only zero-point energy of molecular potential in Born-Oppenheimer picture. This difference is too large for zero-point energy. It is described by the problem of expression of electron-nuclear wave function with Gaussians. The ground-state energy for electron-nuclear wave function is reported by previous research<sup>3)</sup>. In this research, the formulation of wave function in the present research is categorized as translation and rotation-contaminated (TRC)-NOMO. In the formulation of electron-nuclear wave function, the coordinates for translational motion can be separated converting the coordinates in the wave function such as,

$$\Psi_{\text{total}} = \Psi_{\text{tr}}\Psi_{\text{tf}} , \quad (4-27)$$

where  $\Psi_{\text{tr}}$  is wave function for translational motion and  $\Psi_{\text{tf}}$  is wave function for translation free part. This formulation is categorized as translation-free (TF)-NOMO and the ground-state energy is  $H = -1.073631$  a.u. In this previous research, the energy of TRC-NOMO is reported as  $H = -1.051219$  a.u. The value of present research is slightly lower than this value. The slight improvement may be ascribed to the optimization in the position of the Gaussian functions. Indeed, in another previous research for NOMO, the energy of H<sub>2</sub> molecule is reported as  $H = -1.069$  a.u.<sup>4)</sup> in the framework of TRC-NOMO. This value agrees with the energy of  $H = -1.0684$  a.u. in the previous research.

However in the scheme of TF-NOMO, the energy is still high. In a previous research using explicitly correlated Gaussian (ECG) as basis function, the energy of H<sub>2</sub> is reported as  $H = -1.164$  a.u.<sup>5)</sup>. Explicitly correlated Gaussian involves explicitly correlated term for 2 particles 1, 2 like as  $\exp(r_1 r_2)$ . It is necessary to achieve this value to use 512 terms and there is also difficulty to formulate the wave function. The biggest problem is that the calculation cost is in proportion to  $M!$  ( $M$  is the total number of basis). The time complexity for ECG is factorial time and it is very slow as well as Grid method. There is the tradeoff between accuracy and calculation time.

The CCS method resulted in slightly higher energy but could achieve almost limit value for TRC-NOMO only with  $M = 9$ . The strongest point of the CCS method is polynomial time complexity. When we consider the time-dependent molecular dynamics, the time complexity is the critical issue. From next section, the real time propagation will be simulated and discussed.

## 4.2. Time-dependent dynamics

### 4.2.1. Real time propagation with orbital coefficients fixed

#### 4.2.1.1. Case of $M = 4$

Next, the real time propagation will be considered. First, at  $M = 4$  case, initial values are set at the values after ITP optimization in section 4.1.2.1.1. Figure 4-13 shows the variation of the center positions of Gaussians for real time propagation. We can see that the center positions settle at the initial positions. The optimized ground-state is an equilibrium state for the parameters and they do not change in real time propagation. The calculation results reflect that appropriately.

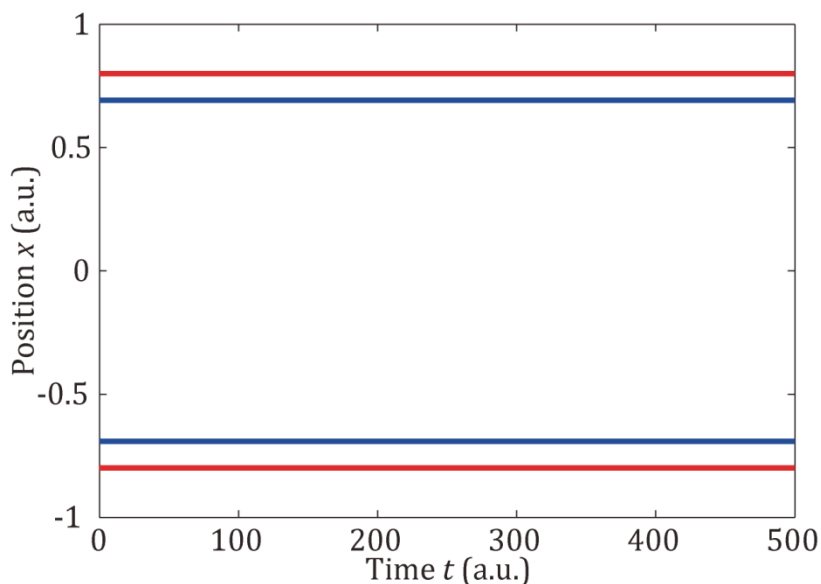


**Figure 4-13** Variations of the center positions of Gaussian bases developed for real time at  $M = 4$ . The red lines represent the bases of the nuclei and the blue lines represent the bases of electrons.

Second, a trajectory from initial values out of the equilibrium point is simulated to examine dynamics when electrons have momenta. The initial values are like below. The initial positions of Gaussians  $q$  are

$$q = \begin{pmatrix} 0.75 & -0.75 & 0.7 & -0.7 \\ 0 & 0 & 0 & 0 \\ 0 & 0 & 0 & 0 \end{pmatrix}, \quad (4-28)$$

and the momenta of Gaussians  $p$  are

$$p = \begin{pmatrix} 0 & 0 & 0 & 0 \\ 0.1 & -0.1 & 0 & 0 \\ 0 & 0 & 0 & 0 \end{pmatrix}. \quad (4-29)$$

Figure 4-14 shows the variation of the center positions of Gaussians for real time propagation. We can see the periodic motion of protons and electrons.

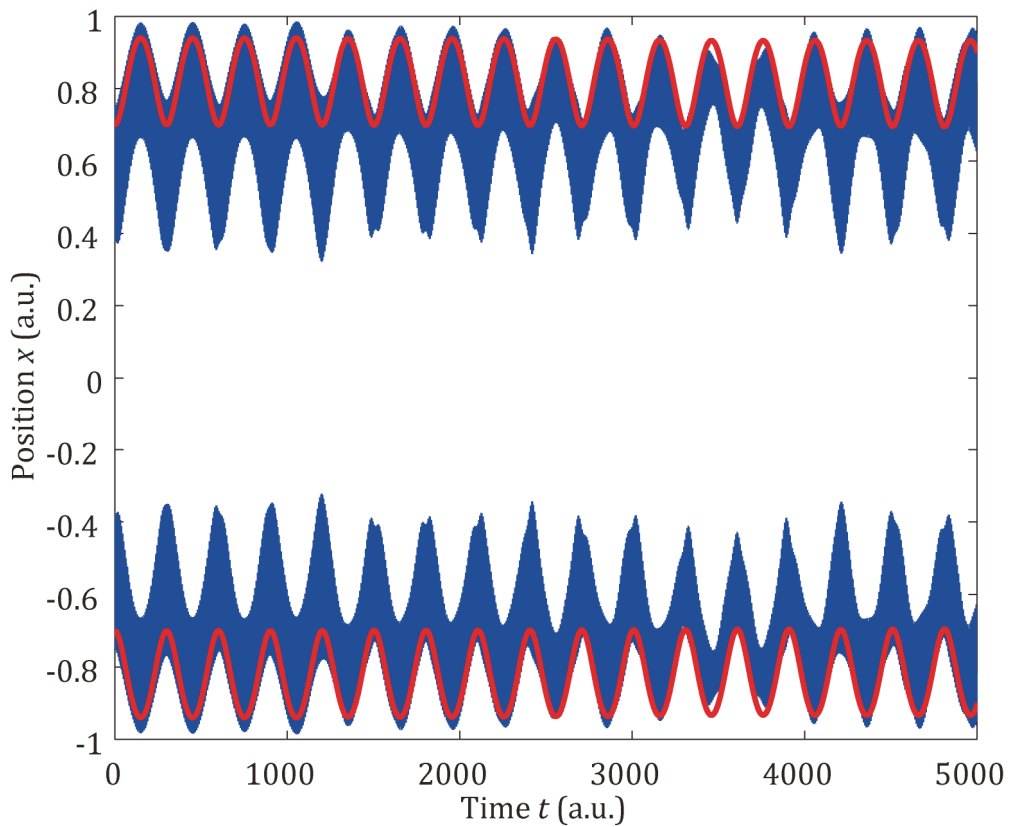


**Figure 4-14 Variations of the center positions of Gaussians for real time propagation at  $M = 4$  with electronic initial momenta. The red lines represent the bases of the nuclei and the blue lines represent the bases of electrons.**

The motions of electrons are not completely periodic and their complexity of 4 particle problem shows up. Only 4 bases are used and orbital coefficients are fixed so apparently the motions of center positions are like classic motion but stable motions after 5000 a.u. are difficult to implement in classical calculation even if soft-core potential is introduced. Then this method can achieve the stable chemical bond with the least number of basis functions.

#### **4.2.1.2. Case of $M = 10$**

Next to the equilibrium state, the real time propagation was calculated and the nuclear motion was examined with a vibrational period at  $M = 10$  case. As a vibrationally excited state, the state 50 a.u. of imaginary time after the initial state in ITP in Figure 4-7 was chosen, and a vibrational motion of nuclei can be observed through time propagation of this state for real time space. Figure 4-15 shows the time variations of center positions of Gaussian bases in real time propagation. The meaning of symbol is the same as in Figure 4-7 and the same coefficients of orbitals were applied. From the numbers of Equation (4-20) to (4-23), it can be considered that G9 and G10 represent the nuclear part of the wave function. Then the red lines of G9 (solid) and G10 (dashed) represent the motions of nuclei. Figure 4-16 shows the expanded motion of G9 and the oscillation of the small amplitude with the period of 299 a.u. (7.2 fs) can be seen.

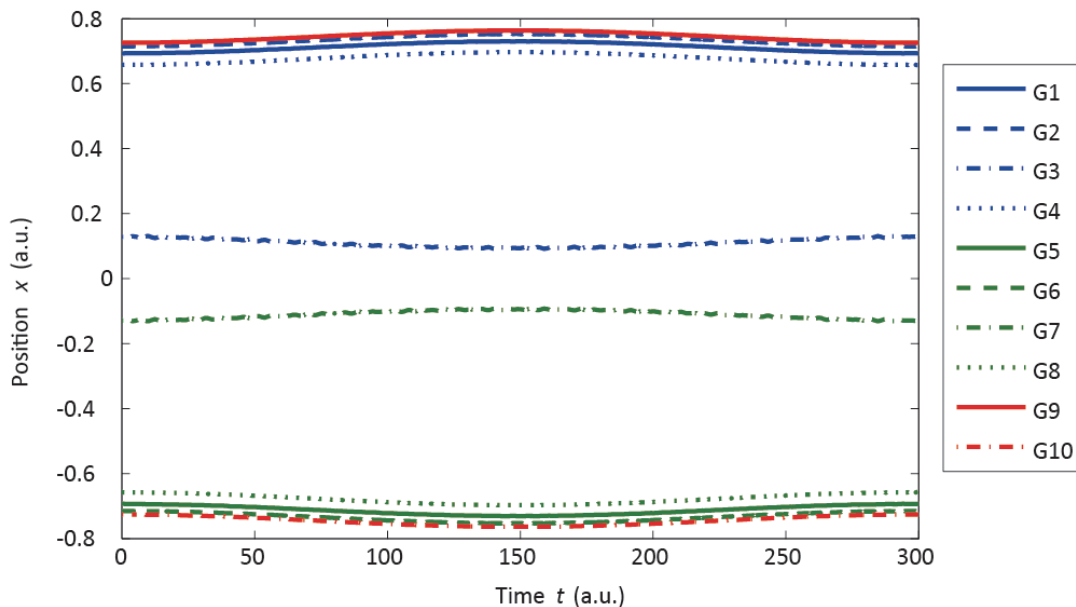


**Figure 4-15** Variations of the center positions of the Gaussian bases in real time. The initial positions of bases are the same as those at  $\tau = 50$  a.u. in Figure 4-7. The coefficients of orbitals are shown in Equation (4-20) to (4-23). The coefficients were fixed through the iterations.

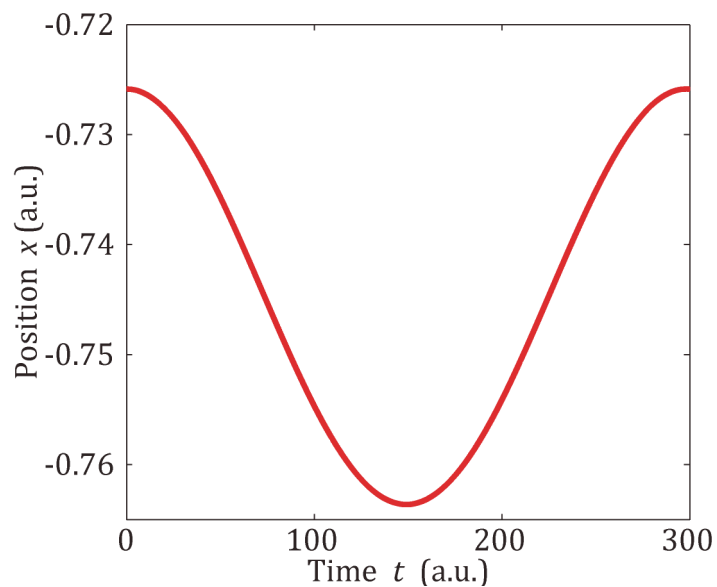


**Figure 4-16** Expansion of the motion of G9 in Figure 4-15.

Figure 4-17 shows the expanded motion of G1 and the oscillation of the electron with

the period of around 2 a.u. (50 as) can be seen. The faster oscillation reflects the lighter weight of electron than that of nucleus.

Figure 4-18 shows the variation of total energy in real time propagation. The variation of value starts from the 8<sup>th</sup> decimal place. The accuracy of Runge-Kutta method is set at under  $10^{-6}$  per step and this variation is less than the error of Runge-Kutta. This indicates that the total energy is correctly conserved through the calculation.

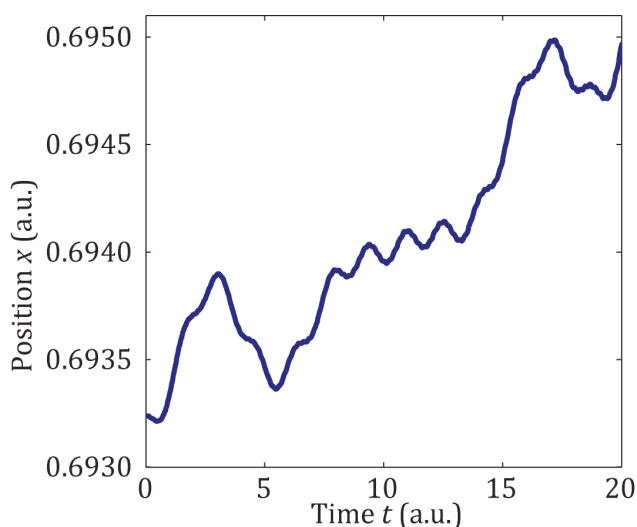


Figure 4-17 Expansion of the motion of G1 in Figure 4-15.

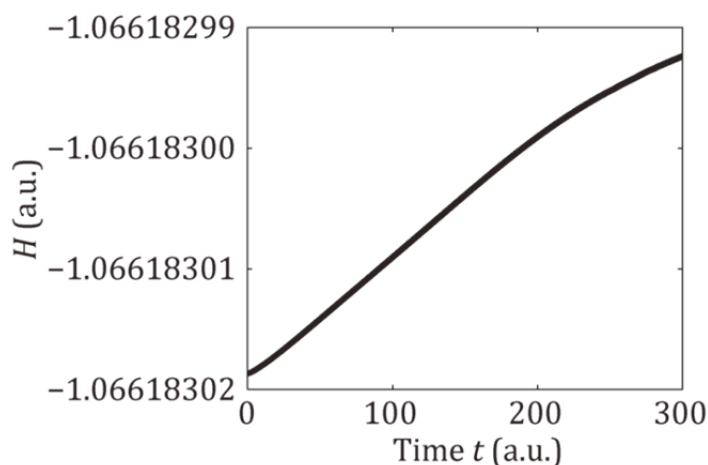


Figure 4-18 Variation of total energy in real time propagation at  $M = 10$

#### 4.2.2. Real time propagation with orbital coefficients varied

In this section, real time propagation with orbital coefficients varied at  $M = 9$  will be simulated. A vibrational period of the ground state of  $H_2$  molecule is estimated in the following manner. By displacing the optimized positions of the respective Gaussian functions by 0.001 a.u. symmetrically with respect to  $x = 0$ , a small amplitude can be induced molecular vibration since the optimized ground-state is a stationary state as we saw in above sections. But in this situation, the electrons are not necessarily in the electronic ground state. The expanded region for the center positions of Gaussians of nuclei and electrons are shown in Figure 4-19 and Figure 4-20. We can see relatively large amplitude of vibration of electrons compared to nuclei. So ITP optimization for 15 a.u. time is executed after displacing and parameters at that time are set at initial values. Then from the different time scale for convergence as seen in Figure 4-9, vibrational excited state with electronic ground state can be achieved.

A vibrational motion of nuclei can be observed through time propagation of this state for real time space. Figure 4-21 and Figure 4-22 show the time variations of center positions of Gaussian bases in real time propagation. Figure 4-21 shows the expanded region for the center positions of protonic Gaussians. Figure 4-22 also shows the time variations of center positions of electronic Gaussians. We can see that the vibrations of electrons are suppressed compared with Figure 4-20 but there are the several components of vibrational periods for nuclei and electrons. The longest period of synchronous motion for electrons and protons is 340 a.u. (8.2 fs) and this value is consistent with the vibrational period of  $H_2$ , 331 a.u. (8.0 fs), obtained from the energy difference between the first vibrationally excited state ( $v' = 1, J' = 0$ ) and the vibrational ground state ( $v'' = 0, J'' = 0$ ) of  $H_2$  in the electronic ground state obtained spectroscopically<sup>6)</sup>. We can also see faster time periods<sup>6)</sup> in addition to the same long time periods for nuclear vibration. Those faster vibrational periods are considered as those related to the electronic excitation. The electronic excitation is discussed in the next section.

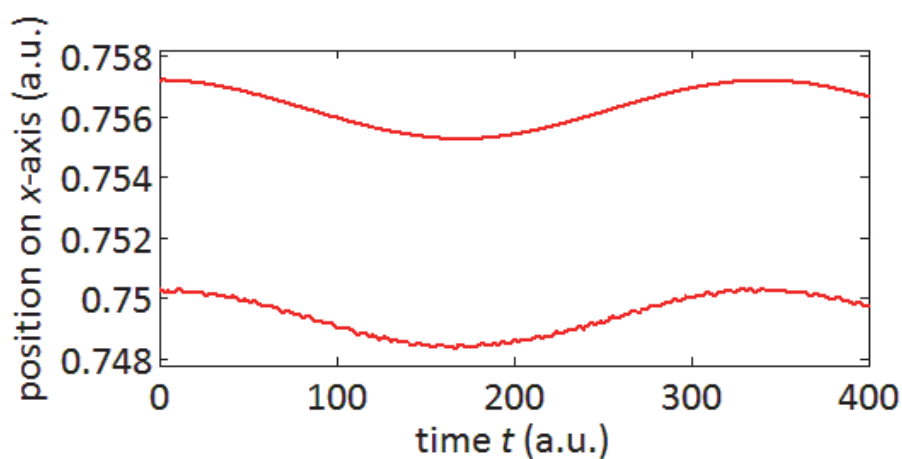


Figure 4-19 Variations of the center positions of the Gaussians of protons in real time after only displacing the optimized positions of the respective Gaussian functions by 0.001 a.u.

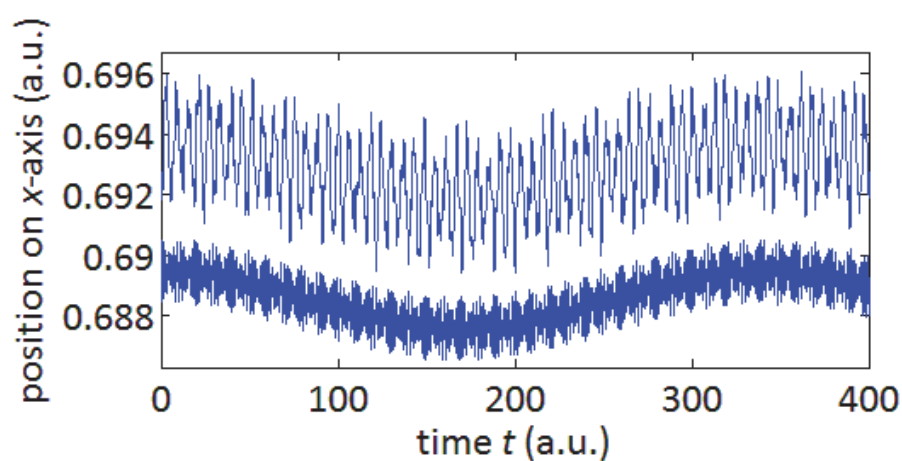


Figure 4-20 Variations of the center positions of the Gaussians of electrons in real time after only displacing the optimized positions of the respective Gaussian functions by 0.001 a.u.

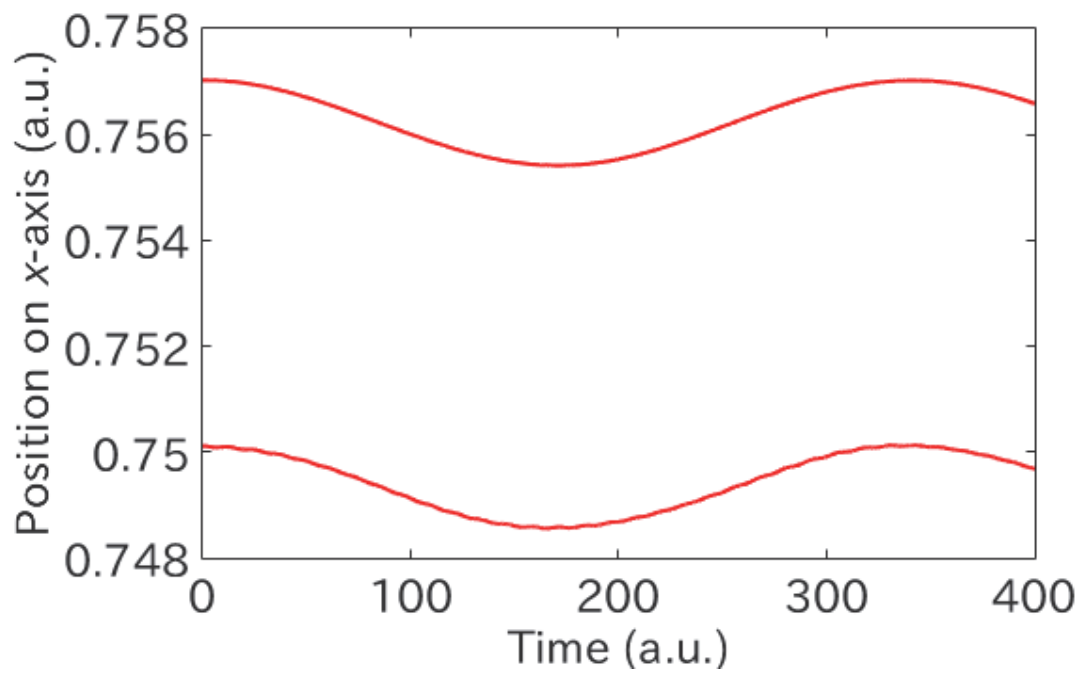


Figure 4-21 Variations of the center positions of the Gaussians of protons in real time.

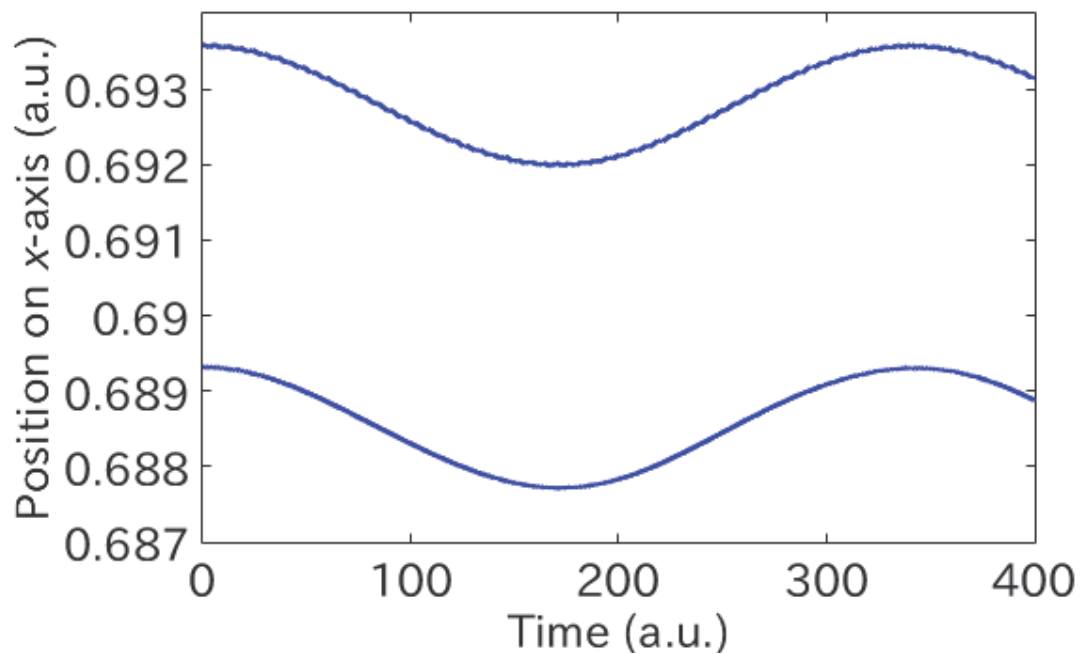


Figure 4-22 Variations of the center positions of the Gaussians of electrons in real time.

### 4.2.3. Electronic excitation represented by floating Gaussian

In order to discuss the interparticle couplings quantitatively, the expectation values of the squared nuclear-nuclear distance,  $r_{pp}^2$ , the squared electron-nuclear distance,  $r_{pe}^2$ , and the squared electron-electron distance,  $r_{ee}^2$ , defined respectively as

$$\begin{cases} r_{pp}^2(t) \equiv \langle \Psi(t) | (\mathbf{R}_1 - \mathbf{R}_2)^2 | \Psi(t) \rangle, \\ r_{pe}^2(t) \equiv \langle \Psi(t) | (\mathbf{R}_1 - \mathbf{r}_1)^2 | \Psi(t) \rangle, \\ r_{ee}^2(t) \equiv \langle \Psi(t) | (\mathbf{r}_1 - \mathbf{r}_2)^2 | \Psi(t) \rangle, \end{cases} \quad (4-30)$$

are evaluated. In deriving the temporal variations, a real-time propagation was performed by the adaptive Dormand-Prince Runge-Kutta method<sup>7)</sup>.

The temporal variations of  $r_{pp}^2$ ,  $r_{pe}^2$ , and  $r_{ee}^2$  of H<sub>2</sub> thus obtained are shown in Fig. 2(a), 2(b), and 2(c), respectively. The oscillation with the period of 340 a.u. (8.2 fs) is seen commonly in  $r_{pp}^2$ ,  $r_{pe}^2$ , and  $r_{ee}^2$ , which is seen in the discussion of the center position of basis functions. This means that not only the distance between the two protons, but also (i) the distance between one electron located in the vicinity of one proton and the other proton and (ii) the distance between one electron located in the vicinity of one proton and the other electron located near the vicinity of the other proton oscillate with the period of the vibrational motion of H<sub>2</sub>. After the Fourier transform of Figure 4-23 (a)-(c), the frequency distributions in Figure 4-24 (a)-(c) were obtained. The distinct peak appearing at 0.003 a.u. in frequency in Figure 4-24 (a)-(c) corresponds to the vibrational frequency of H<sub>2</sub>.

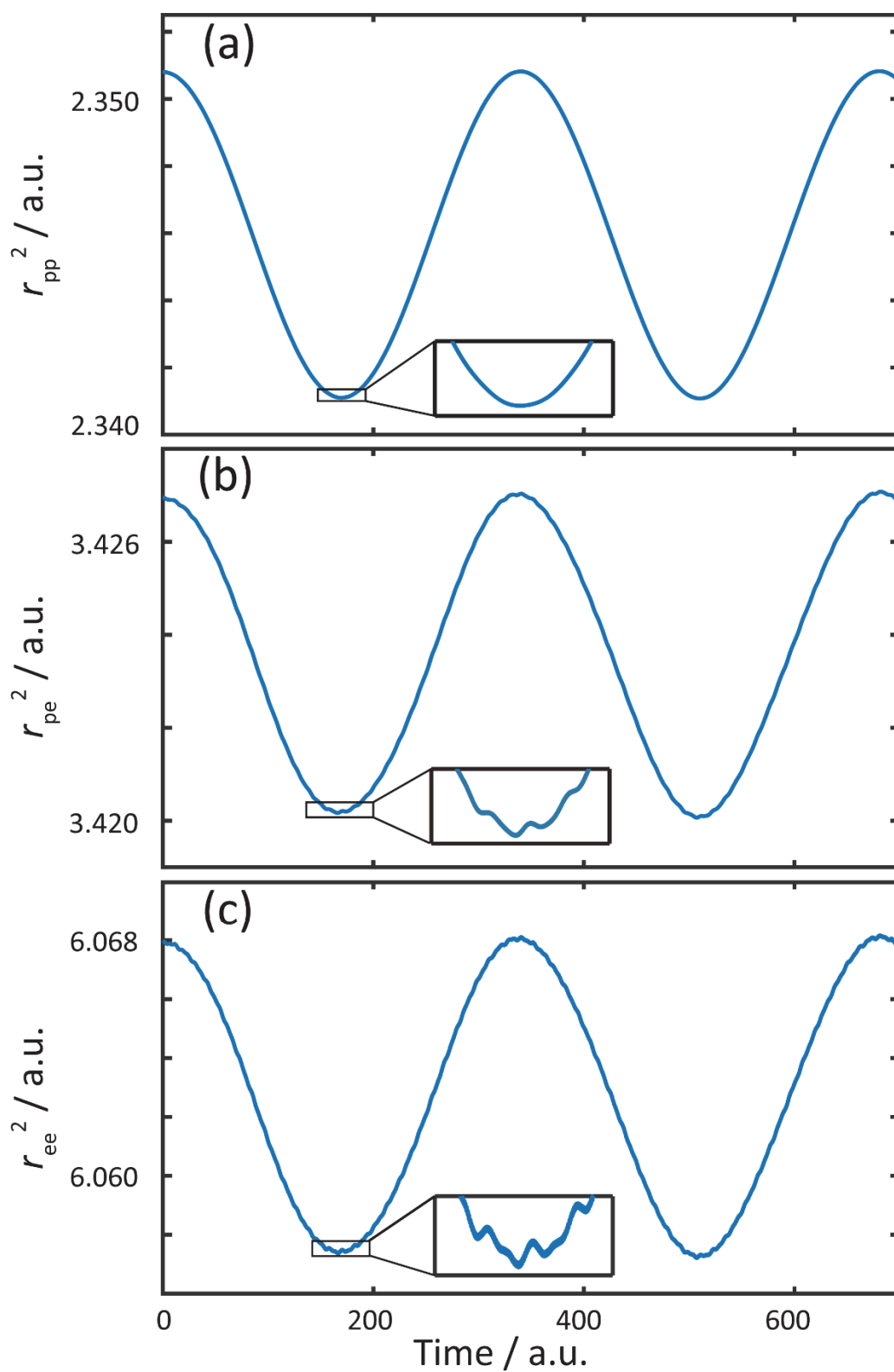
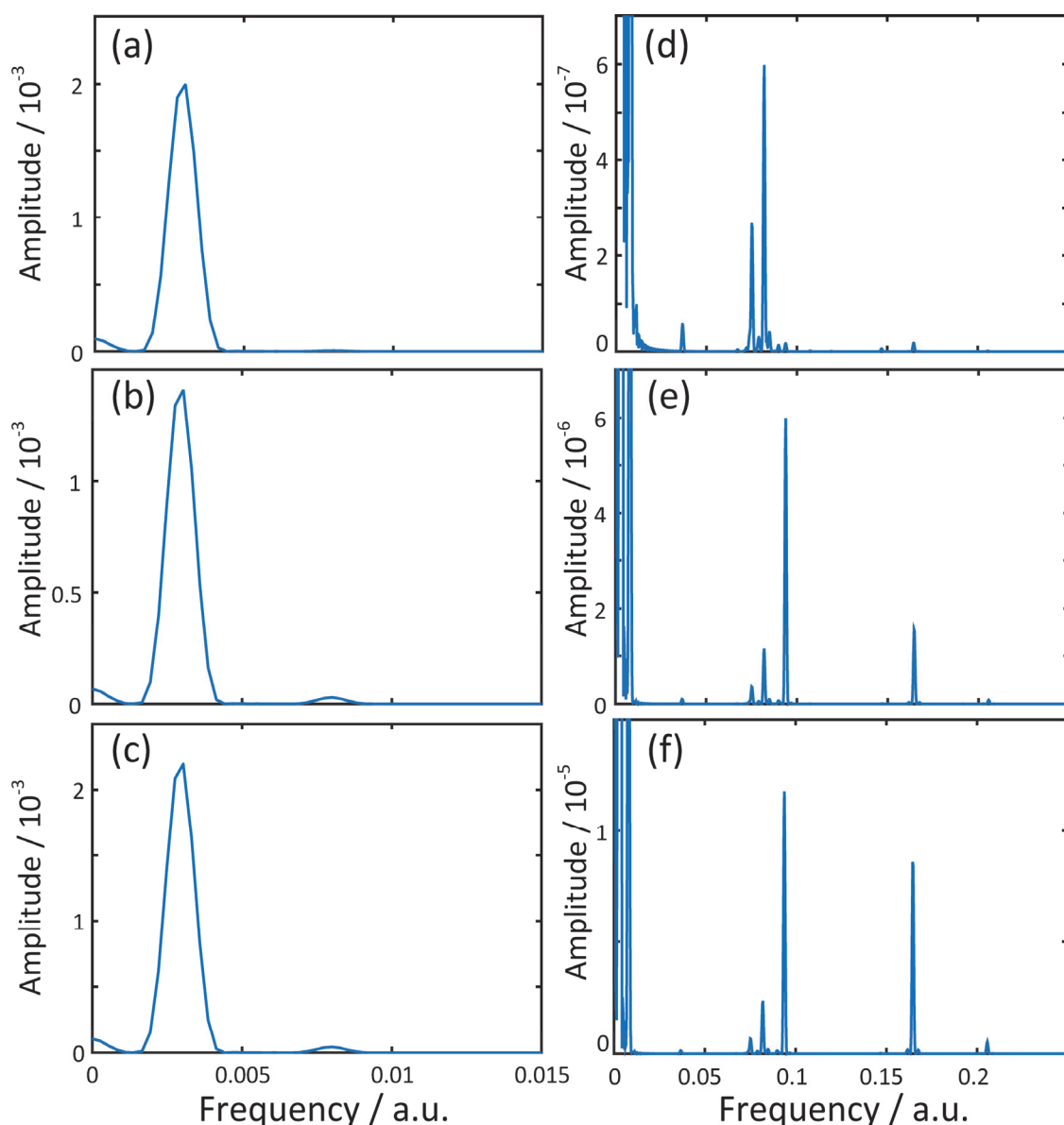


Figure 4-23 Time variation of (a)  $r_{pp}^2$  (proton-proton), (b)  $r_{pe}^2$  (proton-electron), and (c)  $r_{ee}^2$  (electron-electron) of H<sub>2</sub> molecule in the real-time propagation.



**Figure 4-24** Amplitudes of the Fourier transform of (a)  $r_{pp}^2$ , (b)  $r_{pe}^2$ , and (c)  $r_{ee}^2$  of  $H_2$  molecule in the real-time propagation. The right row shows the different scales of the horizontal (frequency) axes for (d)  $r_{pp}^2$ , (e)  $r_{pe}^2$ , and (f)  $r_{ee}^2$ .

The inset figure in each of the three subfigures in Figure 4-23 represents the expanded view of the corresponding parts. It can be seen in the insets of Figure 4-23 (b) and (c) that oscillatory structures appear with the modulation period of around 10 a.u. In order to examine this high frequency component, the high frequency region of the Fourier transformed spectra are expanded as shown in Figure 4-24 (d)-(f). A sharp

feature accompanying two small side peaks in the lower frequency side appear at around 0.094 a.u. and another sharp feature appears at around 0.164 a.u. commonly in Figure 4-24 (e) for  $r_{pe}^2$  and Figure 4-24 (f) for  $r_{ee}^2$ . In addition, in Figure 4-24 (d) for  $r_{pp}^2$ , two sharp features appear at around 0.075 and 0.082 a.u., which are close to the frequencies of the two side peaks appearing in Figure 4-24 (e) and (f). These high-frequency components appearing above 0.05 a.u. can be related to the motion of electrons because the corresponding energy range is in a typical energy range of the electronic excitations.

#### 4.2.4. Assignment of the high frequency components

In order to confirm that these high-frequency components are interpreted by the electronic excitation energies of  $H_2$ , we examine if the spectral features in the spectrum of  $r_{ee}^2$  are interpreted in terms of HF orbitals and if the respective peaks can be interpreted in terms of electronic excitation energies calculated by the time-dependent Hartree-Fock (TDHF) method. The electronic energies of the four lowest excited states, measured from the ground electronic state, thus obtained by the TDHF method are listed in Table 4-2, showing that the first excited state whose symmetry is *ungerade* has a main electron configuration described by the excitation of  $\varepsilon_u^1 \leftarrow \varepsilon_g^0$ . The main electronic configurations for the second excited state (*gerade*), the third excited state (*ungerade*), and the fourth excited state (*gerade*) are  $\varepsilon_g^1 \leftarrow \varepsilon_g^0$ ,  $\varepsilon_u^2 \leftarrow \varepsilon_g^0$ , and  $\varepsilon_g^2 \leftarrow \varepsilon_g^0$ , respectively. In the calculations performed using Gaussian 09, the option of ghost atoms [21] was chosen in order to locate a floating orbital at  $x = 0$ . For the nine basis functions, the same parameters as those listed in Table 4-1 were adopted. The nuclear distance defined as the distance between the centers of G8 and G9 basis functions was set to be 1.5124 a.u., which is the optimized value by the ITP as shown in Table 4-1 and Figure 4-10. This value is consistent with the quantity of  $\sqrt{r_{pp}^2(t=0)} = 1.5332$  a. u. obtained by the floating Gaussian method.

**Table 4-2.** Excitation energies of H<sub>2</sub> from the ground state to the four lowest electronic excited states calculated by the TDHF method using Gaussian 09. The basis set composed of nine Gaussian functions with the parameters shown in Table 4-1 is adopted.

	Energy / eV (Energy / a.u.)	Main Configuration
$\Delta E_1$	16.0041 (0.588140)	$\varepsilon_u^1 \leftarrow \varepsilon_g^0$
$\Delta E_2$	17.9340 (0.659062)	$\varepsilon_g^1 \leftarrow \varepsilon_g^0$
$\Delta E_3$	58.5242 (2.15072)	$\varepsilon_u^2 \leftarrow \varepsilon_g^0$
$\Delta E_4$	63.3917 (2.32960)	$\varepsilon_g^2 \leftarrow \varepsilon_g^0$

We note that the spatial part of the electronic wave function calculated by using the floating Gaussian orbitals can be rewritten in terms of time-dependent orbitals of *gerade* and *ungerade* symmetries. The spatial part of the wave function can be written by a product of electronic and nuclear Slater determinants as

$$\begin{aligned} \langle r_1, r_2, R_1, R_2 | \Psi(t) \rangle &= \Psi(r_1, r_2, R_1, R_2, t) = \langle r_1, r_2 | \Psi_e(t) \rangle \langle R_1, R_2 | \Psi_n(t) \rangle \\ &= \Phi_e(r_1, r_2, t) \Phi_n(R_1, R_2, t), \end{aligned} \quad (4-31)$$

The electronic Slater determinant can be always expressed as

$$\begin{aligned} \Phi_e(r_1, r_2, t) &= \langle r_1, r_2 | \Psi_e(t) \rangle \\ &= \frac{1}{\sqrt{2}} (\phi_R(r_1, t) \phi_L(r_2, t) + \phi_R(r_2, t) \phi_L(r_1, t)), \end{aligned} \quad (4-32)$$

using orbitals  $\phi_R$  and  $\phi_L$ , where  $\phi_R$  is the localized orbital mainly on positive area (right side) and  $\phi_L$  is the localized orbital mainly on negative area (left side) on x-axis.  $\phi_R$  and  $\phi_L$  are expressed using the time-dependent orbitals composed of time-dependent floating Gaussian functions as

$$\begin{aligned} & \phi_R(r, t) \\ &= \frac{\langle r | \phi_{e1}(t) \rangle}{(\langle \phi_{e1}(t) | \phi_{e1}(t) \rangle \langle \phi_{e2}(t) | \phi_{e2}(t) \rangle + \langle \phi_{e1}(t) | \phi_{e2}(t) \rangle \langle \phi_{e2}(t) | \phi_{e1}(t) \rangle)^{\frac{1}{4}}}, \end{aligned} \quad (4-33)$$

$$\begin{aligned} & \phi_L(r, t) \\ &= \frac{\langle r | \phi_{e2}(t) \rangle}{(\langle \phi_{e1}(t) | \phi_{e1}(t) \rangle \langle \phi_{e2}(t) | \phi_{e2}(t) \rangle + \langle \phi_{e1}(t) | \phi_{e2}(t) \rangle \langle \phi_{e2}(t) | \phi_{e1}(t) \rangle)^{\frac{1}{4}}}. \end{aligned} \quad (4-34)$$

where the denominators in Equations (4-33) and (4-34) are taken to satisfy the normalization condition of  $|\Phi_e(r_1, r_2, t)| = 1$ .  $\phi_R$  and  $\phi_L$  have the symmetry of

$$\phi_R(r, t) = \phi_L(-r, t). \quad (4-35)$$

as shown in Table 4-1. Therefore the orbitals  $\phi_R$  and  $\phi_L$  can be decomposed into two components having gerade and ungerade symmetries as

$$\begin{cases} \phi_R(r, t) = \phi_g(r, t) + \phi_u(r, t) \\ \phi_L(r, t) = \phi_g(r, t) - \phi_u(r, t) \end{cases}. \quad (4-36)$$

In terms of  $\phi_g$  and  $\phi_u$ , we can rewrite the electronic Slater determinant as

$$\Phi_e(r_1, r_2, t) = \sqrt{2} \left( \phi_g(r_1, t) \phi_g(r_2, t) - \phi_u(r_1, t) \phi_u(r_2, t) \right). \quad (4-37)$$

The gerade symmetry of  $\Phi_e(r_1, r_2, t)$  is always ensured by the relation of  $\Phi_e(r_1, r_2, t) = \Phi_e(-r_1, -r_2, t)$ . In the same way, the gerade nuclear Slater determinant can be represented in terms of nuclear single particle orbitals with gerade and ungerade symmetries.

Next, we discuss how those ungerade orbitals contribute to the spectra of  $r_{ee}^2(t)$ . To compare with the excited states calculated by Gaussian 09, we assume that the gerade and ungerade orbitals  $\phi_g(t)$  and  $\phi_u(t)$  are approximately represented by the 9 canonical molecular orbitals (MOs) used in Gaussian 09 as

$$\begin{cases} \tilde{\phi}_g(r, t) \approx \sum_{i=0}^4 a_g^i(t) \phi_g^i(r) \\ \tilde{\phi}_u(r, t) \approx \sum_{i=1}^4 a_u^i(t) \phi_u^i(r) \end{cases}, \quad (4-38)$$

where  $\{\phi_g^i(r)\}$  are the set of gerade MOs and  $\{\phi_u^i(r)\}$  the set of ungerade MOs

generated in the HF calculation by Gaussian 09. The time-dependent coefficients of  $a_g^i(t)$  and  $a_u^i(t)$  are calculated from the relationship of Equation (4-38) as

$$\begin{cases} a_g^i(t) = \langle \phi_g^i | \phi_g(t) \rangle \\ a_u^i(t) = \langle \phi_u^i | \phi_u(t) \rangle \end{cases} \quad (4-39)$$

respectively. Here,  $\phi_g(t)$  and  $\phi_u(t)$  can be calculated using the relations represented by Equation (4-36) and Equations (4-33) and (4-34). The expectation value of  $r_{ee}^2(t)$  is calculated by

$$r_{ee}^2(t) = \langle \Phi_e(t) | (r_1 - r_2)^2 | \Phi_e(t) \rangle, \quad (4-40)$$

where we used the normalization condition of the nuclear Slater determinant. By using the expression of Equation (4-37), we can rewrite  $r_{ee}^2(t)$  as

$$\begin{aligned} r_{ee}^2(t) = 4 & \left( \langle \phi_g(t) | r_1^2 | \phi_g(t) \rangle \langle \phi_g(t) | \phi_g(t) \rangle \right. \\ & \left. + \langle \phi_u(t) | r_1^2 | \phi_u(t) \rangle \langle \phi_u(t) | \phi_u(t) \rangle + 2\text{Re} \langle \phi_g(t) | r_1 | \phi_u(t) \rangle^2 \right) \end{aligned} \quad (4-41)$$

using the symmetry of the electronic Slater determinant with respect to  $r_1$  and  $r_2$ . Against those relationships, we can consider the comparison with the electronic states calculated with the MOs of conventional HF methods by replacing  $\Phi_e(t)$  to  $\tilde{\Phi}_e(t)$  where  $\tilde{\Phi}_e$  denotes the function generated by the replacements of  $\phi_g$  and  $\phi_u$  in Equation (4-37) by  $\tilde{\phi}_g$  and  $\tilde{\phi}_u$  defined in Equation (4-38), respectively. The expectation value of  $r_{ee}^2(t)$  is then calculated approximately by

$$\widetilde{r_{ee}^2}(t) = \langle \tilde{\Phi}_e(t) | (r_1 - r_2)^2 | \tilde{\Phi}_e(t) \rangle. \quad (4-42)$$

By evaluating  $\widetilde{r_{ee}^2}$  and after the Fourier transform, the frequency distribution was obtained as shown in Figure 4-25.

Figure 4-25 shows the results of the reproduction of the spectrum in Figure 4-24 (f) based on Equations (4-38) and (4-39). The frequencies of peaks are consistent in Figure 4-24 (f) and Figure 4-25. However, the peak height of Peak 4 is about 30 % smaller in Figure 4-25. On the other hand, the norm of  $\langle \Psi_e(t) | \Psi_e(t) \rangle$  calculated by using Equations (4-37) and (4-38) was 0.998 at  $t = 0$ . Those two observations indicate that the time-dependent motion of the center positions of floating Gaussian basis functions cannot be completely expressed only in the terms of the time variation of

orbital coefficients of the time-independent MOs even if the reproduced norm is as accurate as 99.8 %.

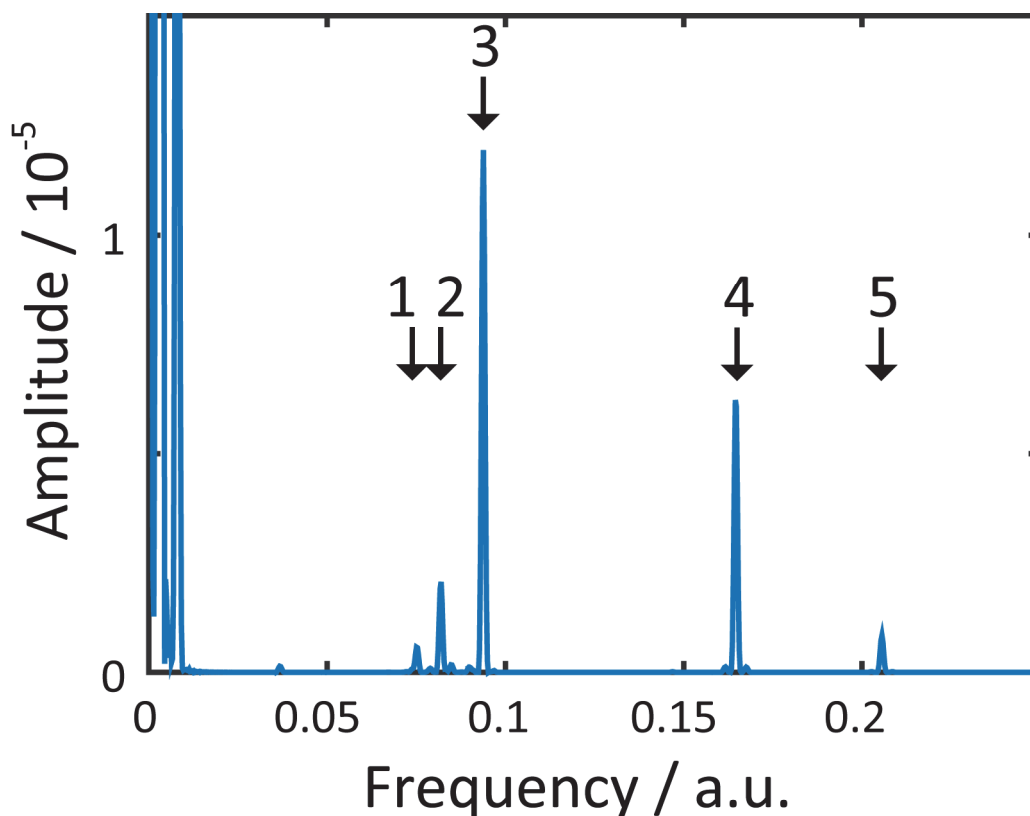


Figure 4-25 The amplitude of the Fourier transformed spectrum of  $r_{ee}^2$  of  $H_2$  by the calculation using the HF canonical MOs with the time-dependent coefficients shown in Equation (4-39). The peak numbers represent the assignments listed in Table 4-3.

The frequency of each peak can be assigned with the help of orbital energy calculated by HF calculations as follows. For example, the term of  $\langle \phi_g(t) | r_1^2 | \phi_g(t) \rangle$  is approximately evaluated by using Equation (4-38) as

$$\langle \tilde{\phi}_g(t) | r_1^2 | \tilde{\phi}_g(t) \rangle = \sum_{ij} a_g^{i*}(t) a_g^j(t) \langle \phi_g^i | r_1^2 | \phi_g^j \rangle . \quad (4-43)$$

In order to interpret the frequency components in  $r_{ee}^2(t)$  by canonical orbital energies, MOs used by TDHF, we will assume the following relationship as

$$a_g^j(t) \phi_g^j(r) \approx a_g^{j'} e^{-i\varepsilon_g^j t / \hbar} \phi_g^j(r) , \quad (4-44)$$

where  $\varepsilon_g^j$  denotes the canonical orbital energy of the  $j$ -th gerade orbital. Therefore, the right-hand side in Equation (4-43) can be written as

$$\sum_{ij} a_g^{i*}(t) a_g^j(t) \langle \phi_g^i | r_1^2 | \phi_g^j \rangle \approx \sum_{ij} a_g^{i'*} a_g^{j'} e^{-i(\varepsilon_g^j - \varepsilon_g^i)t/\hbar} \langle \phi_g^i | r_1^2 | \phi_g^j \rangle . \quad (4-45)$$

Here we notice that the energy difference of two orbitals approximately corresponds to the energy difference of two electronic Slater determinants. For example, if we define five lowest energies of electronic states in the HF calculation as

$$\begin{cases} E_g^0 = E(\Phi_{00}^{gg}) \\ E_u^1 = E(\Phi_{01}^{gu}) \\ E_g^1 = E(\Phi_{01}^{gg}) \\ E_u^2 = E(\Phi_{02}^{gu}) \\ E_g^2 = E(\Phi_{02}^{gg}) \end{cases} , \quad (4-46)$$

where  $\Phi_{ij}^{gu}$  means the Slater determinant composed of two canonical orbital as

$$\Phi_{ij}^{gu}(r_1, r_2) = \frac{1}{\sqrt{2}} (\phi_g^i(r_1) \phi_u^j(r_2) + \phi_g^i(r_2) \phi_u^j(r_1)) , \quad (4-47)$$

the energy differences in Table 4-2 are expressed using the relationships of Equations (4-46) and (4-47) as

$$\begin{cases} \Delta E_1 = E_u^1 - E_g^0 \\ \Delta E_2 = E_g^1 - E_g^0 \\ \Delta E_3 = E_u^2 - E_g^0 \\ \Delta E_4 = E_g^2 - E_g^0 \end{cases} . \quad (4-48)$$

The frequency related to the energy difference of two gerade states can be involved in the term of  $\langle \tilde{\phi}_g(t) | r_1^2 | \tilde{\phi}_g(t) \rangle$ . In the same manner,

$$\begin{aligned} \langle \tilde{\phi}_u(t) | r_1^2 | \tilde{\phi}_u(t) \rangle &= \sum_{kl} a_u^{k*}(t) a_u^l(t) \langle \phi_u^k | r_1^2 | \phi_u^l \rangle \\ &\approx \sum_{kl} a_u^{k'*} a_u^{l'} e^{-i(\varepsilon_u^k - \varepsilon_u^l)t/\hbar} \langle \phi_u^k | r_1^2 | \phi_u^l \rangle , \end{aligned} \quad (4-49)$$

and the frequency related to the energy difference of two ungerade states is turned out to be involved in this term. Also, the term of  $\text{Re} \langle \tilde{\phi}_g(t) | r_1 | \tilde{\phi}_u(t) \rangle^2$  can be expanded as

$$\begin{aligned} \langle \tilde{\phi}_g(t) | r_1 | \tilde{\phi}_u(t) \rangle^2 &= \sum_{ijkl} a_g^{i*}(t) a_u^k(t) \langle \phi_g^i | r_1 | \phi_u^k \rangle a_g^{j*}(t) a_u^l(t) \langle \phi_g^j | r_1 | \phi_u^l \rangle \\ &\approx \sum_{ijkl} a_g^{i'*} a_g^{j'*} a_u^{k'} a_u^{l'} e^{-i\{(\varepsilon_u^k - \varepsilon_g^i) + (\varepsilon_u^l - \varepsilon_g^j)\}t/\hbar} \langle \phi_g^i | r_1 | \phi_u^k \rangle \langle \phi_g^j | r_1 | \phi_u^l \rangle. \end{aligned} \quad (4-50)$$

We can observe the sum of two energy differences of the ungerade state and the gerade state in Equation (4-50) such as  $\Delta E_1$  and  $\Delta E_3$  in Equation (4-48). Therefore, even if the electronic Slater determinant  $\tilde{\Phi}_e$  is gerade, the frequency related to the energy of ungerade states can be observed in  $r_{ee}^2(t)$ .

**Table 4-3** The energies of Peak 1 to Peak 5 in the Fourier transformed spectra of  $r_{ee}^2$  of  $H_2$  in Figure 4-25 and those obtained by the TDHF method with the assignment in terms of the electronic excitation energies obtained by the TDHF method.

Peak Number	Peak Energy <sup>a)</sup> / eV (Peak Frequency / a.u.)	Peak Energy <sup>b)</sup> / eV (Peak Frequency / a.u.)	Assignment <sup>c)</sup>
1	12.9 (0.0752)	11.1366 (0.065136)	$\Delta E_1 + (\Delta E_3 - \Delta E_4)$
2	14.0 (0.0820)	14.0742 (0.082318)	$\Delta E_1 + (\Delta E_1 - \Delta E_2)$
3	16.0 (0.0938)	17.9340 (0.104893)	$\Delta E_2$
4	28.15 (0.1646)	24.5862 (0.143801)	$\Delta E_3 - \Delta E_1$
5	35.16 (0.2056)	32.0082 (0.187211)	$\Delta E_1 + \Delta E_1$

a) Peak energies in Figure 4-25 obtained by the floating Gaussian method.

b) Peak energies obtained by the TDHF method.

c) Peak energies in b) are calculated by the energy difference of the electronic states calculated by the TDHF method shown in Table 4-2.

Table 4-3 shows the assignments of the peaks in Figure 4-25 using the

excitation energies calculated by TDHF in Table 4-2 along the rules of Equations (4-45), (4-49), and (4-50). The largest deviation between the energies of peaks and the assignments is 14 % in Peak 4. The deviation of 14 % is reasonable in consideration of the deviation of 30 % in the amplitude of Peak 4 between Figure 4-25 and Figure 4-24 (f). In this way, we can explain why the energy of  $\Sigma_u$  state can contribute to the spectrum of  $r_{ee}^2$ . Therefore, the frequency values  $> 0.05$  a.u.<sup>-1</sup> in the amplitude of Fourier transformation of inter-particle distances are interpreted as energy differences related to the electronic excitation as the assignments shown in Table 4-3.

#### 4.2.5. Mass dependence of non-adiabatic coupling

Considering that the appearance of Peak 3 and Peak 4 in the Fourier transformed spectra of  $r_{pp}^2$  is ascribable to the non-adiabatic electron-nuclear couplings, the heights of Peak 3 and Peak 4 can be good indicators representing the extent of the non-adiabatic couplings. Because the extent of the couplings is considered to be influenced sensitively by the ratio of the mass of an electron with respect to the mass of a nuclei in a two-electron homonuclear diatomic molecule, the  $r_{pp}^2$  value of D<sub>2</sub> was calculated by the floating Gaussian method, and the frequency distribution was obtained by the Fourier transform in the same manner as in the case of H<sub>2</sub> as shown in Figure 4-26.

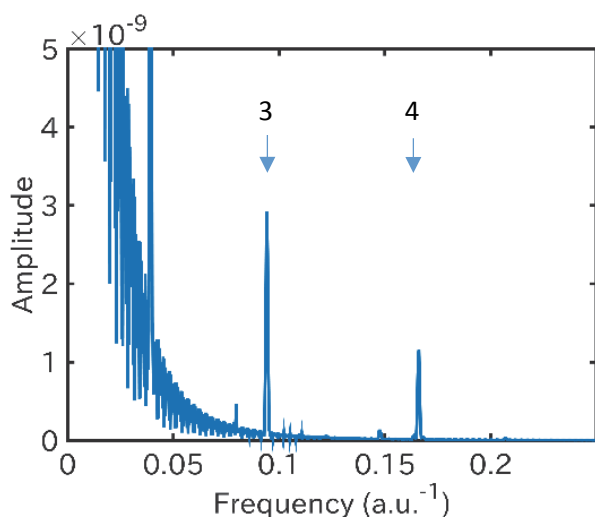


Figure 4-26 Amplitude of Fourier transformation of  $r_{pp}^2$  of D<sub>2</sub>. The peaks of frequencies

related to Peak 3 and 4 in Figure 4-25 are shown in the figure.

Figure 4-26 shows the amplitude of Fourier transformation of  $r_{pp}^2$  of  $D_2$ . The height of Peak 3 appearing at the frequency of 0.0943 a.u. and the height of Peak 4 appearing at the frequency of 0.1660 a.u. were found to be  $8.83 \times 10^{-7}$  and  $3.46 \times 10^{-7}$ , relative to the height of the lowest frequency component representing the molecular vibration. In the case of  $H_2$ , the relative heights of Peak 3 and Peak 4 are  $8.55 \times 10^{-6}$  and  $8.95 \times 10^{-6}$ , respectively, and are found to be larger than in the case of  $D_2$  by one order of magnitude, which clearly shows that the non-adiabatic electron-nuclear coupling becomes more evident when the relative mass of nuclei becomes lighter.

## References

1. H. Nishizawa, Y. Imamura, Y. Ikabata and H. Nakai, "Development of the explicitly correlated Gaussian-nuclear orbital plus molecular orbital theory: Incorporation of electron-electron correlation" *Chem. Phys. Lett.* **533** (2012).
2. Y. Kurokawa, H. Nakashima and H. Nakatsuji, "Free iterative-complement-interaction calculations of the hydrogen molecule" *Phys. Rev. A* **72**, 062502 (2005).
3. H. Nishizawa, M. Hoshino, Y. Imamura and H. Nakai, "Evaluation of electron repulsion integral of the explicitly correlated Gaussian-nuclear orbital plus molecular orbital theory" *Chem. Phys. Lett.* **521**, 142-149 (2012).
4. H. Nakai, "Simultaneous determination of nuclear and electronic wave functions without Born–Oppenheimer approximation: Ab initio NO MO/HF theory" *Int. J. Quantum Chem.* **86**, 511-517 (2001).
5. D. B. Kinghorn and L. Adamowicz, "High accuracy non-Born–Oppenheimer calculations for the isotopomers of the hydrogen molecule with explicitly correlated Gaussian functions" *J. Chem. Phys.* **113**, 4203-4205 (2000).
6. G. D. Dickenson, M. L. Niu, E. J. Salumbides, J. Komasa, K. S. E. Eikema, K. Pachucki and W. Ubachs, "Fundamental Vibration of Molecular Hydrogen" *Phys. Rev. Lett.* **110**, 193601 (2013).
7. MATLAB, in *version 8.5.0 (R2015a)* (The MathWorks Inc., Natick, Massachusetts, 2015).

## 5. Application of laser fields to H<sub>2</sub> molecule

With the CCS method, the center position of Gaussian basis is regarded as the time-dependent variable and it can follow the motion against the electric force in intense laser fields. In this chapter, the motion of each floating Gaussian basis of H<sub>2</sub> in intense laser fields with different carrier-envelope phases (CEPs) will be demonstrated against nuclear-electron wave function as a 4-particle problem.

### 5.1. Demonstration with 1.5 cycle pulse laser

The laser field  $E(t)$  applied to the molecule is expressed as

$$E(t) = E_0 \varepsilon(t) \sin(\omega t + \phi), \quad (5-1)$$

where  $E_0$ ,  $\varepsilon(t)$ ,  $\omega$ , and  $\phi$  denotes the peak intensity, pulse envelope, frequency and CEP respectively. The peak intensity  $E_0$  of laser pulses applied in the simulation is 0.3 a.u. The cycles of the carrier are 1.5 cycles and the wavelength is 780 nm. The polarization direction is  $x$ -axis. Figure 5-1 (a) shows the profile of electric field of these pulses and their envelope. 3 trajectories with different CEPs were calculated. The number of Gaussian bases of the wave function adopted for time propagation in these laser field is 4. One basis is assigned for each particle in H<sub>2</sub> and the total number is 4. Figure 5-1 (b)-(d) show the time variations of center positions of Gaussian bases with CEPs of  $\phi = 0, 2.0345$ , and  $\pi/2$  respectively. Blue solid lines represent the center positions of bases of electrons and red dashed lines represent those of nuclei. In Figure 5-1 (b), one electron is ejected at the peak intensity of the pulse and the other electron remains bound in the core. In Figure 5-1 (c), a single ionization occurs but the recollision of the electron to the bound electron can be observed. This is a characteristic phenomenon observed in intense laser field experiments. Furthermore the double ionization after the recollision can be observed in Figure 5-1 (d). This double ionization occurs after interaction of two electrons during  $t = 50 \sim 100$  a. u. and can be recognized as a non-sequential double ionization in contrast to a sequential double ionization. From the comparison of Figure 5-1 (c) and (d), we can see that a small change of the CEP has a large impact on the fate of the molecular ionization.

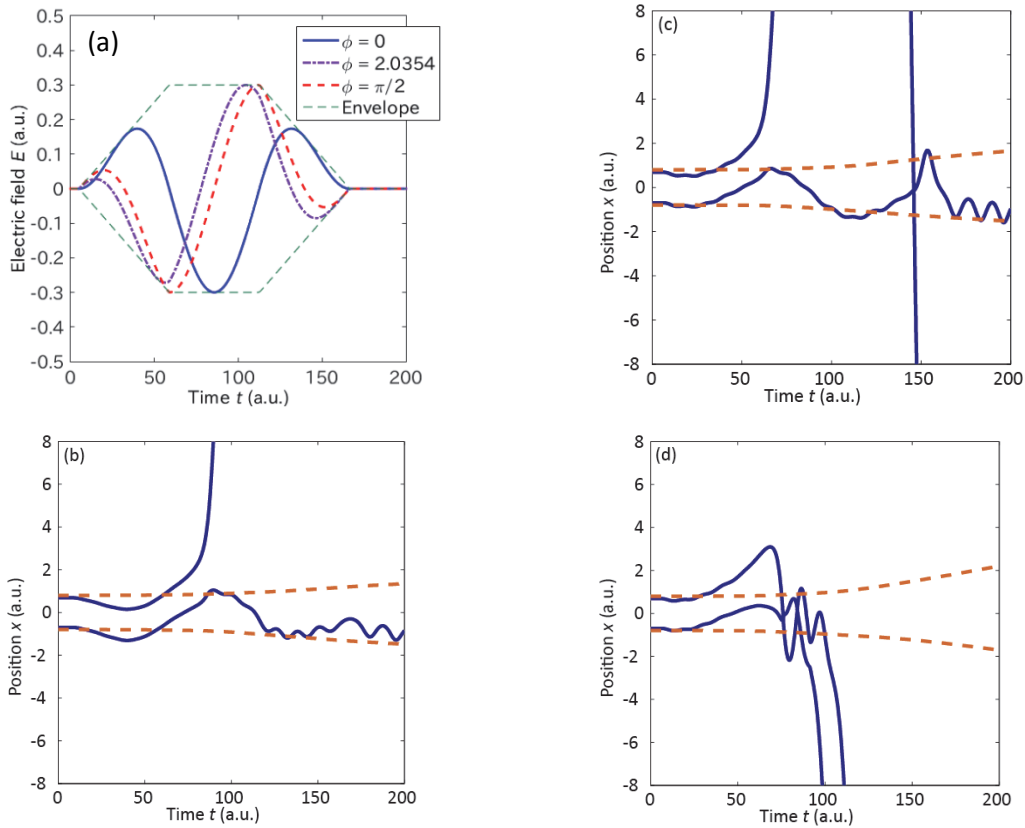


**Figure 5-1 (a):** Electric field amplitudes of three pulses adopted in the simulation. Three lines with legends represent carriers and dashed lines represent the envelope. **(b):** Variations of the center positions of the Gaussian bases with the CEP of  $\phi = 0$ . **(c):** Results with the CEP of  $\phi = \pi/2$ . **(d):** Results with the CEP of  $\phi = 2.0354$  radian. On (b)-(d), solid lines show the center positions of electronic bases and dashed lines show those of nuclear bases.

## 5.2. Ionization dependence on CEP and cycle of pulses

In the above section, we saw the influence of the CEP difference on the trajectories in intense laser fields. Next, the effect of the difference of the laser condition is examined by changing the numbers of the cycle, the CEP and the intensity of pulses. The dependence of ionization count of  $H_2$  molecule on such parameters will be simulated.

### 5.2.1. Laser condition

The laser field  $E(t)$  applied to the molecule is expressed as

$$E(t) = E_0 \varepsilon(t) \sin\left(\omega t + \phi - cycle \times \pi + \frac{\pi}{2}\right), \quad (5-2)$$

where  $E_0$ ,  $\varepsilon(t)$ ,  $\omega$ , and  $\phi$  denotes the peak intensity, pulse envelope, frequency and CEP respectively. The polarization direction is  $x$ -axis. The wavelength is 780 nm and the envelope is sin-square shape like as

$$\varepsilon(t) = \begin{cases} \sin(\omega t / (2 * cycle))^2 & \text{while } 0 < \omega t / (2 * cycle) < \pi \\ 0 & \text{elsewhere} \end{cases}. \quad (5-3)$$

The laser pulse shapes are illustrated as Figure 5-2 for these parameters. The peak intensity  $E_0$  of laser pulses applied in the simulation is 0.25 or 0.3 a.u.

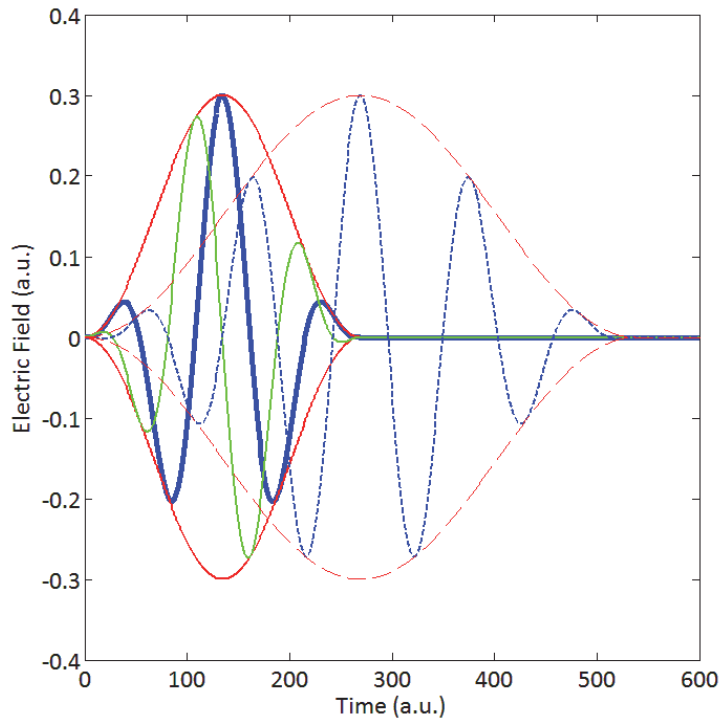


**Figure 5-2 Electric field amplitudes of laser pulse for different CEP and cycles. Red lines show envelope of pulses and blue lines are carriers when the CEPs are 0. The green line shows the carrier when the CEP is not 0.**

An ionization count for a certain condition is determined in a pseudo code like  
 if ( $r_1 < 17.3 \ \&\& \ r_2 < 17.3$ )

ioncount=0; //  $H_2$

elseif ( $r_1 < 14.0 \ \&\& \ r_2 > 17.3$ ) || ( $r_1 > 17.3 \ \&\& \ r_2 < 14.0$ )

ioncount=1; //  $H_2^+$

else

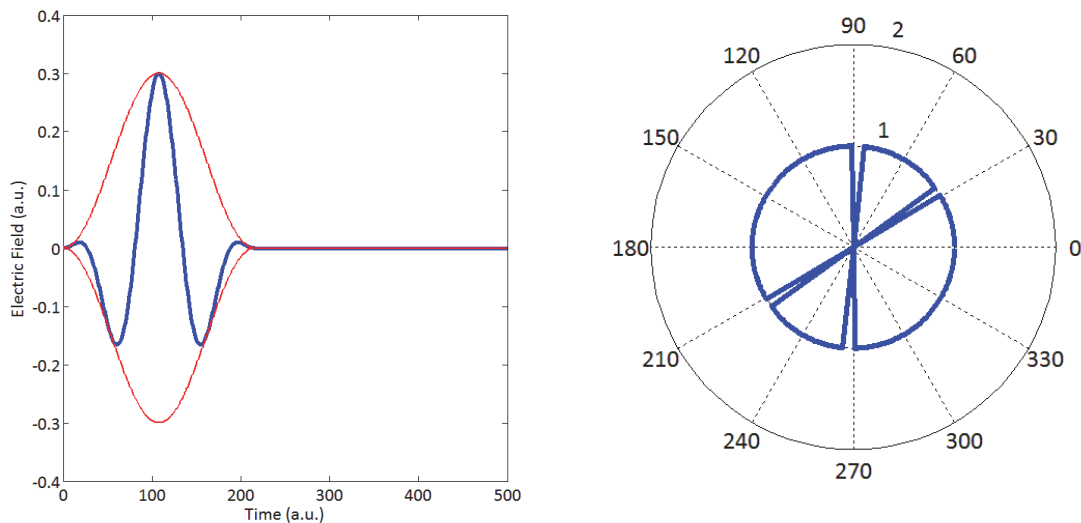
ioncount=2; //  $H_2^{2+}$

Where  $r_1$  is the norm of the center position of Gaussian of electron1 ( $|z_1\rangle$ ) and  $r_2$  is that of electron2 ( $|z_2\rangle$ ).

The step width for the variation of CEP is set at  $\frac{\pi}{90}$  in the simulation.

### 5.2.2. $E_0 = 0.3$ a.u.

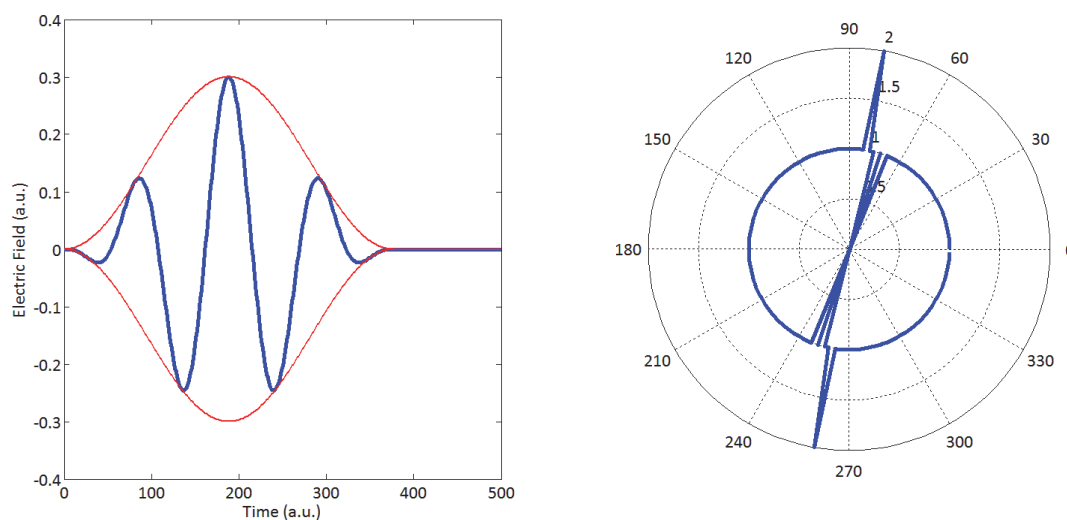
First, for laser parameters, the peak intensity is fixed at  $E_0 = 0.3$  a.u. ( $= 3.2 \times 10^{15}$  W/cm<sup>2</sup>) and calculation results are shown when the cycle number is 2. Figure 5-3 shows the laser pulse shape and ionization count for CEP difference. In this cycle, double ionization does not occur.



**Figure 5-3** laser pulse shape and ionization count for CEP difference at  $E_0 = 0.3$  a.u. and pulse cycle = 2. The left pane shows the laser pulse shape at CEP=0. The red line represents the envelope and the blue line represents the pulse carrier. The right pane shows the ionization

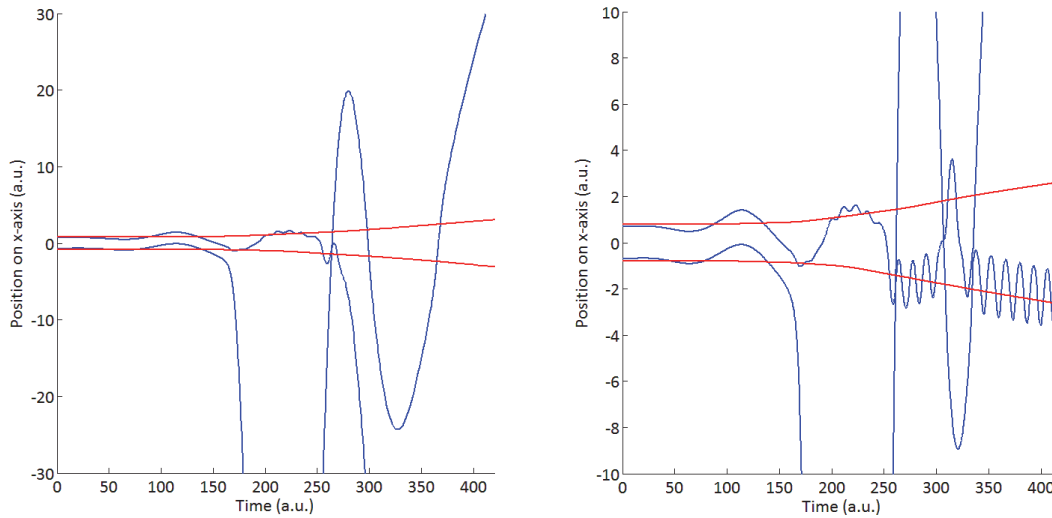
count of H<sub>2</sub> molecule for CEP change.

Figure 5-4 shows the laser pulse shape and ionization count for CEP difference when the cycle is 3.5. In this cycle, double ionization occurs when the CEP is 80 degree.



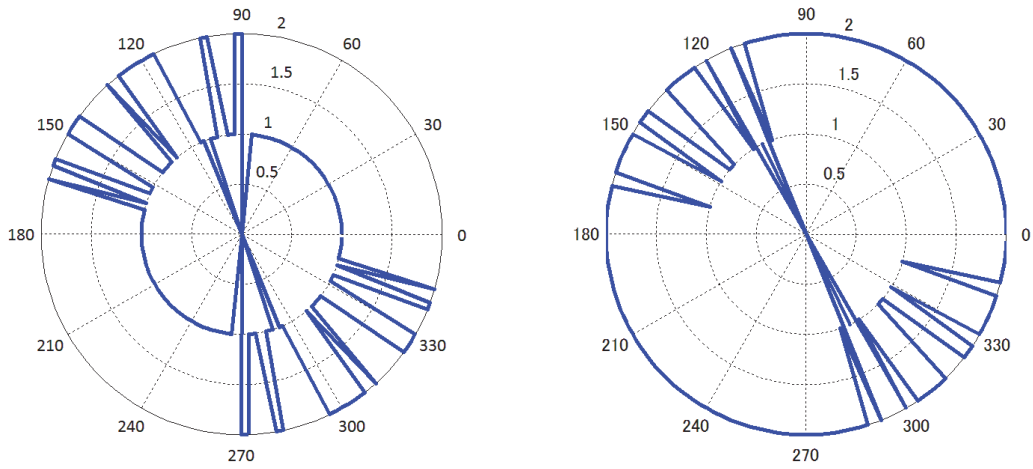
**Figure 5-4 laser pulse shape and ionization count for CEP difference at  $E_0 = 0.3$  a.u. and pulse cycle = 3.5. The left pane shows the laser pulse shape at CEP=0. The red line represents the envelope and the blue line represents the pulse carrier. The right pane shows the ionization count of H<sub>2</sub> molecule for CEP change.**

Figure 5-5 shows trajectories at CEP = 80 degree and CEP = 82 degree. At CEP = 80 degree the ionization is double ionization and at CEP = 82 degree the ionization is single ionization from the right pane in Figure 5-4. We can find the difference of ionization mechanism after  $t = 250$  a.u. in Figure 5-5. At CEP = 80 one electron which once got away from the core came back to the core and collided with the other electron and after that both electrons were ionized. This is the non-sequential double ionization mechanism but at CEP = 82 degree the other electron remained at the core and eventually single ionization was observed. Hence the difference of CEP results at the separation of trajectories and the different ionization mechanism.



**Figure 5-5 Comparison of trajectories at CEP = 80 degree and CEP = 82 degree for cycle = 3.5. The left pane shows variation of center positions of Gaussians at CEP = 80 degree. The right pane shows variation of center positions of Gaussians at CEP = 82 degree. The red lines represent the bases of the nuclei and the blue lines represent the bases of electrons.**

Figure 5-6 shows the comparison of count of the ionized electron for the variation of the CEP at cycle = 4 and cycle = 4.5. First, we can see the major difference at  $0 < \text{CEP} < 90$  degree for double ionization. Figure 5-7 shows the comparison of trajectories at cycle = 4 and cycle = 4.5 for CEP = 30 degree. We can see the divergence around  $t = 320$  a.u. for the double ionization. This is because the sub peak of the laser pulse is stronger in the longer cycle pulse related to the shape of envelope and the strength of sub peak is effecting the second ionization. The double ionization in cycle = 4.5 is sequential double ionization and the strength of the sub peak is mainly dividing the ionization count between cycle = 4 and 4.5. Then the region of  $0 < \text{CEP} < 90$  degree, cycle = 4 case does not have any double ionization but cycle = 4.5 case has always double ionization.



**Figure 5-6 Comparison of count of the ionized electron for the variation of the CEP at cycle = 4 and cycle = 4.5. The left pane shows the ionization count of H<sub>2</sub> molecule at cycle = 4. The right pane shows the ionization count of H<sub>2</sub> molecule at cycle = 4.5.**

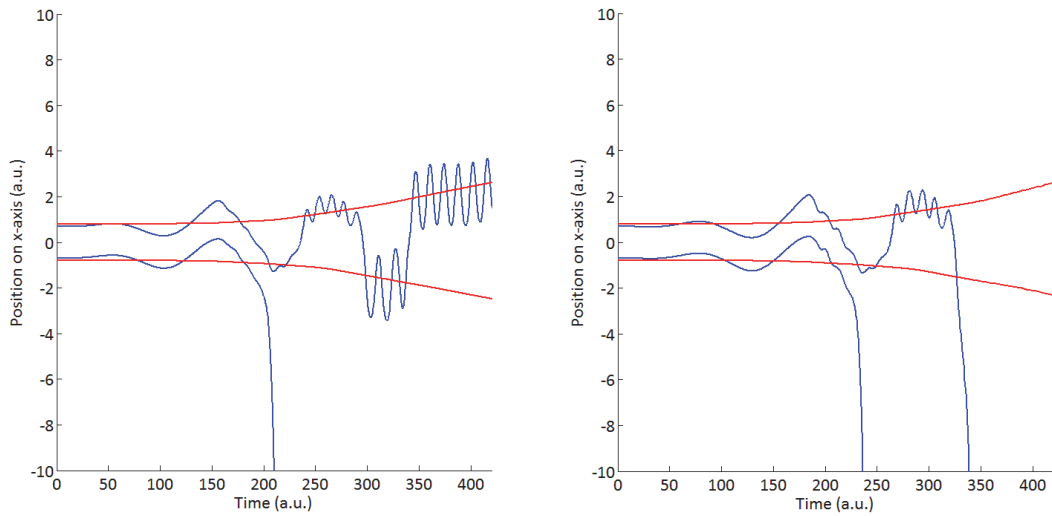


**Figure 5-7 Comparison of trajectories at cycle = 4 and cycle = 4.5 for CEP = 30 degree. The left pane shows variation of center positions of Gaussians at cycle = 4. The right pane shows variation of center positions of Gaussians at cycle = 4.5. The red lines represent the bases of the nuclei and the blue lines represent the bases of electrons.**

Furthermore, Figure 5-8 shows the comparison of trajectories at CEP = 90 degree and

CEP = 120 degree for cycle = 4. From the left pane in Figure 5-6, the double ionization occurs at  $90 < \text{CEP} < 180$  degree. At CEP = 90 degree and CEP = 120 degree, the recollision of the electron to the core occurs around  $t = 270$  a.u. and immediately the other electron is ionizing. These are the non-sequential double ionization and the NSDI is the main mechanism for double ionization at this cycle number.

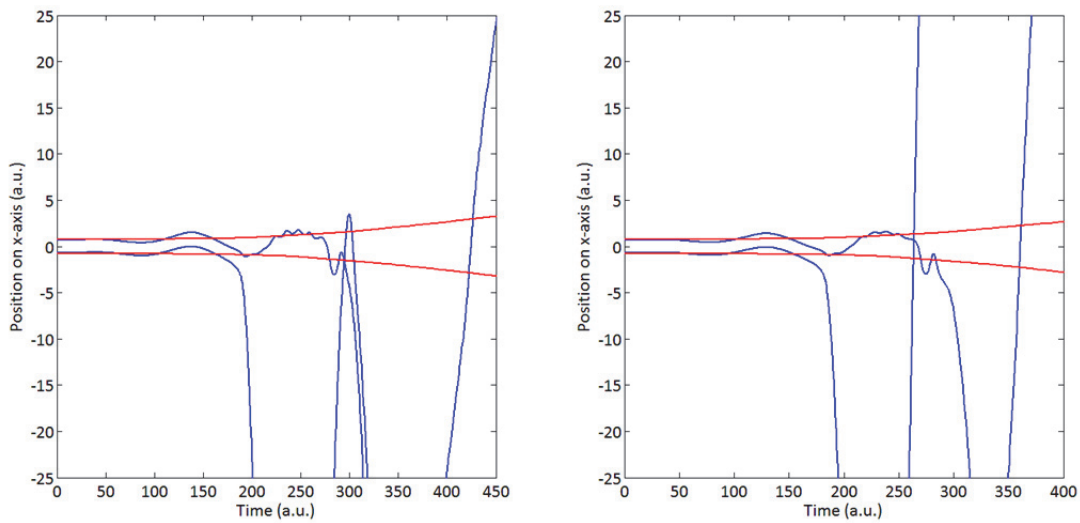


**Figure 5-8 Comparison of trajectories at CEP = 90 degree and CEP = 120 degree for cycle = 4. The left pane shows variation of center positions of Gaussians at CEP = 90 degree. The right pane shows variation of center positions of Gaussians at CEP = 120 degree. The red lines represent the bases of the nuclei and the blue lines represent the bases of electrons.**

Figure 5-9 shows variation of center positions of Gaussians at CEP = 118 degree for cycle = 4.5. From Figure 5-6, ionization count for these CEP and cycle is 0. When we see the detail of trajectory, the recollisions occur 4 times, and at  $t = 420$  and  $520$  a.u., the permutation of electrons occurs. Then, eventually both electrons are captured to nuclei and ionization count is 0. In this case, if the electric field is strong enough for the ionization, some trajectories still show no ionization and the detail of trajectory includes complicated motion of electrons.

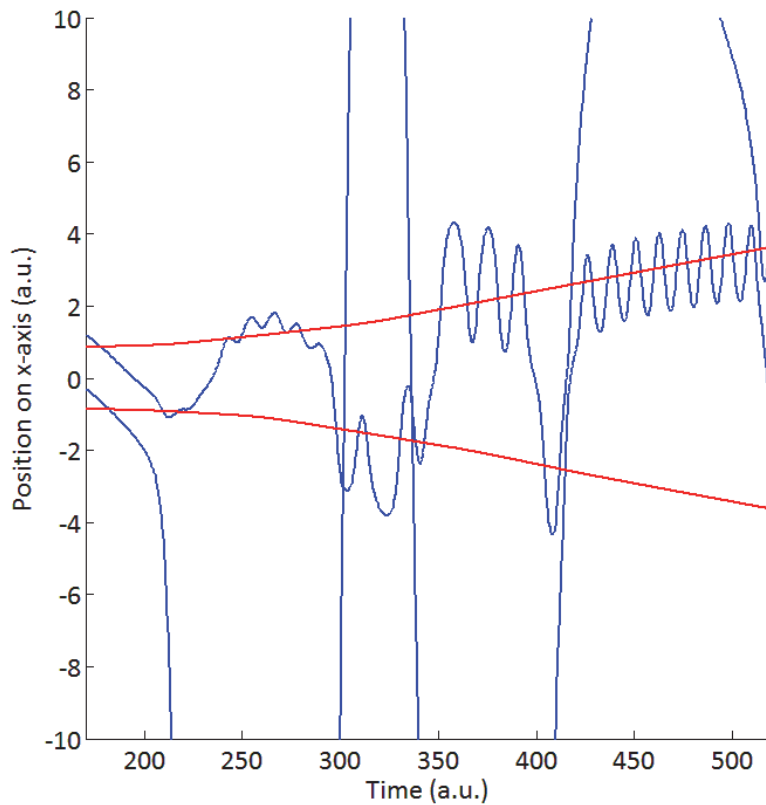


**Figure 5-9** Variation of center positions of Gaussians at CEP = 118 degree for cycle = 4.5. The red lines represent the bases of the nuclei and the blue lines represent the bases of electrons.

For the intensity peak of  $E_0 = 0.3$  a.u. ( $= 3.2 \times 10^{15}$  W/cm<sup>2</sup>), all the figures of ionization count for CEP against the parameter of cycles from 2 to 5 are shown together in Figure 5-10. From 2 cycles to 3 cycles, ionization is limited to single ionization. At 3.5 cycles the first double ionization is observed and this is explained above as non-sequential double ionization. At 4 cycles, the double ionizations start to occur at  $90 < \text{CEP} < 180$  degree and this reason is also described above. From 5 cycles, in the region of  $0 < \text{CEP} < 90$  degree the double ionization also starts to occur and this region is dominated by sequential double ionization. At 5 cycles, the double ionization occurs at almost all the region of CEP. This suggests that 5 cycles is enough to induce double ionization independently of CEP difference. At longer cycles, the envelope is

closer to 1 against CEP change, and the peak and sub peaks tends to be stronger. Then at few cycle pulse in strong laser fields, the increase of cycle number affects directly the ionization count.

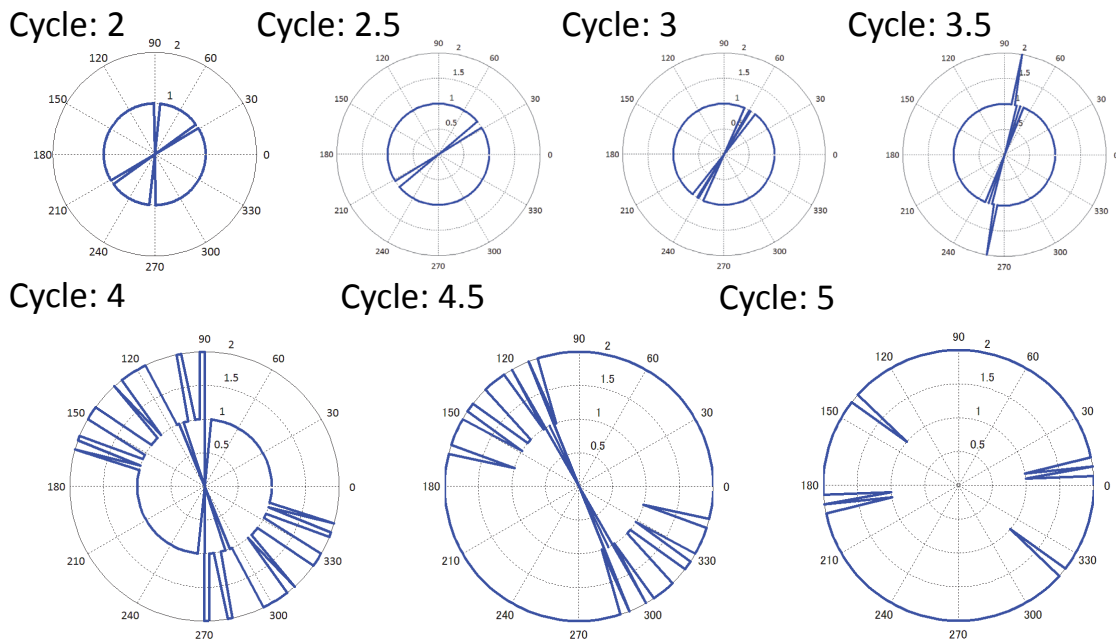


**Figure 5-10** Variation of count of the ionized electron for the CEP difference against the cycle number of the pulse at  $E_0 = 0.3$  a.u. Figures show results for cycle 2 to 5 with 0.5 step width. Left top letters of “Cycle:” on each pane shows the cycle number of the applied laser pulse.

### 5.2.3. $E_0 = 0.25$ a.u.

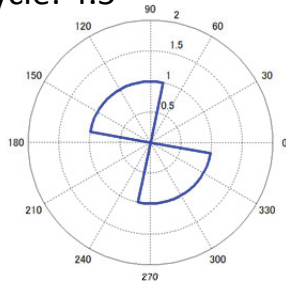
Next, the peak intensity is fixed at  $E_0 = 0.25$  a.u. ( $= 2.2 \times 10^{15}$  W/cm<sup>2</sup>) and the ionization count for CEP difference is simulated changing cycle number of laser pulse. Figure 5-11 shows the ionization count for CEP from 4.5 cycle number to 9. Under 4 cycles, the ionization is not observed at this peak intensity. From the 6 cycles, the double ionization is observed. At the 6 and 6.5 cycles, the double ionization is observed between the CEP of 0 to 90 degree, and the double ionization is mainly observed between the CEP of 0 to 90 degree. Figure 5-12 shows the comparison of trajectories at cycle = 6 and cycle = 7 for CEP = 34 degree. The recollision of the

electron to the core occurs around  $t = 350$  a.u. at the left pane and  $t = 450$  a.u. in the right pane. After those, the other electrons are ejected from the core. These are the non-sequential double ionization and the NSDI is the main mechanism for double ionization at this cycle number.

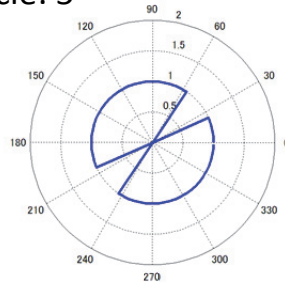
Cycle:  $\sim 4$

ionization count: 0

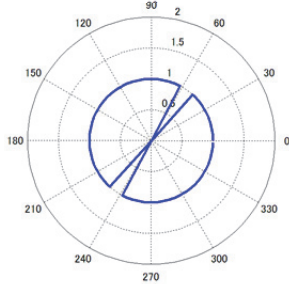
Cycle: 4.5



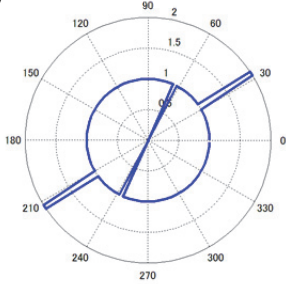
Cycle: 5



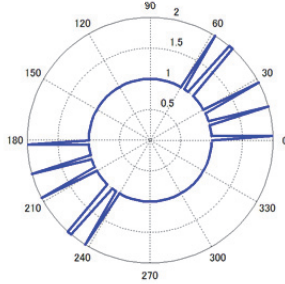
Cycle: 5.5



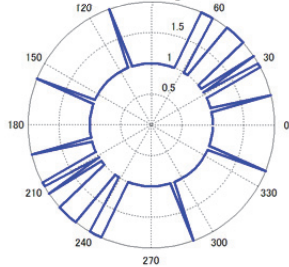
Cycle: 6



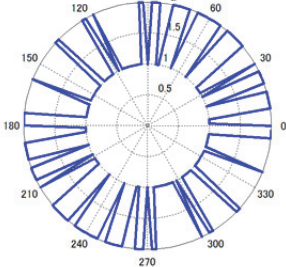
Cycle: 6.5



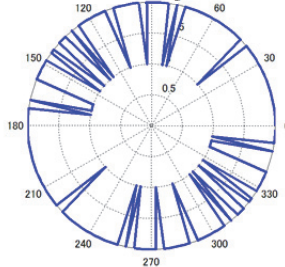
Cycle: 7



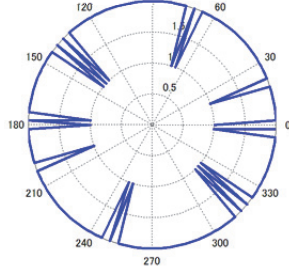
Cycle: 7.5



Cycle: 8



Cycle: 8.5



Cycle: 9

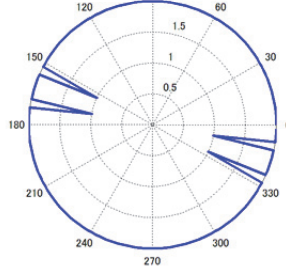


**Figure 5-11** Variation of count of the ionized electron for the CEP difference against the cycle number of the pulse at  $E_0 = 0.25$  a.u. Figures are shown for cycle 4.5 to 9 with 0.5 step width.

Left top letters of “Cycle:” on each pane shows the cycle number of the applied laser pulse. Until 4 cycle the ionization counts are all zero and figure are not shown.

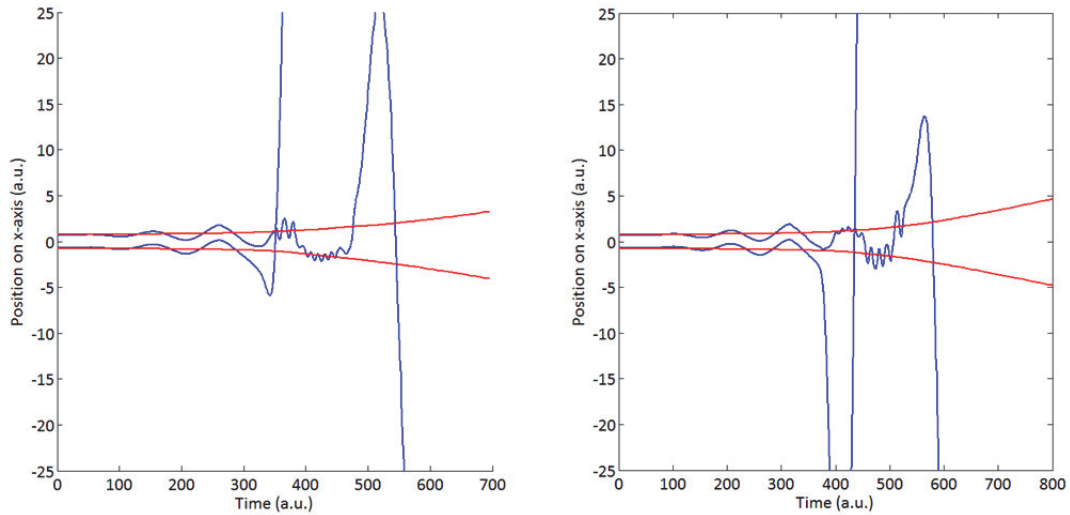


**Figure 5-12 Comparison of trajectories at cycle = 6 and cycle = 7 for CEP = 34 degree. The left pane shows variation of center positions of Gaussians at cycle = 6. The right pane shows variation of center positions of Gaussians at cycle = 7. The red lines represent the bases of the nuclei and the blue lines represent the bases of electrons.**

Figure 5-13 shows the comparison of trajectories at CEP = 110 degree and CEP = 158 degree for cycle = 7. The recollisions of the electrons to the cores occur around  $t = 450$  a.u. at the both cycles. After those, the other electron is ejected from the core. In those CEPs, the NSDI is also the main mechanism for double ionization.

Those situations indicate that the NSDI is the main mechanism for the double ionization at the beginning of the double ionization against the increase of cycle numbers. Compared to the case of  $E_0 = 0.3$  a.u., the larger number of cycles is required to induce the double ionizations. Furthermore, the region of starting angles of CEPs for the NSDIs are different between  $E_0 = 0.3$  a.u. and 0.25 a.u. Hence, we could see that the effects of CEPs for differentiate the ionization field and its mechanisms and trajectories.

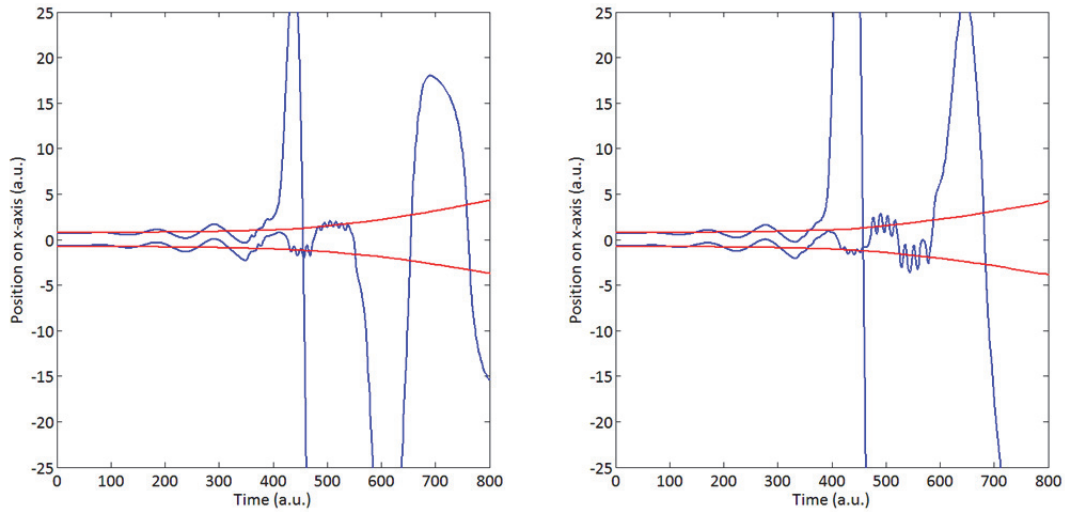


**Figure 5-13 Comparison of trajectories at CEP = 110 degree and CEP = 158 degree for cycle = 7. The left pane shows variation of center positions of Gaussians at CEP = 110 degree. The right pane shows variation of center positions of Gaussians at CEP = 158 degree. The red lines represent the bases of the nuclei and the blue lines represent the bases of electrons.**

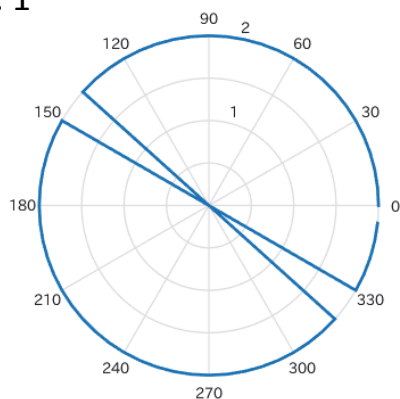
#### **5.2.4. $E_0 = 1$ a.u. and 0.1 a.u.**

On the above discussion, I discussed the case when the peak intensity is  $E_0 = 0.3$  a.u. and 0.25 a.u. This is because if the peak intensity is much larger than  $E_0 = 0.3$  a.u., all the electron will be ejected or if the peak intensity is much smaller than  $E_0 = 0.1$  a.u., no ionization occurs. Figure 5-14 shows the ionization counts for the CEP difference at  $E_0 = 1$  a.u. with 1 cycle (left pane) and at  $E_0 = 0.1$  a.u. with 9 cycle (right pane). In the left pane, the double ionization occurred for all the CEP angles even for 1 cycle number. The point which is zero is the lack of count because the calculation of trajectory was truncated for too long calculation time. The reason is guessed that the multicollinearity appeared. Oppositely, no ionization was observed at  $E_0 = 0.1$  a.u. with 9 cycle in the right pane even for 9 cycle number. The reason why the ionization count varies drastically for the peak intensity is first that the peak intensity in the scale of  $W/cm^2$  is proportional to the square of the peak electric field intensity  $E_0$ . Another reason is that the number of basis functions is small. I used 4 bases for 4 particles with

fixed orbital coefficients and trajectories will be deterministic in that situation because the small probability for the ionization cannot be expressed.

$E_0 = 1$  a.u.

Cycle: 1



$E_0 = 0.1$  a.u.

Cycle: 9

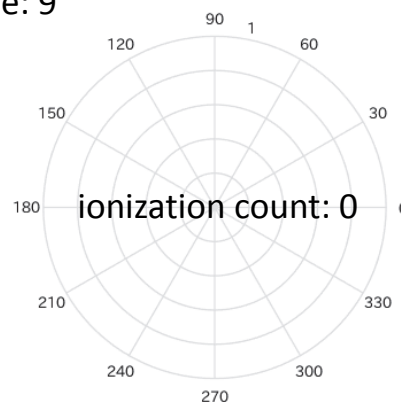


**Figure 5-14** Counts of the ionized electron for the CEP difference at  $E_0 = 1$  a.u. with 1 cycle (left pane) and at  $E_0 = 0.1$  a.u. with 9 cycle (right pane). Left top letters of “Cycle:” on each pane shows the cycle number of the applied laser pulse. The step size for CEP was 6 degree. In the left pane, the calculation of trajectory was not finished at CEP = 146 degree and 326 degree and plotted as 0 count.

## 6. Summary and perspectives

### 6.1. Summary

In Chapter 1, the object of the present research was described with experimental facts. In the molecular dynamics in intense laser fields, there are unique phenomena such as ionization of molecules, recollision of electron, non-sequential double ionization, and ultrafast proton migration. The calculation cost such as required memory size and time complexity is the critical problem in the simulation of dynamics in intense laser field. In conventional grid calculation, huge memory is required to express the electron-nuclear wave function and the time complexity is exponential time for number of particle. It suggests that it is practically difficult to apply the grid method to investigate the electron-nuclear mechanics in intense laser field.

The approach of the present research is CCS method. In CCS, the basis function is expressed with floating Gaussian which has a time-dependent center position and momentum. Floating Gaussian is suitable to follow the electronic motion in intense laser field and its time complexity is polynomial time for the total number of basis. Hence, CCS method is expected to be a good approach for this problem.

In Chapter 2, first the general EOMs were derived for the parameters  $\xi_i$  in the wave function. The analytical expressions of integrals with floating Gaussian functions were formulated. For  $H_2$  system, the wave function consists of Slater determinants of protons and electrons as described in Chapter 3. Each determinant is expressed with orbital function electrons or protons. Orbital functions are expressed with the linear combination of CCS. The analytical forms of tensor  $c_{ij}$  and differential of Hamiltonian were derived clearly. Also each integral of Gaussian was derived analytically. Hence the EOMs of electron-nuclear wave function were prepared.

The methods for optimization to the ground-state were introduced. One is gradient descent method (GDM) and the other is imaginary time propagation (ITP) method. The parameters are complex number in the present research, and then GDM should be modified for that case. In chapter 4, the optimizations of GDM and ITP were compared in the case of  $M = 4$  and the convergence was much faster in ITP

optimization. The optimized energy was  $H = -1.0665$  a.u. in the case of  $M = 10$  with orbital coefficients fixed and it was  $H = -1.0684$  a.u. in the case of  $M = 9$  with orbital coefficients varied. If the orbital coefficients were allowed to change, the total energy agreed with the limit of TRC-NOMO.

After we obtained the ground-state, real time propagation was simulated. In  $M = 4$  case, it was confirmed that the bases did not move at the equilibrium points and stable oscillation and bonds were achieved against some initial momenta. The vibrational period of nuclei was 299 a.u. in the case of  $M = 10$  with orbital coefficients fixed and it was 340 a.u. in the case of  $M = 9$  with orbital coefficients varied. The experimental value of vibrational period is 331 a.u. and the result in  $M = 9$  case was closer to the value. We could also observe the same vibrational periods in the calculation of squared inter-particle distances. Furthermore, the electronic excited states were by the MOs of the conventional HF calculation and the energies of electronic excited states calculated by the TDHF method. Through the Fourier transform analysis, we could observe the high frequency components related to the electronic excited states in the squared inter-nuclear distance. In the Born-Oppenheimer picture, electrons are always at ground-state and the nuclei will move slowly as a harmonic oscillator. The amplitude of the peak heights of those electronic frequency components depended on the mass of nuclei. Hence, we could confirm the non-adiabatic coupling between nuclei and electrons.

In Chapter 5, the laser field was introduced to the simulation and the molecular dynamics depending on the laser parameters was calculated. First the calculations for laser pulses of  $E_0 = 0.3$  a.u., 1.5 cycle, and three different CEPs were shown. In strong few cycle pulses, the difference of CEP critically affected ionization pathways and the non-sequential double ionization was observed. Next, changing the cycle number, the ionization count against the CEP difference was simulated for the laser pulses with the sin-square envelopes at  $E_0 = 0.3$  a.u. and 2.5 a.u. Then we could observe that the ionization counts were higher in  $E_0 = 0.3$  a.u. than in  $E_0 = 0.25$  a.u. and higher for longer cycles. We could see that there are regions where SDI and NSDI mainly

contribute respectively. For longer cycles, the ionization counts tended to be isotropic. The simulation was done in  $M = 4$  and this was least value for 4-particle system. However, we could clearly see the effect of laser parameters such as CEP, peak intensity, and cycle number against the ionization yields. Those non-adiabatic *ab initio* calculations can be achieved due to the small calculation cost with floating Gaussian basis functions.

## 6.2. Perspectives

In the present research, the width of Gaussian  $\gamma$  was fixed through the simulation. To treat  $\gamma$  as time-dependent parameter, the EOM for  $\gamma$  should be derived analytically. It might be more complicated to derive than other parameters, but more accurate calculation would be obtained by using the time-dependent  $\gamma$ . For example, the small amplitude of ionization can be expressed with widening of width of Gaussian.

In the calculation of the trajectories in laser fields in Chapter 5 was done with 4 Gaussians with orbital coefficients fixed. However, there was difference for the ground-state calculation between  $M = 4$  case and  $M = 9$  case. If the trajectory is calculated with at  $M = 9$  with orbital coefficients varied, more accurate and interesting results can be obtained. However, the calculation time per 1 trajectory is about couple of minutes for  $M = 4$  case but more than days for  $M = 9$  case. There is also the problem of instability when the orbital coefficients are allowed to change. Then it requires careful treat to expand the basis set for numerous calculation of trajectories.

The strong point of CCS is the polynomial time complexity for the number of Gaussian basis functions. The interesting object is a lager system than  $H_2$  molecule. Furthermore, the formulation for nuclei should be adopted for lager systems. Proton is especially light particle in nuclei and hybrid formulation for light proton and heavy nucleus (e.g. quantum mechanical treatment to proton, regarding heavy nucleus as Coulomb point) may be an efficient way to adapt the electron-nuclear wave function to the larger system. Matrix assisted laser desorption/ionization (MALDI) is one phenomenon of protein in the laser field. Another example of dynamics in the protein

is a proton pump at a biological membrane. The eventual goal is to adopt this method to the larger substance such as protein and discover interesting phenomena or control of reactions using laser field through calculations using floating Gaussian basis functions.

## Acknowledgements

I would like to thank Prof. Kaoru Yamanouchi from center of my heart for his grate supervision throughout my Ph.D. study, and for the opportunities to research in the outstanding environment. I am really grateful to have the chance to study in Bielefeld. I also would like to thank Prof. Tsuyoshi Kato for his valuable comments and advises for my research. I appreciate Dr. Erik Lötstedt for his kind supports. I am also grateful to Dr. Katsunori Nakai especially for his help on the calculations on the servers and Dr. Tamas Szidarovszky for his advises.

I would like to thank Prof. Farhad Faisal for his many advises for the research and extensive supports in Bielefeld. I also would like to thank Dr. Wanda Faisal and Dr. Klara De Decker for warm and strong supports in Bielefeld.

I would like to thank all my mates in Prof. Yamanouchi's group. I am grateful to Dr. Yoshihiro Ide for his kindness in the theory group. I appreciate more than five years shared with Mr. Takao Yamazaki, Mr. Kakuta Ishida and Mr. Shinichi Fukahori. I also appreciate to nice memories with the same grades Mr. Ryoichi Kira, Mr. Kei-ichi Yoshida and Mr. Kazuki Ootaka. Again I would like to thank all the other members.

Thank you for all my dear supporters and family.

Yuichi Ichikawa  
June 13, 2016  
Hongo, Tokyo